ISTANBUL TECHNICAL UNIVERSITY ★ GRADUATE SCHOOL

BADLAND SYSTEMS IN TURKEY: A HOLISTIC APPROACH TO UNDERSTAND THE FORMATION, CONTROLLING FACTORS AND GEOMORPHOLOGIC CHARACTERISTICS

Ph.D. THESIS

Aydoğan AVCIOĞLU

Department of Solid Earth Sciences

Geodynamics Programme

OCTOBER 2023

ISTANBUL TECHNICAL UNIVERSITY ★ GRADUATE SCHOOL

BADLAND SYSTEMS IN TURKEY: A HOLISTIC APPROACH TO UNDERSTAND THE FORMATION, CONTROLLING FACTORS AND GEOMORPHOLOGIC CHARACTERISTICS

Ph.D. THESIS

Aydoğan AVCIOĞLU
(602192002)

Department of Solid Earth Sciences

Geodynamics Programme

Thesis Advisor: Assoc. Prof. Dr. Tolga GÖRÜM
Thesis Co-Advisor: Asst. Prof. Dr. Ömer YETEMEN

OCTOBER 2023

ISTANBUL TEKNİK ÜNİVERSİTESİ ★ LİSANSÜSTÜ EĞİTİM ENSTİTÜSÜ

TÜRKİYE'DEKİ KIRGIBAYIR SİSTEMLERİ: OLUŞUMLARINI, KONTROL EDEN FAKTÖRLERİNİ VE JEOMORFOLOJİK KARAKTERLERİNİ ANLAMAK ÜZERİNE BÜTÜNSEL BİR YAKLAŞIM

DOKTORA TEZİ

Aydoğan AVCIOĞLU
(602192002)

Katı Yer Bilimleri Anabilim Dalı

Jeodinamik Programı

Tez Danışmanı: Doç. Dr. Tolga GÖRÜM
Eş Danışman: Dr. Öğr. Üyesi Ömer YETEMEN

EKİM 2023

Aydoğan Avcıoğlu, a Ph.D. student of İTU Graduate School student ID 602192002, successfully defended the dissertation entitled "BADLAND SYSTEMS IN TURKEY: A HOLISTIC APPROACH TO UNDERSTAND THE FORMATION, CONTROLLING FACTORS AND GEOMORPHOLOGIC CHARACTERISTICS.", which he prepared after fulfilling the requirements specified in the associated legislations, before the jury whose signatures are below**.**

Thesis Advisor :	**Assoc. Prof. Dr. Tolga GÖRÜM** İstanbul Technical University	.....
Co-advisor :	**: Assist. Prof. Dr. Ömer YETEMEN** İstanbul Technical University	.....
Jury Members :	**Prof. Dr. Atilla ÇINER** Istanbul Technical University	.....
	Prof. Dr. Cengiz YILDIRIM Istanbul Technical University	……
	Prof. Dr. Tuncer DEMİR Akdeniz University	……
	Assist. Prof. Dr. Abdullah AKBAŞ Istanbul University	……
	Dr. Mariano Moreno de las Heras Universitat de Barcelona	……

Date of Submission : 25.07.2023

Date of Defense : 19.10.2023

To my family,

FOREWORD

Badlands are extremely rugged, outstanding, and iconic landforms and they draw attention with their fast erosion rates, susceptibility to land degradation, high carbon flux, and geo-touristic potential. This study reveals and documents, for the first time, the existence of badland landscapes in Turkey by utilizing a comprehensive holistic approach; their spatial distribution and territorialization, weathering dynamics, and topographic imprints.

First, I would like to express my sincere gratitude to my supervisor and great mentor Assoc. Prof. Dr. Tolga GÖRÜM, who believed in me, trusted me, and always made me feel his unwavering support and hearty friendship. You have always been a source of inspiration for me and consistently instilled the mindset of thinking big and going beyond my limits. I am also grateful for the constant support, help, and kindness I received from my co-supervisor, Assist. Prof. Dr. Ömer YETEMEN, throughout this journey. I am sure that we'll always pursue our collaboration and friendship.

In addition, special thanks go to Assist. Prof. Dr. Abdullah AKBAŞ, Dr. Mariano Moreno de las HERAS, Assoc. Prof. Dr. Ali MOHAMMEDI, and Assoc. Prof. Dr. Orkan ÖZCAN, you always supported, motivated, and encouraged me throughout this journey.

I would like to thank Dr. Wolfgang SCHWANGHART, Dr. Uğur ÖZTÜRK, and Prof. Dr. Axel BRONSTERT for their great hospitality and collaboration during my 1-year visit in Potsdam, the Institute of Environmental Science and Geography at Universitat Potsdam. Also, I am thankful to Dr. Milica Kasanin GRUBIN, Nevena ANTIC, and Dr. Toma TOSTI for the great help in laboratory analyses and hospitality during the visit in Belgrade University.

I also thank Prof. Dr. Atilla ÇINER, Prof. Dr. Cengiz YILDIRIM, Prof. Dr. Tuncer DEMIR, Asst. Prof. Dr. Abdullah AKBAŞ, and Dr. Mariano Moreno de las HERAS for being examiners of this thesis.

The important thanks are necessary to a number of friends who helped me during this journey and fieldworks; Toygar family, Onur ALTINAY, Tunahan AYKUT, Cihan YILDIZ, Seçkin FIDAN, Abdüssamet YILMAZ, Furkan KARABACAK, Emrah ÖZPOLAT, Deniz YAZICI, Kamal RANA, and Joaquin Vicente C FERRER.

Furthermore, I thank to TUBITAK and my co-supervisor, Assist. Prof. Dr. Ömer YETEMEN for the project support, 2232 International Fellowship for Outstanding Researchers Program of the Scientific and Technological Research Council of Turkey (TUBITAK) through grant 118C329, I received funding during my Ph.D. I thank TUBITAK 2214a program for their support my stay in Potsdam, Germany for a year. I also thank to my supervisor Assoc. Prof. Dr. Tolga GÖRÜM for his support in the last months of Ph.D. through his NATO – Science for Peace and Security Programme project.

I would like to express my heartfelt gratitude and pay tribute to Prof. Dr. Cengiz AKBULAK who has passed away, as he was the first to inspire me and believe in me.

Above all, my heart overflows with immense gratitude and overwhelming emotions as I reflect upon the extraordinary impact my parents, Mürvet and Mehmet AVCIOĞLU, my dear sister Melike YAMAN and my brother-in-law Doğan YAMAN, and my beloved spouse and soulmate, Burcu AVCIOĞLU, have had on my life. Their unwavering love and boundless encouragement have been the very bedrock of my existence, propelling me forward through every triumph and tribulation.

July 2023

Aydoğan AVCIOĞLU

(Jeomorfolog)

TABLE OF CONTENTS

ABBREVIATIONS

A **:** Drainage/contribution area
appox. : Approximately
A1 **:** 1st sample from arid region
A2 :2nd sample from Arid region
A3 :3rd sample from Ardi region
A4 :4th sample from arid region
EC **:** Electrical conductivity
EG **:** Eluent Generator
CAP **:** Central Anatolian Plateau
CDS **:** Conductivity Detector
CR-ATC : Continuously Regenerating Anion Trap Column
C1 : 1st sample of Cappadocia
C2 : 2nd sample of Cappadocia
DEM **:** Digital Elevation Model
DTM **:** Digital Terrain Model
HGM **:** General Directorate of Mapping of Turkey
H1 **:** 1st sample of humid region
H2 **:** 2nd sample of humid region
E **:** East
EAP **:** East Anatolian Plateau
e.g., **:** For example
FR **:** Refrigerator
FZ **:** Freezer
ICP-OES **:** Inductively coupled plasma—optical emission spectrometry
i.e., **:** that is
KOH **:** Potassium hydroxide
L **:** Lamp
MAP **:** Mean annual precipitation
min. : Minute
MTA **:** Mineral Research and Exploration General Directorate

M1 : 1st sample in Mediterranean region

M2 : 2nd sample in Mediterranean region

M3 : 3rd sample in Mediterranean region

NAF : North Anatolian Fault

NAFZ : North Anatolian Fault Zone

NDVI : Normalized Differences Vegetation Index

N : North

NTP : North Turkish Province

Op : Positive openness

On : Negative openness

R : Room temperature

RRIM : Red Relief Image Mapping

S : Slope

SAR : Sodium Absorption Ratio

SE : South East

S : South

SP : Single Pump

™ : Trade Marker

µL : Millionth of a liter

USLE : Universal Soil Loss Equation

Vol : Volume

WAHG : Western Anatolia Horst Graben

WAEP : Western Anatolia Extensional Province

SYMBOLS

cm	**:** centimeter
cm^3	**:** cubic centimeter
kg	**:** Kilogram
km^2	**:** Kilometer square
Ma	**:** Million year
mL/min	**:** Milliliter per minute
mm	**:** Millimeter
mM	**:** Millimolar
m.	: Meter
m.a.s.l	**:** Meters above mean sea level
m^2	**:** Square meter
mm sec^{-1}	**:** Millimeter per second
mm y^{-1}	: Millimeter per year
mmol/kg	**:** Millimole per kilogram
Na^+	**:** Sodium
Ca^{2+}	**:** Calcium
Mg^{2+}	**:** Magnesium
K^+	: Potassium
CO_3^{2-}	: Carbonate
Cl^-	**:** Chlorine
SO_4^{2-}	**:** Sulphate
NO_3^-	**:** Nitrate
θ	**:** Theta
°	**:** Degree
°C	**:** Degree Celsius
R^2	**:** Coefficient of determination
%	**:** Percentage
~	**:** Around/on the order of

LIST OF TABLES

LIST OF FIGURES

Page

BADLAND SYSTEMS IN TURKEY: A HOLISTIC APPROACH TO UNDERSTAND THE FORMATION, CONTROLLING FACTORS AND GEOMORPHOLOGIC CHARACTERISTICS

SUMMARY

Badlands are extremely rugged, outstanding landscapes that can be seen in all ice-free climate regions over erosion-susceptible unconsolidated materials, and they have drawn attention with their spectacular and iconic. The distribution of badlands is primarily influenced by the occurrence of loose and unconsolidated rocks (such as marl, sandstone, mudstone, etc.). These lithological units, in conjunction with various environmental elements such as climate, tectonics, vegetation, and topography, collectively shape the appearance and dynamics of badland landscapes. Since badlands have the largest sediment flux and erosion rates, they are considered to be erosional hot spots. However, the morphological characteristics, origins, regional characteristics, and development processes of these badlands are not well known.

Unlike nearly all badland studies conducted at the experimental site and watershed scale, the broader-scale evaluation has been neglected in the analysis of badland distribution, characteristics, and dynamics. The first part of the thesis provides an integrative new insight into badland landscapes by investigating the distribution, characteristics, and controlling factors of Turkish badlands on a broad, regional scale. Turkish badlands were inventoried using aerial imagery and studied their distribution using *K*-means clustering, an unsupervised machine learning algorithm, based on a set of major conditional geo-environmental factors that control the regional distribution and characteristics of badlands, including tectonics, lithology, topography, climate, and vegetation. Here, a total of 4494 km^2 of badland areas were identified which are non-uniformly distributed across Turkey, substantially clustered in the Central Anatolian Plateau (CAP). According to regional analyses, a total of five badland regions have been determined comprising three major types classified as Semi-arid, Mediterranean, and Montane (humid), together with two transitional types in-between the Semi-arid and Montane badland regions. The results indicate that temperature seasonality, mean annual precipitation, and precipitation seasonality are predominantly assigned to the badlands clusters. The clastic rocks are revealed as the most crucial and inevitable factor for the development of Turkish badlands, which are represented in a wide geologic time-scale (Cretaceous to Quaternary) and diverse lithological units (i.e., lacustrine, volcaniclastics, and terrestrial). Neogene and Paleogene terrestrial clastics (77 %) constitute the majority of the lithologic settings of these badland landscapes. The active and complex tectonic history of Turkey has portrayed the fundamental frame of the identified badland regions, by providing a susceptible environment (i.e., development of sedimentary basins) and promoting badland development through successive base-level changes. Furthermore, tectonically-modulated (i.e., formation of orogenic belts, and uplifting of CAP) climate dynamics outline the distribution pattern and differentiation of the regional characteristics of badlands in Turkey. Overall, the regional-scale approach to badland mapping and regional synthesis may decipher not only the tectonic and climatic

conditions of the identified badlands regions but may also contribute to the implementation of future effective strategies for the detection and mapping of erosion-susceptible and high sediment flux areas in very broad spatial contexts of similar unexplored territories.

An ever-present intricate association between weathering and erosional processes is largely controlled by climate disparities. Weathering as a predisposing process for natural hazards, landform evolution, and sediment mobility hosts key uncertainties in our understanding of how climate controls differential weathering types and rates. Here, the second part of thesis shows an approach to test the hypothesis controlling of weathering trends with the influence of seasonal characteristics of precipitation and temperature, which has been not well understood in badland landscapes, yet. Previous studies have adopted a rainfall simulation approach either in the field or laboratory, which is essential but is also limiting in that only steady climate conditions can be monitored in understanding weathering dynamics. In this context, by taking advantage of the laboratory environment to accomplish the aim of this part, the climate settings were simulated by exposing samples collected from four different climates and sedimentary environments previously defined as characteristic badland landscapes in Turkey to the seasonal precipitation and temperature conditions in twelve sequential seasons mirroring 3-years in order to understand the weathering rebounds. The pH, electrical conductivity (EC), ion, and surficial changes have been used as chemical and physical proxies, respectively, in referring to certain types and trends of weathering. Based on the incontrovertible influence of sediment physicochemical properties (especially high SAR values) on weathering processes, the findings reveal that sinusoidal trends attaining their peak level in spring in Na^{+}, which overcomes other ions, contribute to an accelerated dispersion degree with concurrently decreasing pH in marly sediments in the arid region. Additionally, the recurrent increase pattern of Ca^{2+}, particularly in winter seasons, can enhance the extent of sediment aggregations in Mediterranean sandy mudstones. In conclusion, consistent with previous studies, wetting–drying cycles are crucial in physical weathering and regolith behavior, which resulted in cyclic deep crust formations in the spring and summer seasons due to the higher swelling capacity of samples. Overall, this study demonstrates how seasonal changes in climate regulate the degree of chemical and physical weathering processes in badland landscapes.

The combination of bedrock weathering, climate seasonality, and the controversial contributions of hillslope and river erosion processes, as part of the earth's dynamic systems, is what primarily develop badland environments. Although modern definitions make it clear that gully channels dominated by overland flow, mass movements dominated by gravitational processes, and piping driven by subsurface processes are all necessary for badland initiation, the questions remain to be tackled regarding their topographic position in the landscape. The third and last part of thesis focused on this problem by comparing Turkish badlands and globally known badland sites in order to understand the geomorphometric and topographic imprints of badlands. As a result, the topographic character of badlands at the sub-catchment scale may provide an adequate example of a transitional domain from a diffusive erosional process to a fluvial erosion process.

TÜRKİYE'DEKİ KIRGIBAYIR SİSTEMLERİ: OLUŞUMLARINI, KONTROL EDEN FAKTÖRLERİNİ VE JEOMORFOLOJİK KARAKTERLERİNİ ANLAMAK ÜZERİNE BÜTÜNSEL BİR YAKLAŞIM

ÖZET

Kırgıbayırlar, kutup iklim bölgeleri dışında erozyona duyarlı pekleşmemiş anakayalar üzerinde görülebilen son derece engebeli, olağanüstü yeryüzü şekilleridir. Dikkat çekici ve sıra dışı görünüşleri ile ikonik bir arazi meydana getirmektedirler. Kırgıbayır arazilerinin dağılımında öncelikle gevşek ve pekleşmemiş kayaçların (marn, kumtaşı, çamurtaşı vb.) varlığı önemli rol oynamaktadır. Bu litolojik birimler, iklim, tektonizma, bitki örtüsü ve topoğrafya gibi çeşitli çevresel unsurlarla birlikte, kırgıbayır arazilerinin görünümünü ve dinamiklerini toplu olarak şekillendirmektedir. Kırgıbayırlar, sahip oldukları yüksek sediman akışı ve erozyon hızlarından dolayı, literatürde erozyonel sıcak noktalar olarak kabul edilir. Bu özelliklerine karşın, kırgıbayır arazilerinin morfolojik özellikleri, kökenleri, bölgesel özellikleri ve gelişim süreçleri iyi bilinmemektedir.

Neredeyse tümü deneysel alan ve havza ölçeğinde yürütülen kırgıbayır arazileri üzerine olan çalışmalarda, kırgıbayırların mekansal dağılımı, özellikleri ve dinamiklerinin analizinde bölgesel ölçekli değerlendirme ihmal edilmiştir. Bu yüzden tezin ilk bölümü, Türkiye'deki kırgıbayır arazilerin mekansal dağılımını, özelliklerini ve bu dağılımı kontrol eden faktörleri geniş ve bölgesel ölçekte araştırarak kırgıbayır arazilerine bütünsel yeni bir bakış açısı sunmaktadır. Bu kapsamda Türkiye'deki kırgıbayırların, hava fotoğrafları kullanılarak mekansal envanteri çıkarılmış ve tektonizma, litoloji, topoğrafya, iklim ve bitki örtüsü gibi kırgıbayırların bölgesel dağılımını ve özelliklerini kontrol eden bir dizi jeo-çevresel faktör temelinde, gözetimsiz (ing: unsupervised) bir makine öğrenimi algoritması olan K-ortalamalar kümeleme yöntemi kullanılarak mekansal dağılım desenleri incelenmiştir. Burada, Türkiye genelinde eşit olmayan bir şekilde dağılmış ve büyük ölçüde Orta Anadolu Platosu'nda (OTP) kümelenmiş toplam 4494 km^2 kırgıbayır arazisi tespit edilmiştir. Bölgesel analizlere göre, Yarı-kurak, Akdeniz ve Dağlık (nemli) olarak sınıflandırılan üç ana tip ile Yarı-kurak ve Dağlık Kırgıbayır bölgeleri arasında iki geçiş tipinden oluşan toplam beş adet kırgıbayır bölgesi belirlenmiştir. Sonuçlar, sıcaklık mevsimselliğinin, ortalama yıllık yağışın ve yağış mevsimselliğinin kırgıbayır arazilerinin bölgelerin belirlenmesinde daha fazla katkıya sahip olduklarını göstermektedir. Türkiye'deki kırgıbayırların gelişimi için en önemli ve kaçınılmaz faktör olarak, geniş bir jeolojik zaman ölçeğinde (Kretase'den Kuvaterner'e) ve çeşitli litolojik birimlerde (gölsel, volkaniklastikler ve karasal kırıntılılar) temsil edilen kırıntılı çökel kayaçlar ortaya çıkmaktadır. Neojen ve Paleojen karasal kırıntılı çökelleri (%77) kırgıbayır arazilerinde en yaygın litolojik birimleri oluşturmaktadır. Türkiye'nin aktif ve karmaşık tektonik geçmişi, kırgıbayır arazilerinin gelişiminde, birbirini izleyen taban seviyesi değişiklikleri ile kırgıbayır arazilerinin gelişimi için duyarlı bir ortam sağlayarak (kırıntılı çökel kayaçların depolanması), tanımlanan kırgıbayır bölgelerinin temel çerçevesini çizmiştir. Ayrıca, tektonik olarak düzenlenmiş (orojenik kuşakların oluşumu ve Anadolu platosunun yükselmesi) iklim dinamikleri, Türkiye'deki kırgıbayır arazilerin bölgesel özelliklerinin dağılım

desenlerini ve farklılaşmasını ana hatlarıyla belirlemektedir. Genel olarak, kırgıbayır arazilerinin haritalanması ve bölgesel sentezine yönelik bölgesel ölçekli yaklaşım, yalnızca belirlenen kırgıbayır bölgelerinin tektonik ve iklimsel koşullarını deşifre etmekle kalmayıp, aynı zamanda benzer tespit edilmemiş bölgelerin çok geniş mekansal bağlamlarında erozyona duyarlı ve yüksek sediman akışlı alanların tespiti ve haritalanması için gelecekte etkili stratejilerin uygulanmasına da katkıda bulunabilir.
Ayrışma ve erozyonel süreçler arasında her zaman var olan karmaşık bir ilişki, büyük ölçüde iklim farklılıkları tarafından kontrol edilmektedir. Doğal tehlikelere, yeryüzü şekillerinin evrimine ve sediman akışına zemin hazırlayan bir süreç olarak ayrışma, iklimin farklı ayrışma türlerini ve hızlarını nasıl kontrol ettiğine dair anlayışımızda önemli belirsizlikler barındırmaktadır. Burada, tezin ikinci bölümünde, kırgıbayır arazilerinde henüz iyi anlaşılmamış olan yağış ve sıcaklığın mevsimsel özelliklerinin ayrışma hızlarını kontrolü üzerine hipotezi test etmek adına bir yaklaşım gösterilmektir. Daha önceki çalışmalarda ya arazide ya da laboratuvarda yağış simülasyonu yaklaşımı benimsenmiştir, fakat bu yaklaşım, ayrışma dinamiklerinin anlaşılmasında önemli olmakla birlikte, yalnızca sabit iklim koşullarının izlenebilmesi açısından da sınırlayıcıdır. Bu bağlamda, bu bölümün amacına ulaşmak için laboratuvar ortamından yararlanılarak, ayrışma süreçlerinin bu hipoteze tepkisini anlamak için Türkiye'de daha önce kırgıbayır özellikleri bakımından tanımlanan dört farklı iklim ve sedimanter ortamdan toplanan örnekler, 3 yılı yansıtan on iki ardışık döngüde yağış ve sıcaklık koşullarına maruz bırakılarak, iklimin sıcaklık ve yağış parameterleri simüle edilmiştir. pH, elektriksel iletkenlik (EC), iyon ve yüzeysel değişiklikler, belirli ayrışma türlerine ve eğilimlerine atıfta bulunmak için sırasıyla kimyasal ve fiziksel ayrışma göstergeleri olarak kullanılmıştır. Sediman fizikokimyasal özelliklerinin (özellikle yüksek SAR değerleri) ayrışma süreçleri üzerindeki yadsınamaz etkisine dayanarak, bulgular, diğer iyonların önüne geçen Na^{+} katyonunun ilkbaharda en yüksek seviyeye ulaşan döngüsel eğilimlerin, kurak bölgedeki marnlı sedimanlarda eşzamanlı olarak azalan pH ile hızlandırılmış bir dağılma (ing: dispersivity) derecesine katkıda bulunduğunu ortaya koymaktadır. Buna ek olarak, özellikle kış mevsimlerinde tekrarlayan Ca^{2+} artış deseni, Akdeniz kumlu çamurtaşlarında sediman agregasyon hızının artışını işaret edebilir. Sonuç olarak, önceki çalışmalarla tutarlı olarak, ıslanma-kuruma döngüleri fiziksel ayrışma ve regolit davranışında çok önemlidir ve bu da örneklerin daha yüksek şişme kapasitesi nedeniyle ilkbahar ve yaz mevsimlerinde döngüsel derin kabuk oluşumlarıyla sonuçlanmıştır. Genel olarak bu çalışma, iklimdeki mevsimsel değişikliklerin kırgıbayır arazilerindeki kimyasal ve fiziksel ayrışma süreçlerinin hızını nasıl kontrol ettiğini göstermektedir.

Ana kayanın ayrışması, iklimin mevsimselliği ve dünyanın dinamik sistemlerinin bir parçası olarak yamaç ve flüvyal erozyon süreçlerinin tartışmalı katkılarının birleşimi, öncelikle kırgıbayır arazilerini geliştiren olgudur. Her ne kadar çağdaş tanımlar kırgıbayır oluşumunun yüzeysel akışın hakim olduğu oluk erozyonu (gully), yerçekimi süreçlerinin hakim olduğu kütle hareketlerinin ve yeraltı süreçlerinin yönlendirdiği borulama erozyonunun bir fonksiyonu olduğunu açıkça ortaya koysa da, kırgıbayırların topoğrafik konumlarına ilişkin temel ilgili sorular hala ele alınmayı beklemektedir. Tezin üçüncü ve son bölümü, kırgıbayır arazilerin jeomorfometrik ve topoğrafik izlerini anlamak için Türkiye'deki ve dünyaca bilinen kırgıbayır arazilerini karşılaştırarak bu soruna odaklanmıştır. Sonuç olarak, alt havza ölçeğindeki kırgıbayır arazilerin topografik karakteri olarak, yamaç aşındırma sürecinden flüvyal aşındırma sürecine geçiş alanı için uygun bir örnek sağlayabileceği tespit edilmiştir.

1. INTRODUCTION

Badlands can be defined as extensively eroded areas (e.g., intensive gully networks) with sparse vegetation, characterized by rugged terrain featuring sharp-edged, rounded, and domed ridges (i.e., biancana) on soft bedrock and unconsolidated sediments. The term "Badlands" is derived from the 18th-century French term "mauvaises terres pour traverser," which was used by early explorers in North Dakota to characterize harsh and barren environments (Fairbridge, 1968; Moreno-de las Heras & Gallart, 2018). Badlands are present in all continents, excluding Antarctica, and play a critical role in establishing local erosion and sedimentation rates through gullies and rills, rendering them unsuitable for agricultural purposes. Even though badlands often only constitute a small portion of the overall terrain and only appear as scattered patches, they are significant regional sources of sediment generation because of their severe soil erosion (Higuchi et al., 2013; Yang et al., 2021). Their development and production are intricately associated with the existence of unconsolidated materials, tectonic activity, seasonal climate fluctuations, and anthropogenic activities changing over time.

Moreno-de las Heras and Gallart (2018) proposed that the formation, stability, and rejuvenation of badlands are influenced by the convergence of four factors related to terrain stability: relief vigor, weathering and erosion-prone soft lithology, erosive climate, and environmental conditions or disturbances that limit vegetation growth. Topographic gradients, dynamic base-level conditions, sensitivity to bedrock weathering, and soil erosion are all facilitated by the underlying tectonics and lithology at regional and local scales. Climate conditions and anthropogenic activities (i.e., deforestation) further contribute to denudation instability in these landscapes by influencing the balance between vegetation growth potential and erosive processes. Badlands can originate as primary landforms in arid and semi-arid, erosive climates acting on susceptible lithologies, such as marine-derived, unconsolidated river sediments, marl, and mudrock with dispersive characteristics prone to subsurface erosion. They may also form in humid mountainous environments as secondary

erosive landforms, initiated by landslide scars resulting from extreme flood events or as active gully systems triggered by land use changes and human interventions (Moreno-de las Heras & Gallart, 2018; Torri et al., 2018).

Even though badlands are present throughout the world, with the exception of the polar regions, only a small portion of them have been documented or investigated until now. The majority part of the studies originates from the Mediterranean basin, especially Spain and Italy (Figure 1.1; Martínez-Murillo & Nadal-Romero, 2018). The primary emphasizes have been placed on the role of lithology (Moreno-de las Heras & Gallart, 2016a; Piccarreta et al., 2006) and weathering processes on badland dynamics (Faulkner, 2013; Kasanin-Grubin, 2013; Vergari et al., 2013), runoff generation (Arnau-Rosalén et al., 2008; Cantón et al., 2002), vegetation (Alexander & Calvo, 1990; Nadal-Romero et al., 2014) and erosion rate (Regüés & Gallart, 2004) in these badlands landscapes.

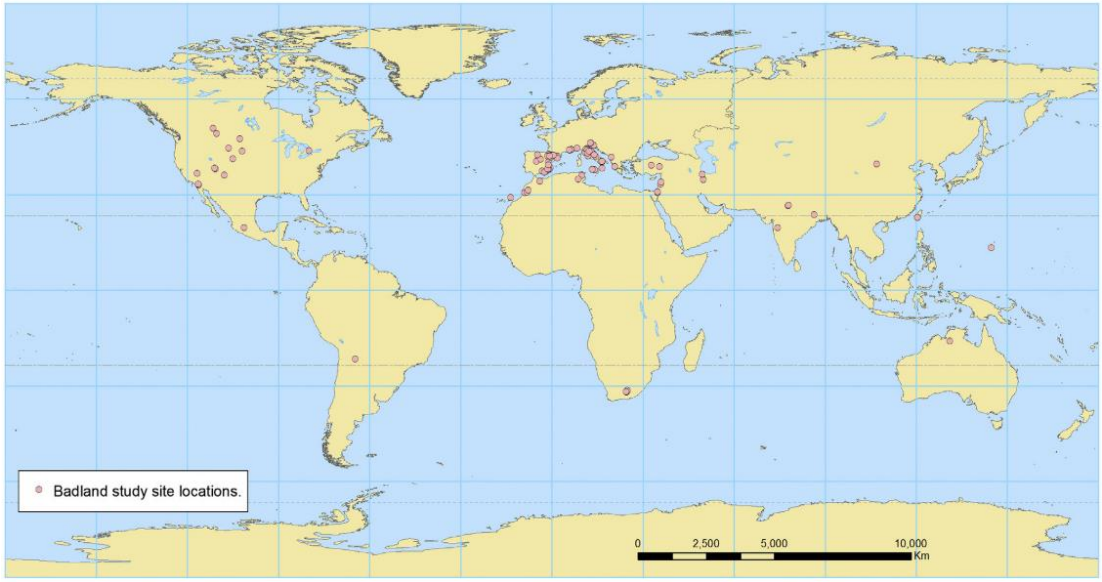

Figure 1. 1: The global badland distribution (Martínez-Murillo and Nadal-Romero, 2018)

On the other hand, in contrast to these well-documented sites, we have little knowledge of unreported badland landscapes that exist in other climatic and tectonic environments, such as the arid and semi-arid margins of the Tibetan Plateau in Asia, the Puna Altiplano Plateau in South America and the Central Anatolian Plateau, Turkey which are located in the prevailing Asian monsoon and continental climates, and tectonically active regions, respectively. These understudied places usually

generate landscapes in which badlands are arranged as spatially continuous, enormous landforms rather than sporadically distributed, limited and constrained forms (Avcıoğlu et al., 2022) and it is necessary to comprehend their geomorphic, erosional, and weathering dynamics.

The type and rate of differential weathering processes that result in unique badland morphologies in varied sedimentary and climatic contexts has received special attention. Faulkner et al., (2000) established the concept of "site signatures," which refer to the relationship between electrical conductivity (EC) and sodium absorption ratio (SAR), the pH-SAR ratio, and the grain size-SAR association. These indicators attempt to understand the underlying mechanisms by which the parent rock's grain size, geochemistry, and mineralogical properties determine the interesting limits between erodibility and weathering. Furthermore, previous studies have shown that the presence and proportion of clay and silt grains are critical factors of badland material, as sediments composed of silt-clay size particles are highly susceptible to weathering, dispersion, piping, and mass movements, resulting in different badland morphologies (Battaglia et al., 2003; Pulice et al., 2012; Vergari et al., 2013). While the role of clay mineralogy in erodibility of sediments has received limited attention (Grabowski et al., 2011), various studies on badlands have demonstrated that certain types of parent materials, such as sediments rich in swelling clays like smectite, exhibit greater susceptibility to erosion compared to sediments containing non-swelling clay minerals like kaolinite and illite (Kasanin-Grubin, 2013; Pardini et al., 1996; Regüés et al., 1995). Additionally, the impact of the climate on weathering have been pointed by utilizing laboratory and field experiments (Cantón et al., 2001; Kasanin-Grubin, 2013; Kasanin-Grubin & Bryan, 2007; Nadal-Romero et al., 2007; Pardini et al., 1996; Regüés & Gallart, 2004; Xie et al., 2022; Yan et al., 2022). This influence has been highlighted by temporal observations which simulate climate conditions. High drying temperatures, according to Xie et al. (2022), greatly promote mechanical disintegration in humid badlands. Kasanin-Grubin (2013) emphasized the importance of rainfall intensity, duration, and drying periods in weathering rate, with following dry and wet periods contributing to the creation of desiccation fractures and rills associated with key mineral types (i.e., smectite and kaolinite).

Over the last four decades, badlands literature has built a consensus on the main types of badlands forms; sharp-edged (i.e., calanchi in Italian), rounded-edged, and

biancane. Even though these landforms suffer from quantitative explanation, the climate-based badland classifications including arid, semi-arid and humid landscapes identify their differences considering their relative age, origin, vegetation, precipitation in Mediterranean basin (Gallart et al., 2002a). The arid badlands generally are characterized by oldest, lowest erosion and more rounded slopes than others. The semi-arid badlands are idenfied as sharp-edged slopes, high drainage density, patchy herbaceous cover, and combination of human activities and natural processes as trigger factors, while the formation humid badlands are highly interconnected with human intervention (i.e., deforestration, over-grazing etc.) and landslides in the range of Mediterranean mountains.

2. PROBLEM STATEMENTS AND OBJECTIVES

Present morphologies and ongoing processes in badlands reveal unearthed crucial pieces of evidence in deciphering the tectonic and climatic evolution of a region. Moreover, knowing the spatial distribution of such intense erosional landforms also contributes to understanding sediment dynamics, carbon fluxes, and interrelated geo-environmental problems like soil loss, reservoir siltation and water quality decrease. Due to their extensive contribution to land degradation and their uncertain responses to driving factors in the present global change context (Nadal- Romero et al., 2021), we need to extend our limited knowledge of badlands distribution over different climatic, tectonic, and anthropo- genic environments. The less-known cognatic section of the Mediterranean basin in terms of badlands, Turkey, offers a natural laboratory to assess the interrelated conditions leading to badlands formation through diverse climatic, tectonic, topographic, and lithological variations.

This thesis seeks to bring a comprehensive large-scale approach by providing a regional assessment on the country scale that explores their broad spatial organization by mapping their diagnostic morphological features and analysing geochemical and geomorphometric properties. In this sense, the essential objectives of this thesis are:

(1) Understanding of regional distribution and characteristics of major badland landscapes in Turkey.

The majority of the research has been conducted on watershed or plot scale assessments to understand the dynamics of surface and weathering processes by considering their local climate, tectonic, and vegetation in badland landscapes. However, there is a lack of regional evaluations of these landscapes to a broader extent in the literature. In order to fill this gap, the first aim of this thesis focuses on the determination of the spatial distribution of badlands in Turkey and to synthesize the distribution characteristics of these badland landscapes, taking into account a set of geo-environmental conditioning factors that mainly hinge on regional differences of tectonic and lithology, climate, local topography, and vegetation characteristics.

(2) How does climate seasonality influence weathering processes in badland landscapes?

The hypothesis that the formation of badlands is strongly linked to seasonal climatic factors has been proposed since the milestone study by Bryan and Yair (1982). However, despite previous laboratory and plot-scale experiments conducted in generally stable climatic conditions, this assumption has not been thoroughly evaluated. Conducting experiments through cycles and observing corresponding variations in geochemical indicators can give support to this overarching hypothesis, and obtained fluctuations in geochemical indicators as a response to simulated wetting and drying conditions may serve as effective proxies for investigating certain types and trends of weathering processes. Thus, the main aim of this part is to explore the key physical and chemical disintegration responses of a variety of badland materials, including unconsolidated sediments (i.e., marl, sandstone) and pyroclastic rocks (i.e., tuffs), in response to seasonal changes in temperature and precipitation. Accordingly, the primary hypothesis of this study is that, depending on the physicochemical properties of parent rocks, seasonal fluctuations in precipitation and temperature regulate the trends of weathering processes (i.e., deflocculation and flocculation).

(3) Determination of topographic positions of badlands.

Even though there are a few classification attempts on badland landscapes regarding their climate, vegetation (Gallart et al., 2002), and morphological differences and evolution (Buccolini & Coco, 2013), identification and quantitative explanation of their morphological distinctions, minimum extents, and topographical position remained extensively unclear. Thus, this part of the thesis aims to reveal the process domains (i.e., gravitational or fluvial processes dominated areas) of selected Turkish badland sites – Tosya and Burdur - with the previously known badland areas; Utah and South Dakota, USA; Murcia and Saldes, Spain; Lombardy and Basilicata, Italy; SW Taiwan. A deeper understanding of the geomorphometric characteristics of the Turkish badlands will be attained by comparing them with various climatic, tectonic, and lithologic contexts thanks to the advantages of the high-resolution digital terrain models (5m) at each site.

3. STUDY AREA

The spatial coverage of this thesis is the country border of Turkey. However, the geomorphometric findings on Turkish badlands (i.e., Burdur and Tosya) are compared with globally recognized sites that exhibit similar badland landforms (Figure 3.1A): Caineville and South Dakota, USA; Murcia and Saldes, Spain; Lombardy and Basilicata, Italy, and Taiwan. These areas have been selected mainly by taking into account different climate and lithological properties within the same country (Figure 3.2). The following section summarizes the general tectonic, geologic, and climatic properties of the first-order physiographic provinces of Turkey.

3.1 General Characteristics of The Study Area

The topography of the Anatolian Peninsula is mainly a result of long-term complex plate tectonic processes. The Horst and Grabens in Western Anatolia, Central and East Anatolian plateaus, the Pontides and Taurides mountain ranges, and troughs of the North and East Anatolian Fault zones are first-order physiographical provinces (Figure 3.1B). The main driving forces that define the outlines of physiographical regions are continental collision in the east and subduction in the west. The Arabian Plate has been colliding with the Eurasian Plate since the Late Eocene/ Oligocene in the east. The collision-related uplift phase started at ca. 10–12 Ma (Okay & Tüysüz, 1999; Bartol & Govers, 2014). The two most important elements of these macro physiographic regions are the Central and East Anatolian plateaus. The margins of these two highly elevated, low-relief major forms are constrained by the Taurides and Pontides orogenic belts with a pronounced topographic relief.

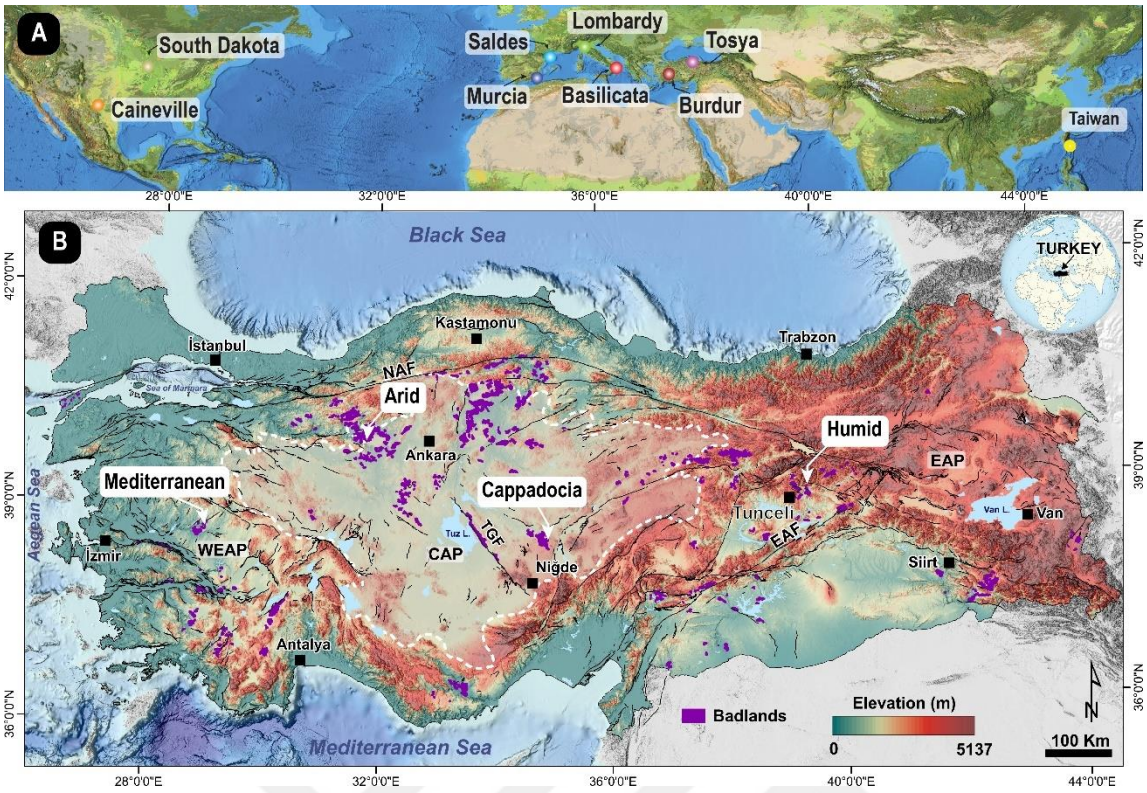

Figure 3. 1: The study sites and badland distribution. A) The location of different badland sites from different countries, B) the purple polygons show major badland distribution in Turkey and white shaded areas point to the sampling sites for geochemical analyses. Black lines show active fault lines (Emre et al., 2013), and dashed white lines delimit the boundary of the Central Anatolian Plateau (CAP). EAP, East Anatolian Plateau; NAF, North Anatolian Fault; EAF, East Anatolian Fault; WAHG, Western Anatolian Horst-Graben System.

Central Anatolia is an orogenic plateau with a high altitude (>900 m.a.s.l.) and low relief (>250 m) topography. The plateau interior has undergone extension with localized strike-slip faulting since the Late Miocene-Pliocene (Genç and Yürür, 2010; Özsayin et al., 2013). The alternating gypsiferous claystone, mudstone, marls, reddish mudstone, fine-grained sandstone, and conglomerates were deposited in the alluvial fans, shallow-lake, and playa lake environment during the late Miocene.

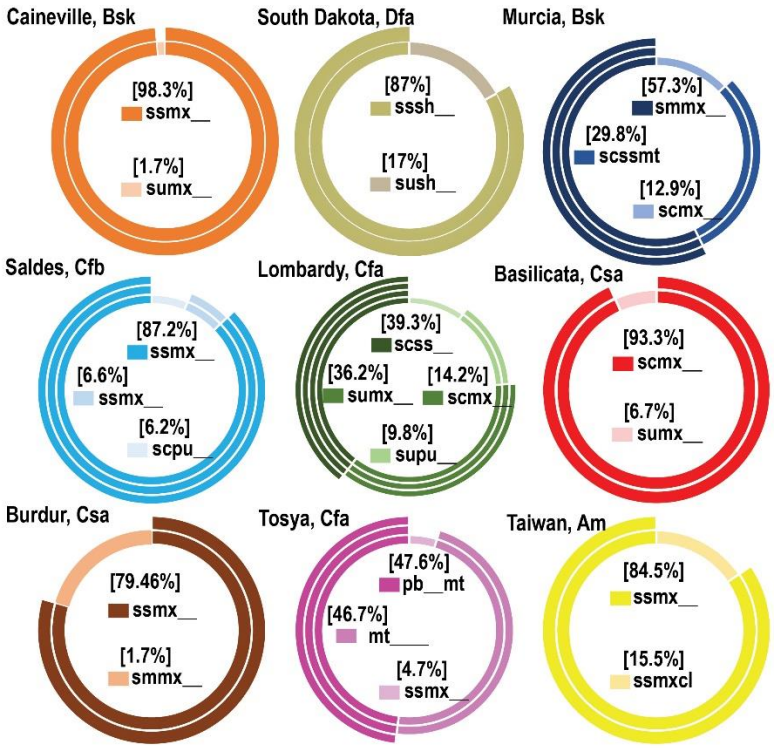

Figure 3. 2: The lithologic and climatic properties of the study sites from Turkey and other countries. The lithology groups are according to Hartmann and Moosdorf, (2012) as follows: sush__; Unconsolidated sediments - Fine grained, sssh__; Siliciclastic sedimentary rocks - Fine grained, scmx__; Carbonate sedimentary rocks - Mixed grain size, scssmt; Carbonate sedimentary rocks - Coarse grained - Metamorphic influence mentioned, smmx__; Mixed sedimentary rocks - Mixed grain size, scpu__; Siliciclastic sedimentary rocks - (Pure) carbonate, supu; Unconsolidated sediments - (Pure) carbonate, sumx; Unconsolidated sediments - Mixed grain size, scss; Carbonate sedimentary rocks - Coarse grained, ssmx__; Siliciclastic sedimentary rocks - Mixed grain size, mt____; Metamorphics, pb__mt; Basic plutonic rocks - Metamorphic influence mentioned, ssmxcl; Siliciclastic sedimentary rocks - Mixed grain - Fossil plant organic material mentioned. Climate groups are according to Peel et al. (2007) as follow: Cfb; Temperate oceanic climate or subtropical highland climate, Bsk; Cold semi-arid climate, Dfa; Humid continental climate, Csa; Temperate, dry summer, hot summer, Cfb; Temperate, no dry season, hot summer, Am; Tropical monsoon.

The sharp-edged composed of very steep (>40 degrees) and shorter slopes, rounded-edged, piping, and calanchi mammellonari were formed west of Ankara due to differential weathering and erosional limits of parent material in arid badlands (Figure 3.3; A1 to A4). Although there are fault-controlled mountain fronts (e.g., Tuz Gölü Fault, Central Anatolian Fault) and individual stratovolcanoes, the relief is very subtle. Evaporites and ignimbrites (Capadoccia Region) are typical basin infills in Central Anatolia where Cappadocia samples have been collected in north of the Niğde (Figure 3.3; C1 and C2).

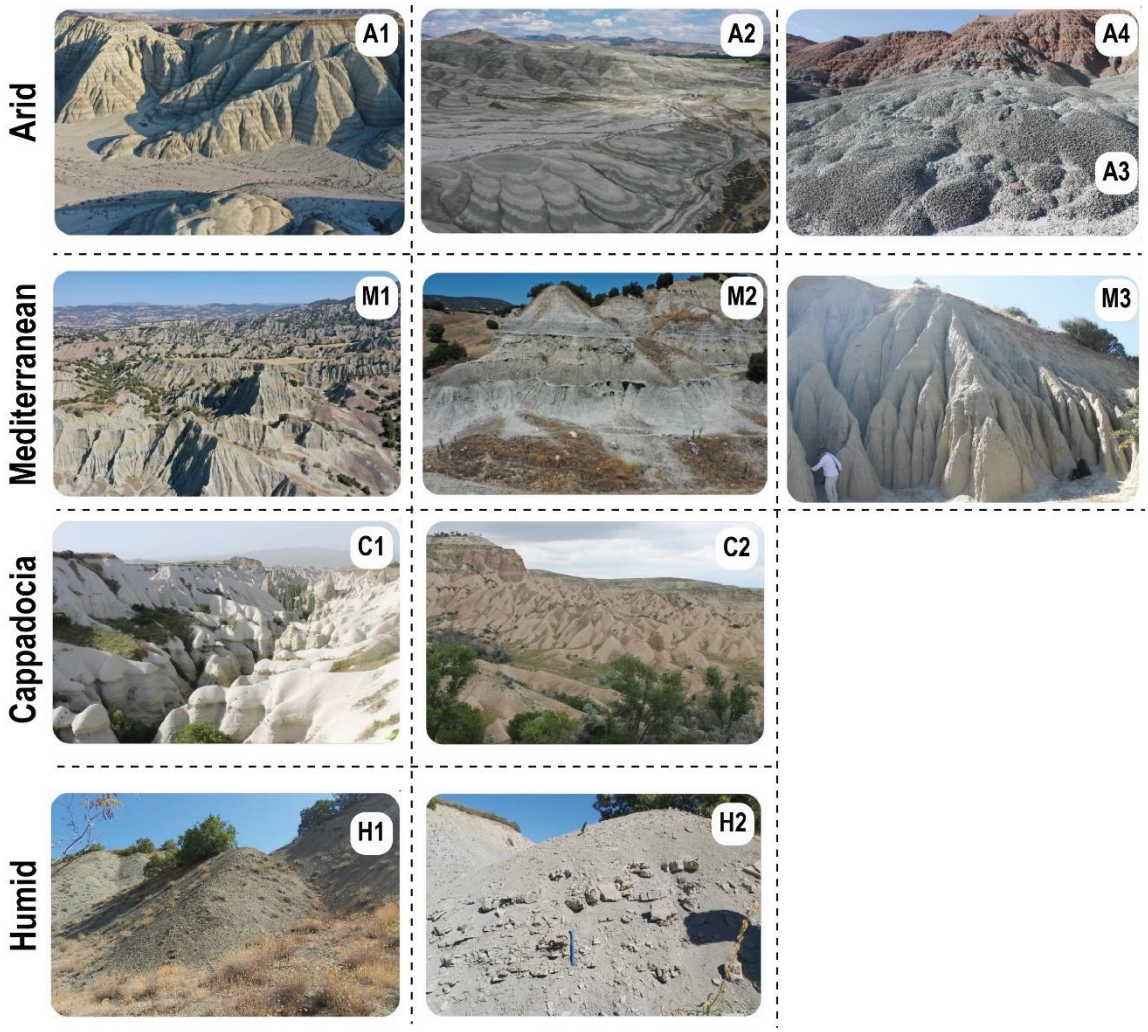

Figure 3. 3: The badland photos of different badlands sites from Turkey where samples have been collected for geochemical analyses

The Anatolian Microplate escapes west along the dextral North Anatolian Fault, and sinistral East Anatolian Fault zones accommodate this motion between collision and subduction. The space-based geodetic rate of this motion is 25 mm yr^{-1} and 11 mm yr^{-1}, in the north and east, respectively (Reilinger et al., 2006). Mountains surrounded by grabens or pull-apart basins characterize the topography of the western Anatolia province between the Marmara, Aegean, and Mediterranean seas. Terrestrial basin infills (e.g., Gediz Graben, Büyük Menderes Graben) and crystalline bedrocks (e.g., Menderes Massif) constitute the geology of Western Anatolia. Existing badlands in this area (Figure 3.3; M1 to M3) are distributed in Miocene and Quaternary unconsolidated sandstones (Maddy et al., 2005; Şen et al., 2014). The sharp and rounded-edged divides and piping are the main landforms of Mediterranean badland

(east of the İzmir) and shrubs -mostly maquis- are the dominant vegetation cover in this area.

The East Anatolian Plateau (EAP) has high topography. The mean elevation of EAP is ~ 1.5 km higher than that of the Central Anatolian Plateau (CAP). The geology of Eastern Anatolia comprises mainly calc-alkaline and alkaline volcanism, indicating fundamental changes in the mantle lithosphere or upper mantle (Keskin, 2007). In Eastern Anatolia, the presence of N–S contraction resulted in the formation of several E-W oriented ramp basins delimited by reverse faults. The uplift rate of Eastern Anatolia is 0.15–0.2 mm yr^{-1} since the onset of the regional uplift ca. 12–10 Ma (McNab et al., 2018). A typical flysch succession consisting of alternation conglomerates, sandstones, siltstones, and limestones (Agostini et al., 2019; Herece and Acar, 2016) constitute the parent material of the badland distribution which is represented by deeply-incised gully channels nearby Tunceli province where samples have been collected to represent mountainous humid areas (Figure 3.3; H1 and H2).

The Eastern Taurides (a fold and thrust belt between the Arabian Platform and EAP) and the Central Taurides define the southern margin of the Central Anatolian Plateau. Multiple oceanic and continental units deformed during the Late Cretaceous-Eocene time made up the basement of the Taurides. Up to 7 Ma old marine deposits at 2 km high above sea level indicate rapid surface uplift of the Taurides since the Late Miocene (Schildgen et al., 2014).

The Pontides delimit the northern margin of the Central Anatolian Plateau. The erosional character of the landscape and absence of notable Neogene units constraint quantify to long-term (Ma) uplift rate of the Pontides. The age of the youngest marine sediments is estimated at Early to Middle Miocene at 1040 m elevation (Tunoğlu, 1991), indicating a 1 km uplift since that time. The most remarkable large restraining bend of the North Anatolian Fault zone (NAFZ) gives rise to the accumulation of strain in a broad region from the north of the plateau to the Black Sea (Yildirim et al., 2011). This strain gives rise to accelerate regional uplift from 0.05 mm yr^{-1} in the interior of the plateau (Çiner et al., 2015) to 1.0 – 0.45 mm yr^{-1} at the central strand and the eastern flank of the NAFZ (Hubert-Ferrari et al., 2021; McClain et al., 2021).

Turkey's macroclimate is identified as the Mediterranean climate with hot/dry summers and wet/cold winters, although there are many sub-climatic regions (Figure

3B; Türkeş, 1996; Peel et al., 2007). As an explicit consequence of the Mediterranean climate conditions, natural vegetation in western Turkey is dominated by maquis and pinus brutias, mainly in the northern face of the badland areas. The Central Anatolian orogenic plateau has complex climatic characteristics due to the influence of the orography on precipitation, seasonal tracks, and the frequency of mid-latitude cyclones. This influence can be distinguished in the plateau margins by creating a gradient in climatic variations between the seafront and the inner section of the plateau. During winter, mid-latitude and Mediterranean cyclones associated with Atlantic-originated (the Icelandic Low) polar air masses reach the Mediterranean, bringing abundant rainfall to orographic barriers in the region, such as the Pontides, Taurides, and the Western Anatolian horst-graben systems (WAHG) (Karaca et al., 2000; Tatli et al., 2004; Sen et al., 2019). On the other hand, summer warm air masses related to the Azores High and the monsoon low extensively prevail over Anatolia, which causes summer dryness as a common characteristic feature of the Mediterranean climate in the territory, except in the North and Northeastern Anatolia (Tatli et al., 2004; Sariş et al., 2010; Akbaş, 2014; Sen et al., 2019). The complex association between topography and climate favors low water-demand vegetation development (e.g., steppes, dry forest, anthropogenic steppe), especially in the Central Anatolian Plateau. On the other hand, the high average elevation (>1.5 km) in the eastern part of Turkey provides a mountainous environment that supports widespread mixed forests and Alpine and sub-alpine grass formations.

4. METHODS AND DATA

The objectives of this thesis will be accomplished by following three main steps. 1) Investigation of badlands distribution and understanding of regional characteristics of the badlands in Turkey by using a machine learning approach. 2) Weathering processes as a response to simulated precipitation and temperature conditions in Turkish badlands will be analyzed with repeated laboratory analyses. 3) The topographic position of badlands will be determined by using the slope-area approach and comparing Turkish badlands with the badlands in different countries.

4.1 Regional Characteristics of Turkish Badlands

4.1.1 Badlands identification and inventory mapping

The aerial images (5m. resolution) provided by the General Directorate of Mapping (HGM) of Turkey and Google Earth Pro^{TM} images for areas where HGM aerial images were not available were used as source data to delineate badland boundaries (Figure 4.1A). The rough badland boundaries have been investigated by taking into account the spatial continuity the badlands (> 1km^2). In the badlands inventory, we specifically omitted minor (<1km^2) and spatially discontinuous badland-like landscapes associated with localized deforestation spots and mining activities. These landscapes were excluded due to their lack of spatial coherence, in which they did not demonstrate a repetitive distribution within an approximate radius of 10 km. The diagnostic morphologic indicators have been considered in the identification of the badlands landforms, such as the presence of highly dissected landforms (gullies and rills), channel density differences, and sparsely or unvegetated areas showing color, tone, and texture contrasts with their adjacent geo-environment.

The Red Relief Image Map (RRIM; Figure 4.1B) mosaics produced with an HGM-based, 5-m digital elevation model (DEM) were used to map precisely and exclude contiguous flat areas and trunk rivers within roughly identified badlands boundaries (Figure 4.1C).

$$I = (Op - On) / 2, \tag{4.1}$$

where *Op* is positive openness, and *On* is negative openness (Figure 4.1D). The stated parameter (*I* - value) appropriately excludes incident light direction dependencies that occur in shaded relief images and express convexity and concavity at the same time (Chiba et al., 2008; Görüm, 2019).

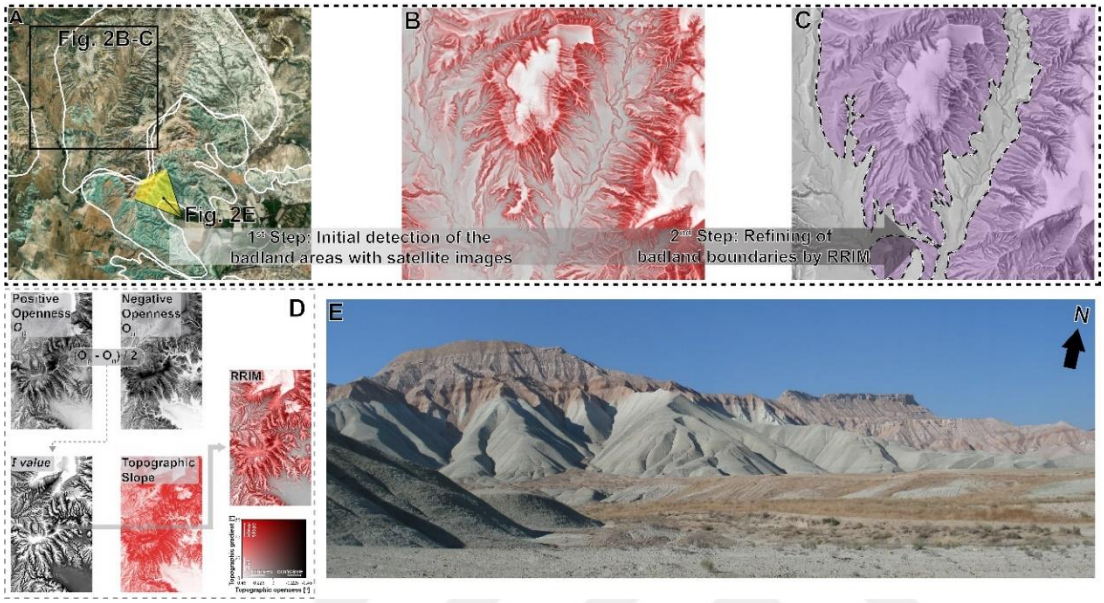

Figure 4. 1: An overview of badland unit identification steps. a) exploring rough morphologies of badland by using high-resolution aerial photos and Google Earth Pro™, b) Refining badland unit boundaries using Red Relief Image Map (RRIM), c) the resultant badland boundaries, d) RRIM visualization procedure steps, e) ground view of the sample area which is subject to badland unit identification

4.1.2 Geo-environmental parameters that control badland distribution

The potential geo-environmental parameters that contribute to badlands formation have been compiled at a 1-km spatial resolution with the aim of understanding and differentiation of the regional characteristics of identified badland distribution. Four main groups of variables have been determined according to their properties: Geology and Tectonics, Topography, Climate, and Vegetation (Table 4.1).

The geology and the Neogene tectonic uplift maps of Turkey (MTA, 2002; McNab et al., 2018) were used to obtain information about geologic settings. The lithologic features have been assessed by reclassifying the 1: 500,000 scale geology map of Turkey by considering the geologic time scale and depositional origin of the sedimentary rocks (Figure 4.2). The climate parameters, the mean annual precipitation (MAP; Figure 4.3A), seasonality both temperature (in Kelvin degrees) and precipitation (Figure 4.3B and 4.3C, respectively) were obtained from the WorldClim2

dataset (Fick & Hijmans, 2017). The aridity index (Trabucco & Zomer, 2018; Figure 4.3D) and the USLE R factor (Figure 4.3E) derived from the Global R-factor dataset (Panagos et al., 2017) R were also included to analyses.

Table 4. 1: The geo-environmental parameters used in defining regional characteristics of badlands.

Category	Parameters	Spatial Resolution	Reference
Geology and Tectonic	Lithology	30m	MTA (2002)
	Tectonic uplift	1km	McNub et al. (2018)
Climate	Precipitation	1km	Fick & Hijmans (2017)
	Precipitation seasonality	1km	Fick & Hijmans (2017)
	Temperature seasonality	1km	Fick & Hijmans (2017)
	Minimum temperature	1km	Fick & Hijmans (2017)
	Aridity	1km	Trabucco & Zomer (2019)
	R factor	1km	Panagos et al. (2017)
Topography	Elevation	1km	Yamazaki et al. (2017)
	Relief	1km	Yamazaki et al. (2017)
	Macro landforms	1km	Görüm (2019)
Vegetation	NDVI	1km	Toté et al. (2017)

All these climate parameters are extensively cited in the literature as critical factors involved in the development of badlands (Cantón et al., 2018; Clarke & Rendell, 2006; Higuchi et al., 2013; Moreno-de las Heras & Gallart, 2018). Multi-Error-Removed Improved-Terrain DEM (Yamazaki et al., 2017) has been used for topographic

analyses (i.e., relief and swath profiles) included elevation (Figure 4.3F). Additionally, the macro landforms of Turkey (Figure 4.4) produced by Görüm, (2019) also were included in data sets for further analyses and determination of badlands characteristics. The average value of May of the 1999–2017 SPOT series of the normalized difference vegetation index (NDVI; Figure 4.2H) for Turkey was obtained from Toté et al. (2017) in order to represent vegetation parameters in the regional analyses.

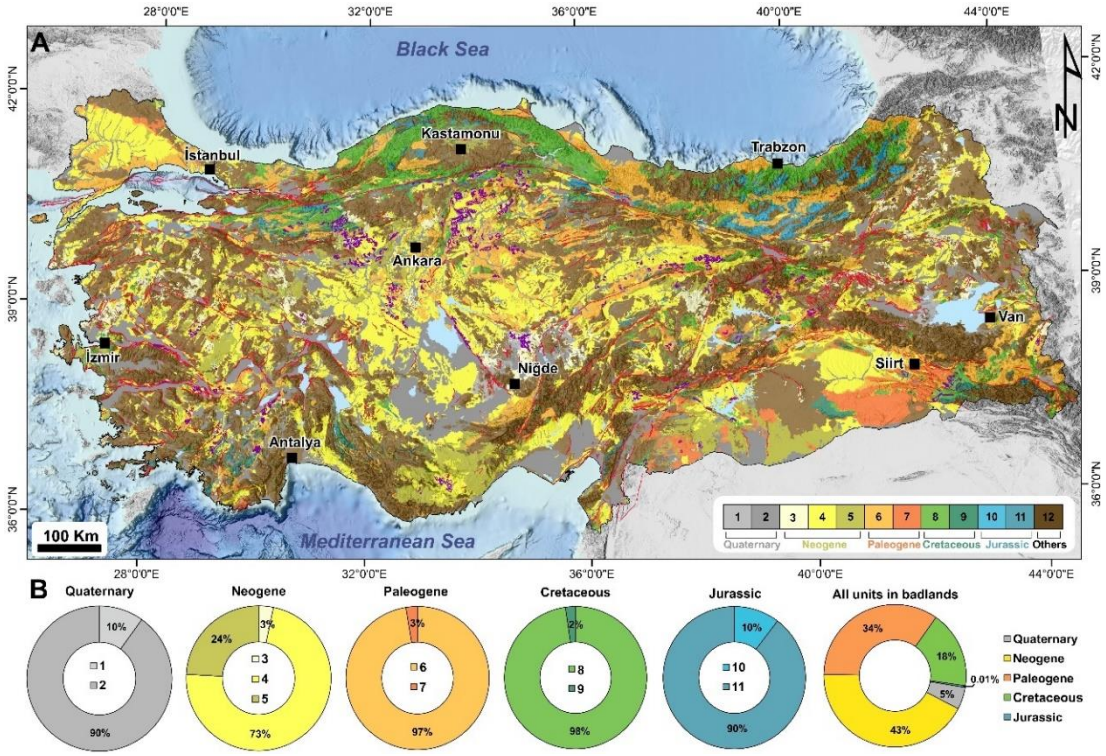

Figure 4. 2: The reclassified lithology map according to the purpose of the study (source: MTA, 2002). a) The lithology groups: Quaternary volcaniclastics (e.g., tuffs) (1), Quaternary clastics (e.g., unconsolidated sandstones) (2), Neogene volcaniclastics (e.g., tuffs, and ignimbrites) (3), Neogene clastics (4), Neogene lacustrine limestone interbedded with clastics (alternation of marls, sandstones, and limestones) (5), Paleogene clastics (6), Paleogene lacustrine limestones interbedded with clastics (e. g., alternation of sandstones, shales, and limestones) (7), Cretaceous clastics&pillow lava (8), Cretaceous lacustrine limestones interbedded with clastics (9), Jurassic clastics (10), Jurassic lacustrine limestones interbedded with clastics (11), others (12), b) the lithology proportions in determined badland areas. Red lines show the main active faults of Turkey (Emre et al., 2013), and purple polygons represent the badland units.

The hydrological unit - at the sub-catchment scale (average size ~ 53 km^2) - developed by the General Directorate of State Hydraulic Works of Turkey was considered a spatial unit for further analyses. Accordingly, we computed the values for each geo-environmental variable at the sub-catchment scale using the zonal mean for continuous

data (e.g., aridity, precipitation, NDVI, etc.) and the zonal majority for categorical data (e.g., lithology data).

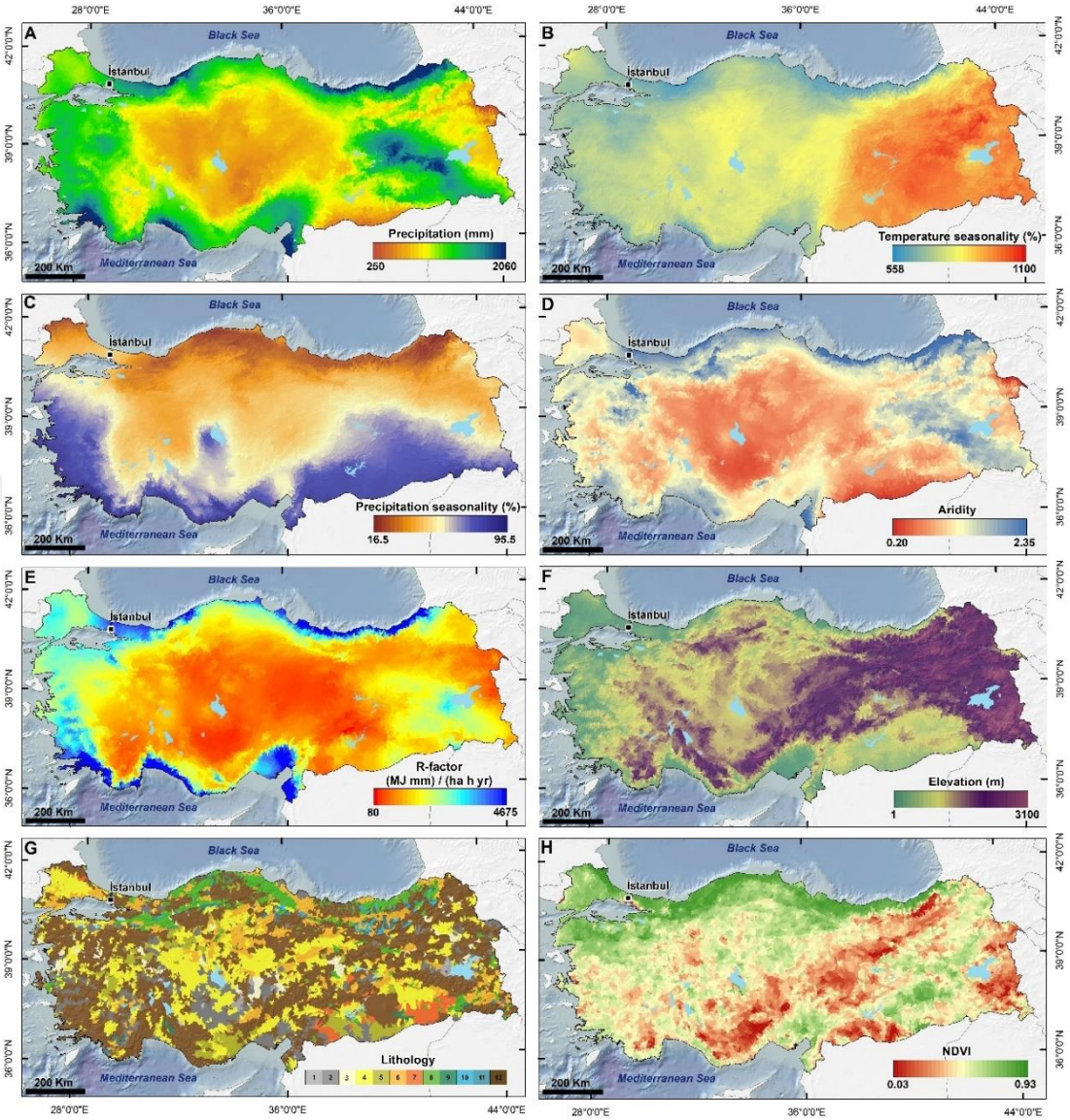

Figure 4. 3: The geo-environmental parameter maps in 1 km^2 spatial resolution, which are evaluated as the conditional factors on badlands clustering. a) Precipitation (mm), b) temperature seasonality (% coefficient of variation), c) precipitation seasonality (% coefficient of variation), d) aridity, e) R factor (Mj mm) / (ha h yr), f) elevation (m), g) lithology, h) NDVI

4.1.3 Data analysis

The one of most common unsupervised machine learning algorithms, *K*-means (MacQueen, 1967; Ball and Hall, 1965; Lloyd, 1982) has been applied to obtain comprehensive and distinctive regions of badlands in terms of the physical aspects that shape their spatial distribution. This technique which finds natural clusters in a given data set is composed of the following main steps: (i) The algorithm generates a random

number of *k* centroids inside the data domain., (ii) by linking each observation with the nearest mean, *k* clusters are formed, and (iii) the algorithm adjusts the centroid of each of the *k* clusters and iterates the previous two steps until the cluster centers' locations and cluster group organization become stable. To determine the ideal number of cluster groups, the R-squared technique (Liu et al., 2010) was used as an internal validation procedure.

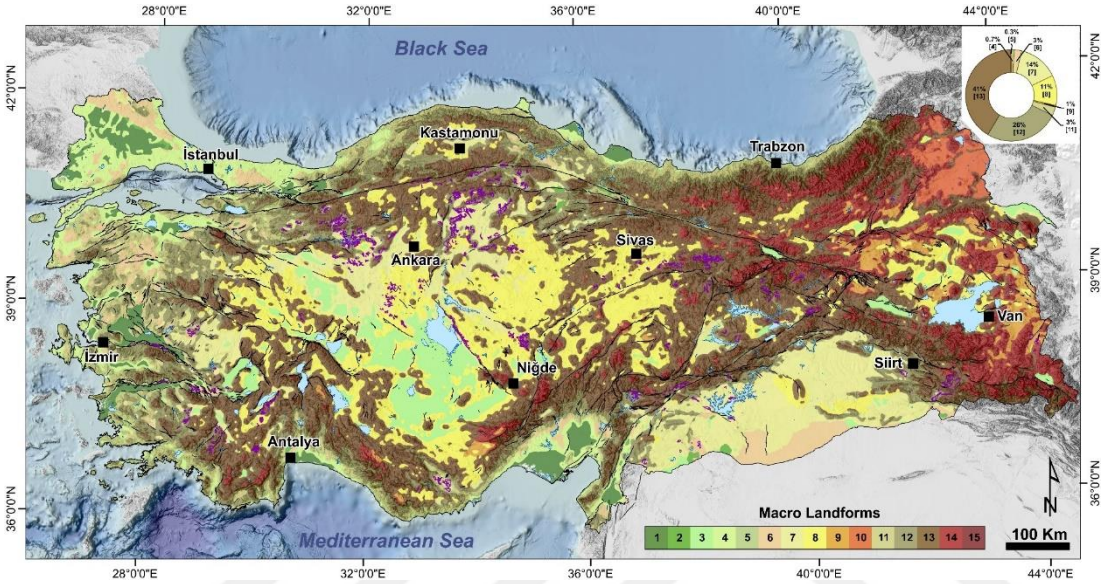

Figure 4. 4: Badlands distribution on macro landforms of Turkey (Görüm,2019): plains (1), mid-altitude plains (2), lowlands (4), rugged lowlands (5), platforms (6), low- (7), and mid-altitude plateaus (8), high (9) and very-high plateaus (10), hills (11), low- (12) and mid-altitude mountains (13), and high (14) and very-high mountains (15). Black lines show the main fault lines of Turkey (Emre et al., 2013), and purple polygons represent the spatial distribution of badlands. The inset shows the macro landforms proportions in determined badlands areas.

In practice, the cluster analysis was performed with geo-environmental parameters ranging from 2-cluster to 7-cluster complexity. Next, the number of cluster groups was determined by taking into account the R-squared technique and the fieldwork-based experiences. The histograms were created displaying the 5^{th}, 95^{th} percentile, and mean values of the geo-environmental factors to better characterize the geographical characteristics of badlands determined by the ideal number of cluster groups.

In addition, in order to investigate spatial changes in the primary analyzed geo-environmental variables and the interactions of these controlling factors with the spatial distribution of badland in the region, the applied swath profiles (comprising mean, maximum, minimum, and standard deviations values of the geo-environmental variables) were utilized to cover the entire extension of Turkey. Two combined swath

profiles were created for precipitation, elevation, aridity, topographic relief, and temperature seasonality across Turkey in the directions of W-E (250 km width 1600 km length) and N-S (250 km width 600 km length).

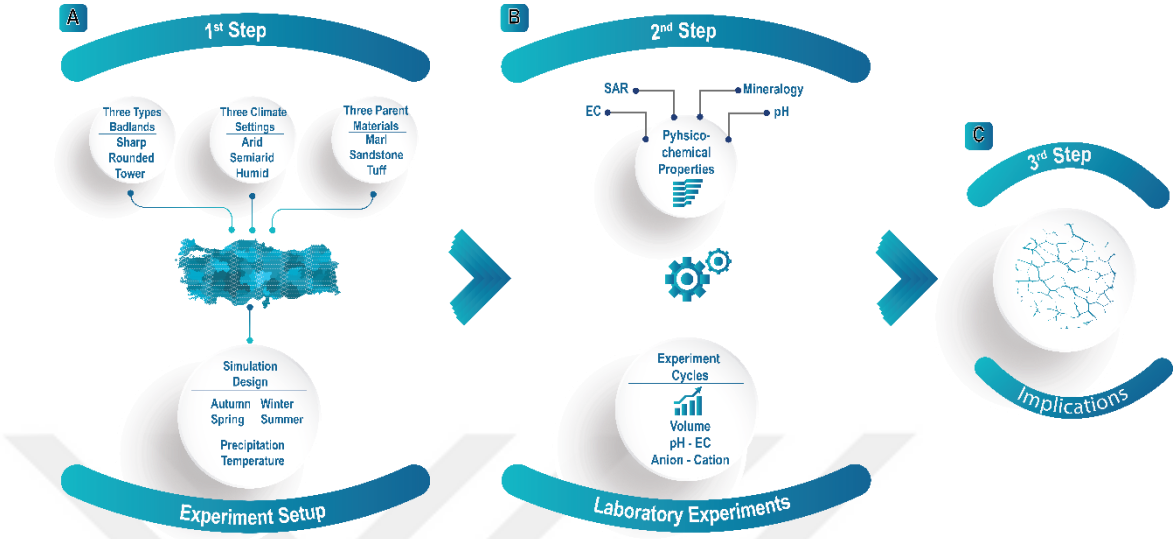

Figure 4. 5: Sequential steps of study, a) experimental setup: sample collection composed of four main lithologies, badland forms, and climate settings, simulation design compiling meteorological data, b) laboratory weathering experiments; analyzing main physicochemical properties of samples and collection of geochemical proxies from treatment of samples with different precipitation and temperature, c) interpretations on weathering processes.

4.2 Weathering Experiments Under Controlled Laboratory Condition

The methodology in this part is divided into three phases (Figure 4.5): Sediment samples from Turkish badland landscapes were collected, and meteorological data was gathered to set up simulations of precipitation and temperature (Figure 4.5a); leachate properties, such as volume, pH, EC, and ions, were measured through a series of experiments with varying precipitation and temperature conditions (Figure 4.5b); and the effects of weathering as a response were also examined (Figure 4.5c).

4.2.1 Sediment sampling

Using a chisel and a hammer, we extracted 11 sediment samples from the unweathered badland parental materials that were about 20 cm below the surface. A total of 3, 4, and 2 samples of the Mediterranean, arid, Cappadocian, and humid (i.e., mountainous humid climate) badlands, respectively, were collected from the four separate study sites, taking into account the significant climatic, lithologic, and badland morphological differences. Even while it is ideal for badland samples to remain intact

during sampling, this is not always achievable because badland sediments frequently have fractures and break up into shards, but they nevertheless serve as a good representation of the unweathered sediment (Kasanin-Grubin, 2013). Two groups of subsamples (each approx. 1 kg) have been determined in the laboratory to achieve two distinct goals: (1) to examine the geochemical properties of parent material of badlands, and (2) to conduct weathering experiments under simulated natural climate conditions.

4.2.2 Setup of climate simulation environments for weathering experiments

In an effort to simulate the field conditions of the study sites as nearly as possible in the laboratory, the 12 simulated climate cycles or seasons that constitute 3-year trials were built up. The badland samples, which were made up of shards with an average size of 1x1.5x1 cm, were put in aluminum sample trays with porous bases (radius=9 cm, depth=4 cm) to enable the collection of leachates and subsequent analyses. Every cycle involved treating samples with precipitation, either in the form of rain or snow, followed by a drying period. Using long-term (1975–2005) climate data for the study locations provided by the Turkish State Meteorological Service (MGM), we calculated the total amount and type of precipitation every season (Table 4.2). According to their seasonal precipitation characteristics, the sample sets were thus exposed to various amounts of rainfall. Depending on the amount of precipitation, a 1.45 mm sec^{-1} rate of precipitation was applied for 16 to 185 seconds (Table 4.2). We used crushed ice consisting of frozen distilled water to mimic snowfall throughout the winter cycles for badland samples from the Cappadocia and humid areas. After the cycles' precipitation phase, the samples were subjected for 24 hours to various conditions—depending on the season and a typical climate region—during the simulations' drying phase. We specifically reproduced room (R), refrigerator (FR), freezer (FZ), and lamb (L) conditions to imitate spring/autumn (15°C), mild winter (4-5°C), winter (-2°C), and summer (25-35°C) average temperatures, respectively.

Table 4. 2: The wetting (precipitation) and drying (temperature) simulation conditions. The values separated by a forward slash (/) indicate precipitation amount (mm.), average temperature (°C), and drying environment, respectively. Drying environments consist of distinct compartments, namely R (room temperature), F (fridge), FZ (freezer), and L (lamp). The arrangement of these compartments signifies various drying conditions within the same season. For instance, RF represents a combination of room temperature and fridge drying. MAP is the mean annual precipitation (mm.) *Refers to snowfall

	Autumn	Winter	Spring	Summer	MAP
Arid	63.6/13.4/R	107.5/2.3/F	89.8/11.3/L	37.1/22.1/L	298
Mediterranean	114.8/16.8/R	211.7/7/F	138.6/15.2/L	26.7/26.4/L	491.8
Humid	185.2/14.3/FR	*331.7/-0.2/FZ	273.2/11.4/FR	24.8/25.6/L	814.9
Cappadocia	79.7/10.4/FR	*108.3/0.03/FZF	149.6/9.4/FR	46.9/20.1/L	384.5

4.2.3 Geochemical analyses

The measurement of leachate volume, pH, and EC after each precipitation period were taken at room temperature without previous mixing, by using a measuring cylinder, pH meter AD 1000 pH/mV & Temperature Meter (Adwa), and Iskra 65967.00 conductometer. The analyses on anion quantification (CO_3^{2-}, CI^-, SO_4^{2-}, NO_3) were carried out with Dionex ICS 3000 (Single Pump (SP), Conductivity Detector (CDS), Eluent Generator (EG), Chromeleon® Chromatography Workstation with Chromeleon 6,7 Chromatography Management Software; Column: IonPac AS15 Analytical, 4x250 mm (P/N 053940), IonPac AG15 Guard, 4x50 mm (P/N 053942), Eluent: 42 mM potassium hydroxide (KOH) (P/N 058900), Flow rate: 1.0 mL/min, Continuously Regenerating Anion Trap Column (CR-ATC) (P/N 060477), Temperature: 30 ˚C, Injection volume: 10 µL, Detection: Suppressed conductivity, ASRS ULTRA II (4 mm) (P/N 061561), recycle mode). The inductively coupled plasma—optical emission spectrometry (ICP-OES) (Thermo Scientific iCAP 6000 ICP-spectrometer, SAD) with autosampler CETAC ASKS-spectrometer, SAD was used in cation quantification (K^+, Mg^{2+}, Na^+, Ca^{2+}) analyses.

The mineralogy of samples was determined by X-ray powder diffraction performed on Philips 1710 PW diffractometer with CuKα 1,2 (1,54178 A°) radiation. X-ray diffraction was recorded over a 2 - 70 ° interval with 0.02 ° step size and a fixed counting time of 1s per step. The samples were prepared for analyses by drying at 105 °C until the constant mass, mixing with wax (sediment: wax = 80:20; Hoechst wax C

micro powder produced by Merck), and pressing into tablets using 25t pressure for 5 min., respectively.

The parameter sodium absorption ratio (SAR) is frequently utilized when an indicator of the sodicity of the material solution is needed. Cations are extracted in water for this index, and the results are calculated according to equation (4.2):

$$SAR = [Na^{+}] / ([Ca^{2+} + Mg^{2+}] /2)^{0.5} \quad (4.2)$$

4.3 Geomorphometric analyses

The topographical position of Turkish Badlands and its comparison with other badland landscapes from different countries have been determined as a quantitative land-surface analysis. The slope-area relation (Willgoose et al., 1991) which is a relationship between drainage area (A in m^2) and slope (S in m/m) has been used in order to determine the topographical position of badland landscapes. According to power law equation (4.3):

$$S = k. A^{\theta} \quad (4.3)$$

In a logarithmic plot ($\log(S) = \log(k) + \theta\log(A)$), where k represents a constant and θ denotes a scaling exponent, representing the gradient or steepness of the slope-area relationship. Empirically, θ exhibits positive values in rounded convex ridges, where dominant diffusive sediment transport processes such as soil creep, rain splash, and bioturbation occur. Conversely, θ exhibits negative values in concave valleys and channels, where fluvial (advective) sediment transport processes erode the landscape. (Tarboton et al., 1992; Istanbulluoglu et al., 2008). This relation has been employed at the watershed scale to elucidate the topographic location of badland landforms within the watershed. Digital terrain models (DTM) and badland areas are needed in order to obtain slope-area diagrams for all areas. For these purposes, freely available and nationwide (i.e., Turkey and Taiwan) DTMs were compiled and badlands boundaries have been delineated according to section 4.1.1.

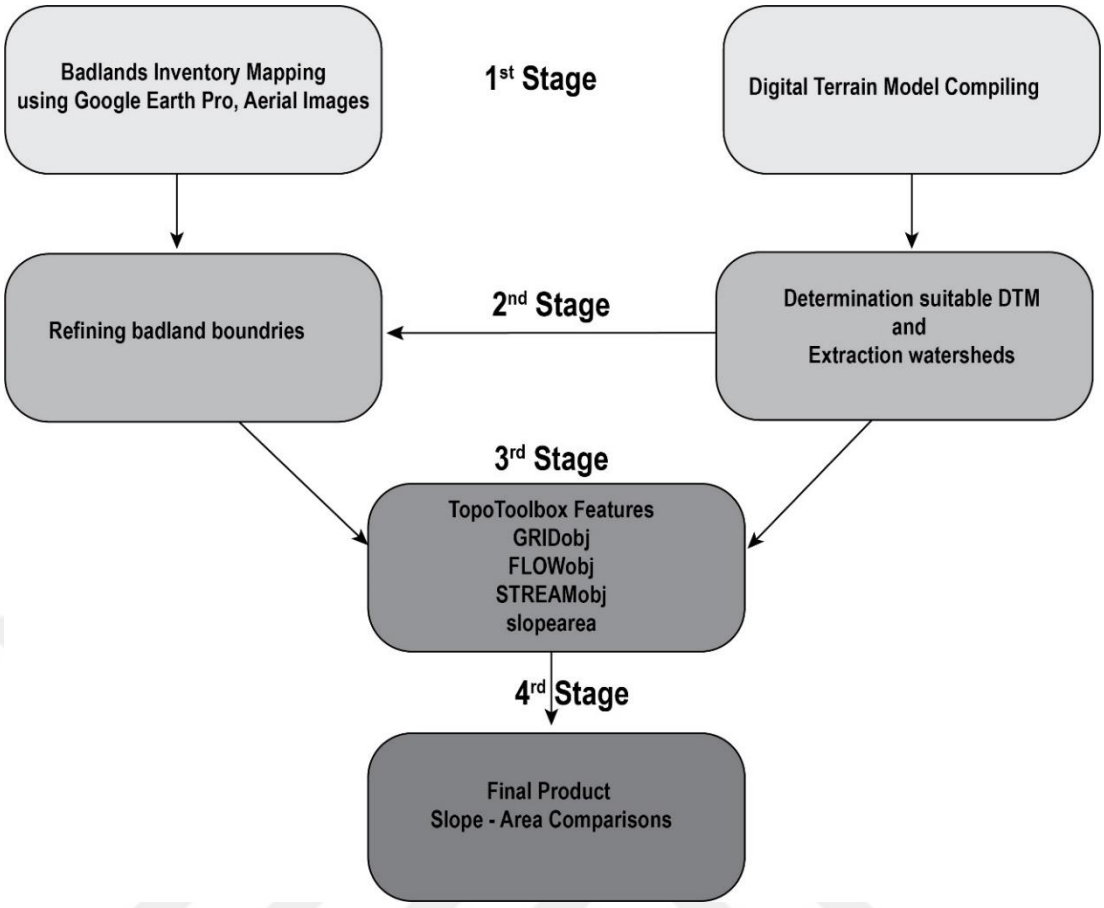

Figure 4. 6: The steps for determining optimum resolution for DTMs and obtaining slope-area plots.

The optimum resolution of DTM has been determined with the swath profiles in Caineville, USA by using 1m to 30m resolution DTM. TopoToolbox 2-MATLAB-based software (Schwanghart & Scherler, 2014) has been used in the pre-processes – extraction of flow direction, contribution area, and slope gradient - of DTMs for geomorphometric analyses. The preparation includes "GRIDobj, FLOWobj, and STREAMobj" of TopoToolbox. As a final product "slopearea" tool has been used in TopoToolbox (Figure 4.6). The *S* values for each log interval of *A* were averaged to reduce the scattering of the slope-area plots caused by the large number of pixels, and this binning method was used in this inquiry to enable the splitting into different process domains. The slope-area diagrams have been utilized for all badland areas with their corresponding watershed.

5. RESULTS

5.1 Regional Distribution and General Geological Setting of Turkish Badlands

A total of 1366 badland units (average size 12 km^2) through our visual inspection. Their regional distribution extends over 4494 km^2 and illustrates the non-uniform spatial distribution of these highly erosive landforms in Turkey (Figure 3.1B).

Density values of badland areas within the sub-catchments vary between 0.00002 and 1.0 km^{-2}, and this variation is divided into five classes whose boundaries are set where there are relatively large differences in the data values using Jenks Natural Breaks algorithm (Figure 5.1A and 5.1B). Most of the identified and delimited badland areas are concentrated in CAP, where they are associated mainly with Neogene and Paleogene lithologies of terrestrial clastics, especially nearby Ankara (Figure 4.2). Although some hotspots stand out for the obtained badlands distributions, the density ratios of badland/micro-catchment areas did not predominate in frequency intervals. (Figure 5.1B). Neogene and Paleogene units are major sub-lithologies with a preponderance ratio (77 %) (Figure 4.2) within the determined geologic units. The Neogene units comprise 43% of the total mapped badlands and are dominated by terrestrial clastics (73% of the Neogene units; Figure 4.2B). Further, the Paleogene units account for 34 % of all mapped badlands, and they are also dominated by clastics of terrestrial origin (97% of the Paleogene units, Figure 4.2B).

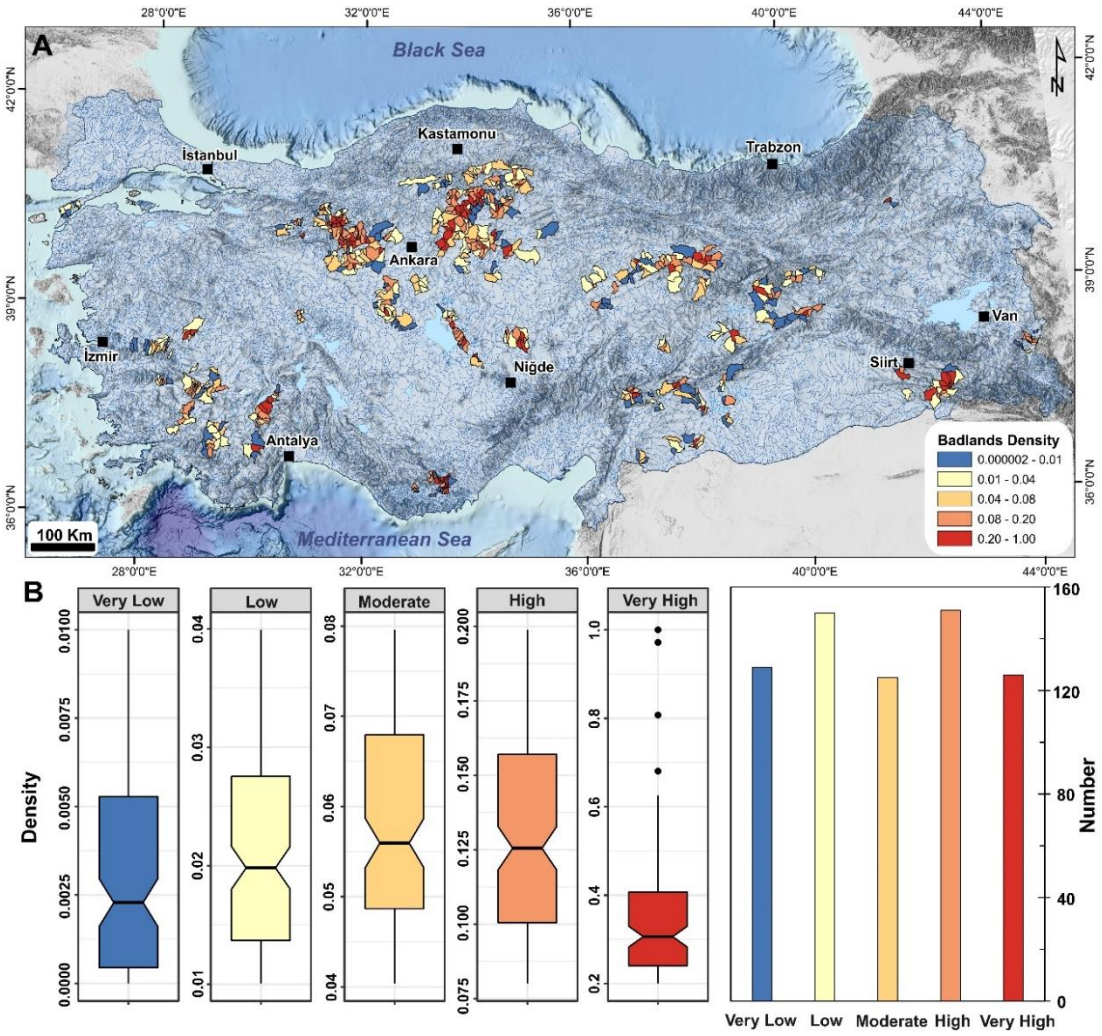

Figure 5. 1: The distribution of badland density. a) The regional badland density map of the study area. Note that badlands densities have been calculated in the sub-basins. b) Box plots show badland densities considering the Jenks optimization method and the histogram that shows the frequency of the density classes of badland units in the study area.

Overall, the obtained pattern of regional distribution of badlands demonstrates a coherence with the Neogene and Paleogene geological units (mostly units 4 and 6), respectively, in CAP and eastern Turkey (Figure 4.2A). The remaining 23% of identified badlands are distributed within Cretaceous, Quaternary, and Jurassic geologic units. Badland areas distributed on the Quaternary deposits are mainly located within the western Anatolia graben system, which lies on tectonically active regions affected by neotectonic movements (Figure 4.2A).

At first glance, the determined badlands distribution suggests that the locations of the badlands are parallel to a general gradient of increasing elevation from W to E, which is also linked to a broad gradient of variations of macro-landforms, from mid-altitude plains in the west to high and very-high mountains in the east (Figure 4.4). An

extensive aggregation of badlands landscapes was observed (67%) in low- and mid-altitude mountains from these spatial gradients of macro-landforms and badlands distribution. By considering the concentration of these badland areas on relatively high topography (>1100 m.a.s.l.), the field visits for validation showed that these mountain badlands are distributed within the mountain hillslopes and side-slope pediments that have been formed by the action of long-term erosion from this high topography. Differently, the low- and mid-altitude plateaus that concentrate nearly 25% of the badland distribution in the CAP region are characterized by paleo-pediment areas on the Neogene deposits (Figure 4.4). Badland areas developed in the southern and northern margins of the CAP are affected by the control of the active tectonic regime and river incision-induced rugged topography. An evident consistency has been found between the distribution of active faults and the presence of badlands for certain areas of the region, for example, south of Kastamonu along with the North Anatolian Fault (NAF), in the extensional regime-dominated areas (e.g., western Anatolia) nearby the Izmir, and fault lines north-west of Niğde (Figure 4.4).

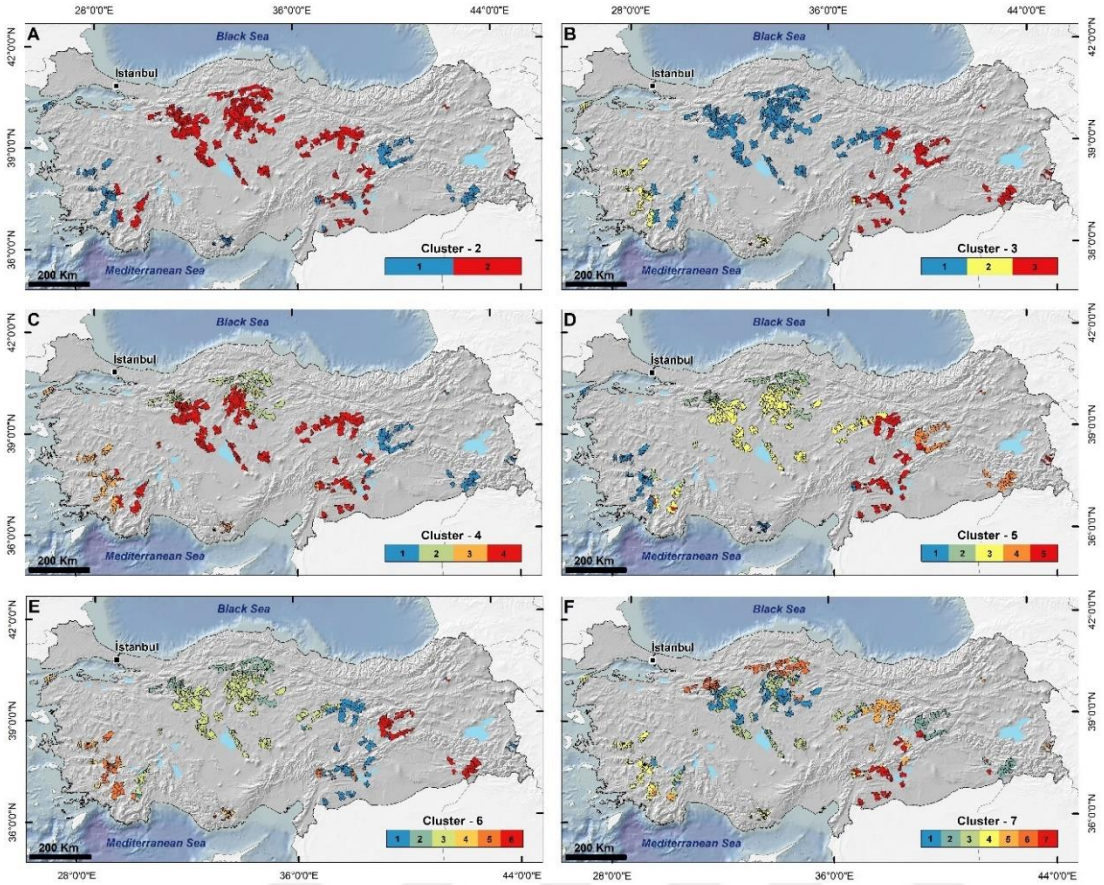

Figure 5. 2: The possible solutions of the K-means clustering analysis in order to find an optimum number of badland regions. a) Cluster-2, b) Cluster-3, c) Cluster-4, d) Cluster-5, e) Cluster-6, f) Cluster-7.

5.2 Cluster Analysis

As a result of the cluster analysis, the different cluster groups of badlands have been generated, ranging from 2 to 7 (Figure 5.2A-F). Cluster-2 representation (Figure 5.2A) shows the most generalized regions, while Cluster-7 (Figure 5.2F) shows a very intricate organization of badland groups. Further internal validation of the cluster analysis indicated that the differences between badland groups decrease abruptly as the number of clusters increases after setting the five groups of Cluster-5 representation (Figure 5.3).

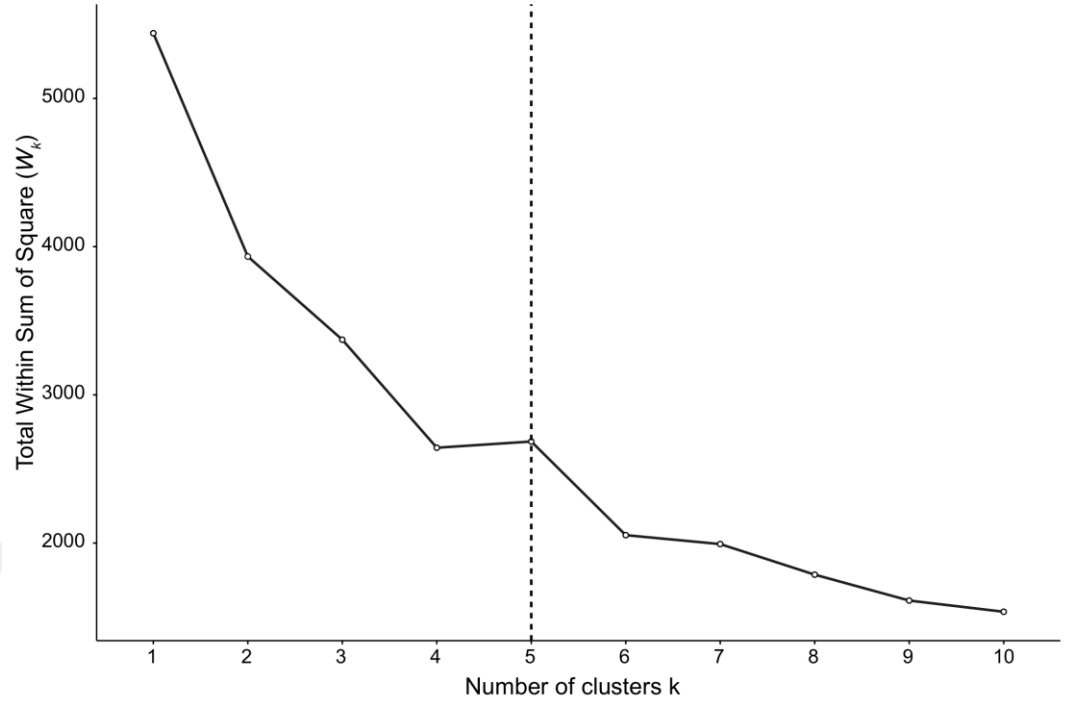

Figure 5. 3: The Elbow Graph which is an internal validation algorithm used in determination of optimum number k-clusters.

Standing on these results, badland mapping, and visual inspections throughout the extensive field validation visits, Cluster-5 represents and differentiates optimally the main physical regions of the territory, by clearly discriminating, for example, the south (Mediterranean climate and mountainous dominated landscapes) and north (NAF-dominated, rugged topography) margins of the Central Anatolian Plateau (CAP), and the pure CAP landscapes (Regions 1, 2 and 3, respectively; Figure 5.2D).

The general characteristics of Cluster-5 (Table 5.1) are particularly influenced by the dominant semi-arid climate of the territory (0.48 mean value for the aridity index), unlike the presence of a high gradient between the minimum (0.25, arid to semi-arid transition) and maximum (0.85, semi-humid) aridity index values of the badlands in the region. Looking at the other climatic geo-environmental factors, mean annual precipitation comes into prominence with a relatively high value (529 mm) when it is compared to the semi-arid conditions.

Table 5. 1: The descriptive statistics of geo-environmental parameters that used in cluster analysis.

Variable	Mean	Std.Dev.	Min	Max	R^2
Temperature Seasonality	810.9922	80.1868	679.72	1015.9	0.8348
Mean Annual Precipitation	529.4075	122.0146	342.412	962.848	0.8344
Precipitation Seasonality	52.6168	16.313	26.0548	90.21	0.7601
R Factor	351.8017	179.8442	115.696	1107.46	0.6744
Aritidy	0.486	0.1096	0.2502	0.8294	0.6527
Lithology	4.9413	1.7559	1	11	0.3631
NDVI	0.5834	0.0979	0.2408	0.8782	0.3229
Elevation	1015.3805	408.7912	78.4872	2910.53	0.3134

The largest precipitation seasonality values of the region (>80 %; Figure 4.3C) are reached in western Turkey, while the overall mean value is sensibly lower (54 mm; Table 5.1). Temperature seasonality shows an undeviating distribution and having the ~ 810 mean value across Turkey extremely variates (>1000), especially in continental eastern Turkey. The USLE R factor shows a significant shift from inland to the shoreline (Figure 4.3E). The elevation values from west to east have a clear increasing tendency (Figure 4.3F). The mean elevation in the micro-catchments hosting the obtained badland distribution is 1015 m. (Table 5.1). The overall mean NDVI value of the studied badland landscapes and sub-catchments is 0.58, corresponding to sparse to moderate vegetation. The descriptive statistics for Cluster-5 (R^2 in Table 5.1) indicate how much the analyzed variables contribute to the optimal sectorization of badland groups. Temperature seasonality and MAP showed the largest R^2 values (0.83), followed by precipitation seasonality, R factor, and aridity (R^2 = 0.6–0.7), all of them contributing largely to discriminating the badland regions of Cluster-5.

Table 5. 2: The characteristics of unweathered samples showing the main geochemical and mineralogical properties before the treatments. Note: EC, electrical conductivity (µS/cm); organic matter (%); SAR, sodium absorption ratio.

Samples	pH	EC (µS/cm)	SAR	Quartz	Smectite	Illite	Kaolinite	Chlorite	Analcime	Calcite	Albite	Other minerals
A1	10.13	702	6.30	0.93	53.25	24.00	0.00	0.00	18.50	2.36	0.89	0.00
A2	9.95	780	31.38	0.91	48.59	23.90	0.00	0.00	21.00	4.27	0.66	0.70
A3	10.42	404	11.18	0.36	72.10	2.40	0.00	0.00	8.50	8.50	0.00	8.14
A4	10.43	506	11.18	0.45	49.93	20.40	0.00	0.00	20.00	4.03	0.00	5.28
M1	8.18	69.8	3.58	32.60	29.30	13.10	2.30	0.00	0.00	0.00	11.80	10.70
M2	10.04	70.9	0.69	27.90	30.31	16.00	5.10	0.00	0.00	0.00	9.80	10.74
M3	8.68	63.4	2.61	22.90	43.60	12.90	6.50	0.00	0.00	0.00	4.80	9.41
H1	9.81	35.7	0.12	13.90	40.60	4.60	1.73	6.40	1.23	18.60	10.80	2.13
H2	9.41	48.7	0.11	12.30	47.32	0.01	0.79	6.30	1.54	16.40	12.80	2.50
C1	8.76	24.3	0.21	19.20	37.24	2.50	0.00	0.00	0.00	0.00	40.50	0.62
C2	9.65	13	0.12	11.70	56.98	2.19	1.18	0.00	0.00	0.00	26.80	0.93

badland regions of Cluster-5. Lithology, NDVI, and elevation contributed marginally to the obtained regional sectorization of badland landscapes (Table 5.1).

5.3 Geochemical and Mineralogical Characteristics of Unweathered Samples

As shown in Table 5.2, the samples exhibit variations in the regional context across all geochemical parameters. The samples in arid region show higher values in average for pH, EC, and SAR. While other geochemical properties show more pronounced variations among regions, the pH values are consistently classified as very strongly alkaline, with average values of 10.23, 9.61, 9.55, and 9.20 in the arid, humid, Mediterranean, and Cappadocia badlands, respectively.

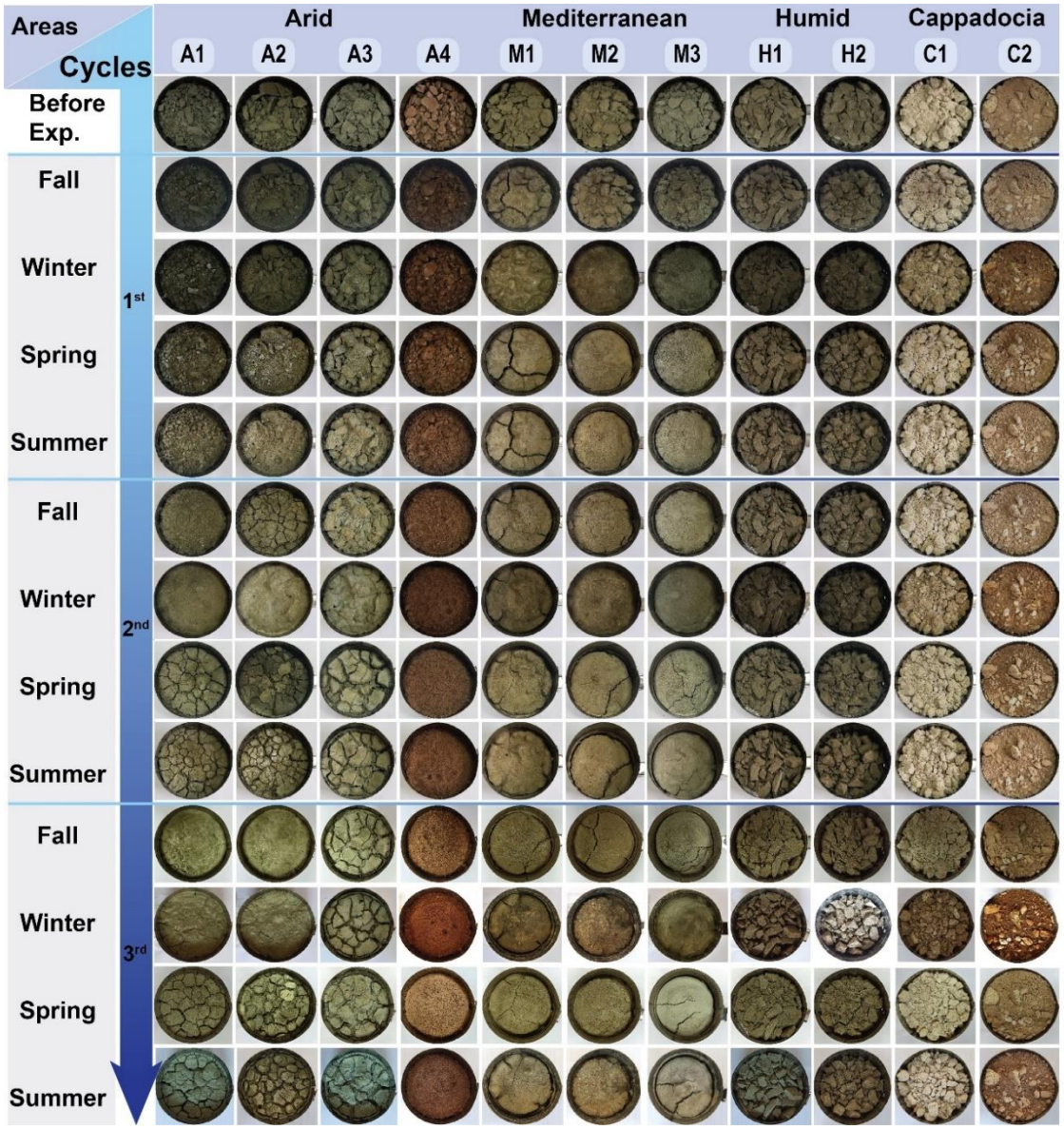

Figure 5. 4: Sequential evolutions of unconsolidated materials recorded by consecutive photos. (*Colour gradients within the same samples throughout cycles does not indicate physicochemical changes, it is because of the dynamic light footage conditions in the laboratory environment.).

The EC values observed in the arid region demonstrate a range between 404 and 780, representing an average increase of 131%, 1317%, and 3106.43% when compared to the Mediterranean, humid, and Cappadocia badlands, respectively. The samples in the arid region exhibit higher levels of dispersity, as indicated by the SAR value of 15.11, when compared to other regions. Regarding the

The samples in arid region display higher average proportions of smectite (55.97%) and illite (17.68%) as clay minerals. Additionally, analcime is notably present,

accounting for 17% of the composition on average. The samples in Mediterranean region exhibits a relatively more uniform distribution of mineral compositions, with smectite 34.40%, quartz %27.8, illite 14%, albite 8.8%, kaolinite 4.63%, and the remaining 10.28% attributed to other minerals. While the smectite (44%) and calcite (17.5%) constitute the majority of the composition of samples in humid badlands, Cappadocia badlands primarily consist of smectite (47.11%) and albeit (33.65%).

5.4 Surficial Responses to Experiments

We have tracked the periodic evolution of the crust, desiccation crack, dispersion, and popcorn formation through serial photographs taken immediately after the drying phase of the samples (Fig. 5.4). While surface alterations in arid and Mediterranean samples throughout cycles were observed, humid and Cappadocia samples maintained their internal stabilities, apart from the minor developed joints in the shard structure of humid samples. Thus, the subsequent results will demonstrate the outcomes from arid and Mediterranean samples.

Although samples were subjected to same experimental conditions in order to simulate behavior precipitation and temperature conditions, within their respective localities, their resulting morphological features were different from each other. The Mediterranean samples have shattered into fine particles after the first cycle. However, arid samples, particularly A3 and A4, maintained their shard structure till the 5^{th} cycle (Figure 5.4). Despite the fact that the Mediterranean region received nearly an order of magnitude higher precipitation (Table 4.2) than the arid region, the samples did not disperse owing to their subtle geochemical differences (i.e., major minerals, pH, EC, SAR, and organic matter content). Instead, after rapid fragmentation in Mediterranean badland samples, often deep cracks (a few mm width), have formed which are highly associated with spring and summer cycles. The surficial responses are periodically shown by arid samples to seasonal contrasts in climate. After completing one hydrological year, represented in 4 successive seasonal cycles, the samples in the arid region exhibited increased instability and dispersion due to their critical susceptibility to swelling and dispersion. This resulted in desiccation cracks and crust formation, except for sample A4, which remained unresponsive after breaking down into fine particles. While the formation of desiccation cracks and crusts in A1 and A2 follows a seasonal pattern, particularly with the spring and summer periods, A3 preserved its

crustal structure from the seventh cycle through to the end of the subsequent cycles. The development of a subtle "popcorn" surface, which denotes the swelling behavior of sediments with high clay content, arose exclusively in the A2 during the latest spring and summer cycles.

5.5 Fluctuations in Leachate Characteristics During The Experiments

5.5.1 Leachate production and ponds formation

The quantity of leachates is strongly influenced by the precipitation amount and drying conditions of both the present and prior seasons coupled with the characteristics of the underlying parent rock. Regardless of the climate type simulated, most samples did not produce enough leachate in the summer seasons of 4^{th}, 8^{th} and 12^{th} cycles, because of rainfall scarcity (Figure 5.5A). Leachate volume showed a marked descending order: Humid>Mediterranean>Arid>Cappadocia (Figure 5.5A). In fact, a 2-order magnitude higher volume of leachates were collected throughout experiments in the humid samples compared to other regions due to the higher mean annual precipitation and relatively more consolidated shards and cracks, allowing higher permeability. The volume of leachates in humid samples also showed a constant periodic variation over the years even if the amount of snowfall in winter is higher than the spring rainfall. The samples in Cappadocia were subjected to slightly higher MAP than the arid samples (384 and 294 mm/year respectively), however, a larger volume of leachates was collected from the arid samples, particularly during fall (1^{st} and 5^{th}) and winter (2^{nd}, 6^{th}, and 10^{th}) of the cycles. Arid samples subjected to the lowest MAP showed a marked decrease during summer. Despite the fact that all samples produced leachate during the initial cycle, only the A3 and A4 samples yielded leachate during the fifth cycle, and sample A3 yielded leachate in the ninth cycle. Leachate were collected in 1^{st} and 2^{nd} for the Mediterranean samples, with the exception of M3. The peaks of leachate amounts were recorded in winter, which commonly coincided with a maximum amount of precipitation.

Temporary pond formation on the surface of samples, which is strongly associated with clogging the pores with fine-grained particles, was observed in arid and Mediterranean samples. While relatively long-lived (>30 min.) ponds were seen in samples A2 (also in 6^{th} cycle) and A4 in the 7^{th} cycle, sample A1 only showed relatively short-lived (30 min.) ponds during 6^{th}, 7^{th}, and 8^{th} cycles. Contrary to arid

samples, ponds were formed in 1st and 2nd year cycles varying from long to short-lived in different Mediterranean samples.

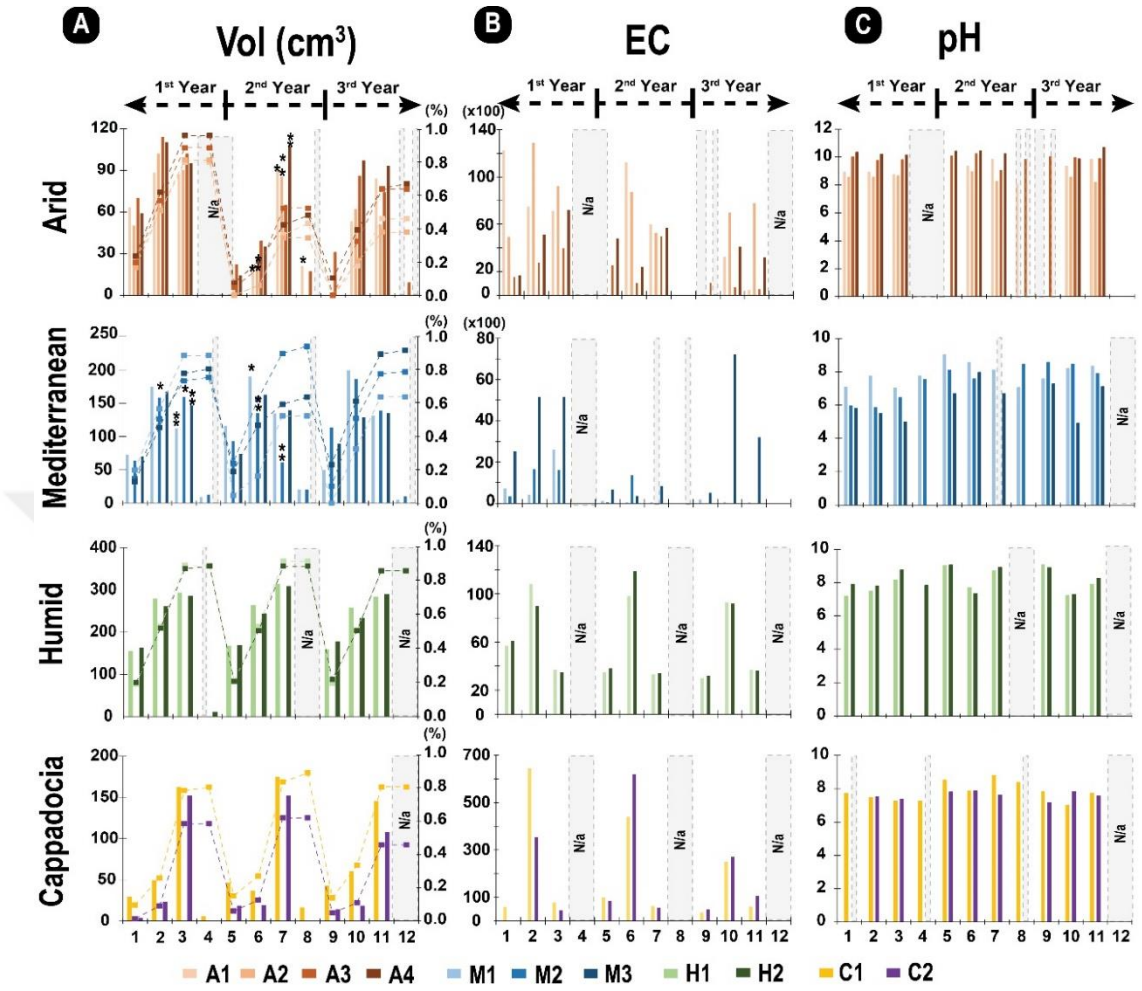

Figure 5. 5: Temporal changes of leachate volume (Vol, cm^3), EC, and pH. Asterisks indicate the pond formations and their durations (*Short lived <30min., **Long-lived >30min.). Dashed lines on the volume graphs show the relative fractions (%) of cumulative leachate to mean annual precipitation in a one year. Grey shaded columns represent cycles with no leachate obtained.

5.5.2 Electrical Conductivity

Notable and largest oscillations have been recorded in electrical conductivity amongst samples (Figure 5.5B). Certain variations were obtained in leachates of arid samples, even if they are fairly similar to each other in terms of their mineralogical compositions. In the leachates of arid samples, the highest value observed (12890 µS/cm) indicated an incremental EC trend during the first-year cycles. Leachates of samples A3 and A4, for example, exhibited an initial increase of 155% and 367% in EC along the first cycle, respectively, followed by irregular variations until the end of

the last-year cycle. Leachates of Mediterranean samples exhibited a comparable pattern of incremental trend for the initial year cycles (258%, 370%, and 105% EC increase for M1, M2, and M3, respectively). Subsequently, the EC values in the Mediterranean samples decreased by an average 48%, leading to inconsistent fluctuations in the third-year cycles. The leachates of Humid and Cappadocia samples showed the most regular temporal seasonal fluctuations. EC remained relatively constant during the fall and spring phases, while marked, abrupt increases were recorded during the winter phases of the cycles. (Figure 5.5B).

5.5.3 pH

The temporal distribution of pH shows constant periodic trends compared to the strong seasonal variations of leachate volume and EC (Figure 5.5C). The pH ranges from acidic (4.9) for some of the leachate obtained from the Mediterranean samples to strongly alkaline (up to 10.5) for arid sample leachates. Additionally, considerable changes have been observed in the Mediterranean samples. During the first year, the pH value of the leachates in Mediterranean samples was moderately acidic, with an average of 6.4. However, in the subsequent two-year cycles, the samples gradually shifted towards being slightly alkaline, with pH values of 7.8 and 7.6 in the second and third years, respectively. In comparison to the leachates from the Mediterranean region, the samples from the arid, humid, and Cappadocia regions displayed relatively minimal variations in pH values during the course of the experiments.

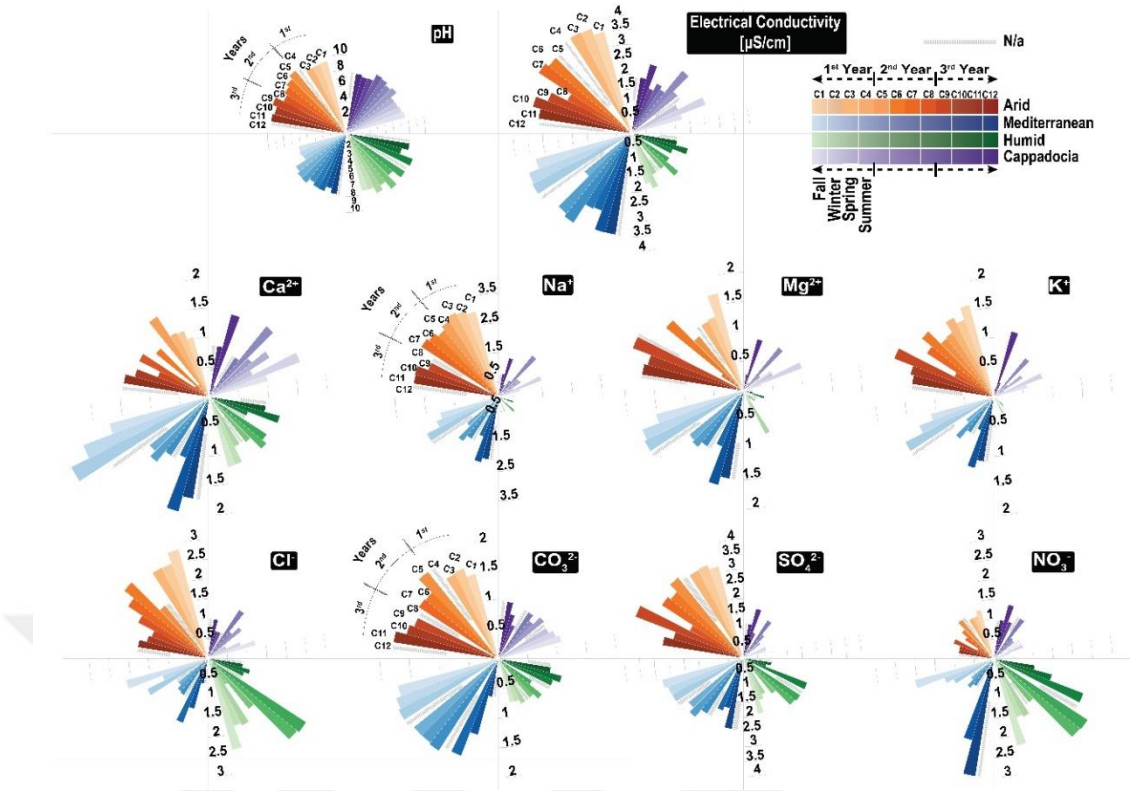

Figure 5. 6: Circular bar plots of region-based results of selected ions, volume, EC, and pH in which samples are represented by their average values with their region. The log10 transformation were utilized for ion concentrations (mmol/kg) and EC (µS/cm).

5.5.4 Ion concentrations

Since the samples from the similar region shared similar geochemical characteristics, such as concentrations of pH, EC, mineralogy, and SAR the conspicuous observations led us to conduct additional analysis in a regional context in order to better understand how seasonal variations influence the geochemical indicators that were thought to be potential proxies for selective weathering processes. The concentrations both in cations and anions substantially vary in all regions, but certain ions (i.e., Na^+, Ca^{2+}, Mg^{2+}, CO_3^{2-}) favorably shows periodic patterns in the leachates of particular samples (Figure 5.6). The seasonal trends (i.e., repeated pattern for same seasons in different years), particularly for K^+, $Mg^{2+,}$ Ca^{2+}, and Na^+ were observed in the leachate of Mediterranean samples after gradual increase of first year. In this context, the winter seasons experienced a notable increase in the second and third years, leading to a pronounced drop in subsequent seasons (i.e., spring) and preceding seasons (i.e., fall) in these leachates.

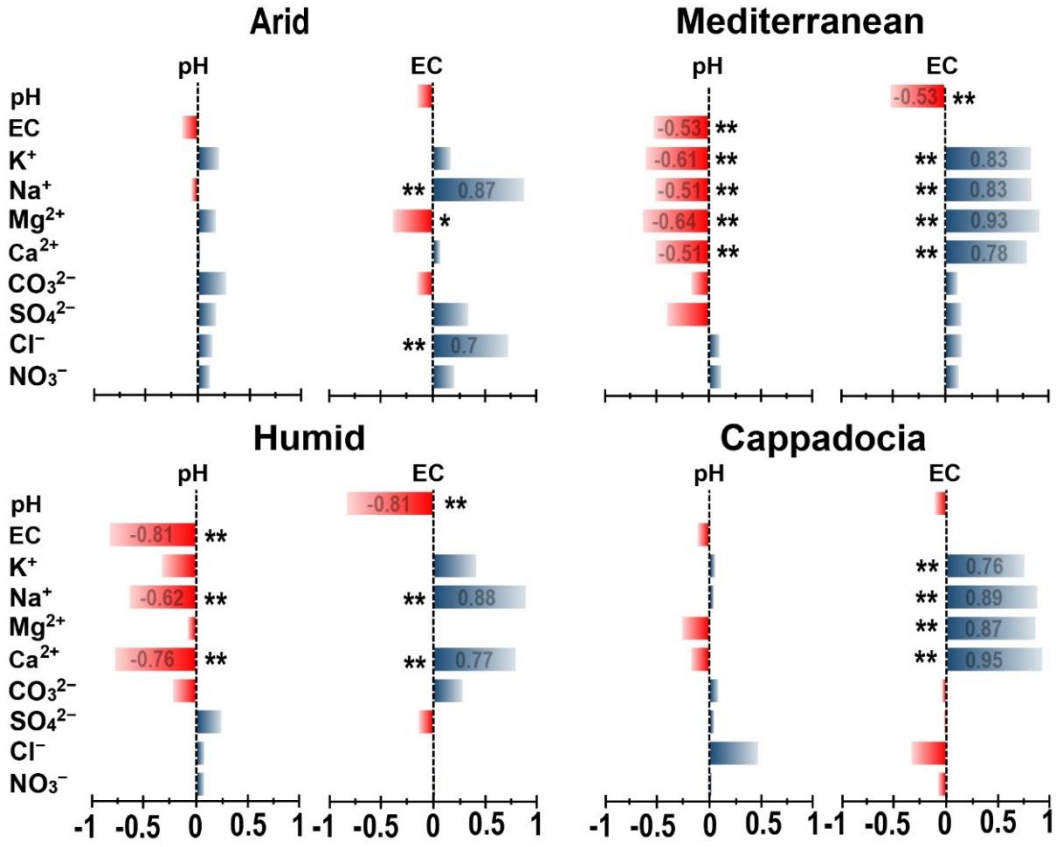

Figure 5. 7: Multilevel correlations coefficients between pH – EC and ions. (the level of significance; * $p < 0.05$ and ** $p < 0.001$).

However, after an ever-increasing level of all cations in Mediterranean leachates, a subsequent decline of 45% and 64% during the second and third annual cycles were observed in the same region, respectively. The Na^+, in particular, demonstrates a sequential annual pattern characterized by an initial gradual increase from fall to spring, followed by a substantial decrease during summer in the leachates of arid samples. The leachates of Humid and Cappadocia samples exhibited higher inconstant ion releases during the cycles in comparison to EC values. Nevertheless, some degree of recurrent cyclic patterns in K^+, Mg^{2+}, and Ca^{2+} in cation releases, portraying fluctuations between upward and downward trends, were also observed in leachate of humid samples. The irregular releases have been observed in the most of the anions (Cl^-, SO_4^{2-}, and NO_3^-) in all regions, while NO_3^- showed a notable increment of %6258 after marked decline from 1st to 8th cycle in the leachates of Mediterranean samples.

The multilevel correlation coefficients indicated that pH and EC as crucial controlling indicators of the weathering rates have a significant ($p < 0.05$) relationship with the cations in the leachate of Mediterranean samples through simulated climate cycles

(Figure 5.7). While pH showed negative correlation with cations, EC illustrates positive correlation in this region. On the other hand, majority of the anions have statistically insignificant relation with EC and pH in all region. The leachates in arid samples shows only positive significant correlation between Na^+ and Cl^- ions and EC (r^2 = 0.87 and 0.7, respectively) while Na^+ and Cl^- in leachate of humid samples are significantly correlated with both pH (negatively) and EC (positively). The cations also are significantly correlated with EC in the leachates of Cappadocia samples (r^2 = 0.86 in average).

5.6 Geomorphometric Properties

The swath profiles show noticeable variations in different resolution of DTM for the minimum, maximum, and mean elevation values taken from Caineville (Utah), USA (Figure 5.8).

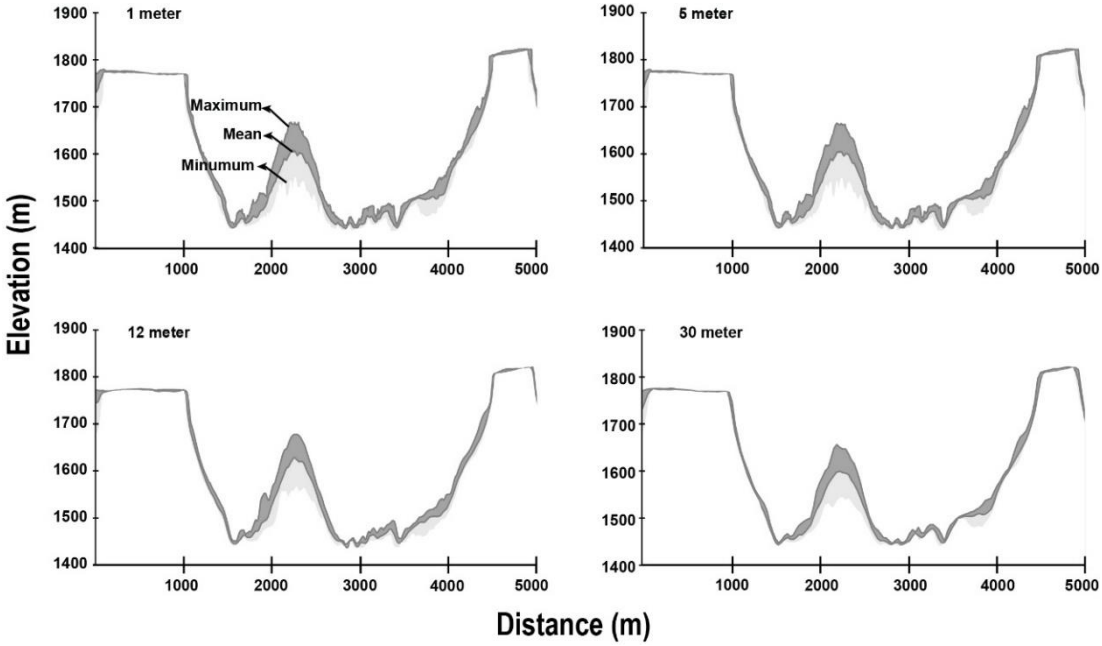

Figure 5. 8: The swath profiles taken from the Caineville badlands areas show minimum, mean, maximum elevation values in order to determine optimum resolution of DTM for geomorphometric analyses.

When comparing DTMs with resolutions of 1, 5, 12, and 30m to determine the appropriate resolution, it was observed that the 1m and 5m DTMs effectively captured the recurring channels and divides. However, DTMs with coarser resolutions beyond 5m exhibited a more generalized representation in the swath profile, indicating a loss of information pertaining to the channels and divides (Figure 5.8). Therefore, in order

to obtain same resolution for DTMs in every study sites, the 5m resolution has been considered as a suitable DTM for further determination of topographic positions of badlands.

The figure 5.9 shows the comparison of slope-area relation both in badland areas and their corresponding catchment and different study sites. Even though contributions areas of catchments can be up to 10^8 m^2, these values are limited maximum up to 10^5 m^2 (in Tosya, Turkey). While maximum contribution values illustrate higher values, the mean contribution area is 328m^2 in all badland areas. Tosya comes into prominence with highest mean contribution area (627m^2) among the other badland areas.

The binned values primarily portray a convex shape up to 10^3 m^2 in the catchments while this convex shape is not evident in badland areas apart from Taiwan, Burdur, and Tosya. The slope area bins of badlands compared to their corresponding catchments generally show higher *S* values for similar values of contributing area (the high *S* values are generally considered as predisposing factors for accelerated erosion landform initiation and development). Surprisingly, despite the fact that the gradient values in Lombardy's badland areas appear to be higher than their catchment, badland areas (0.57 m m^{-1}) are steeper than catchment (0.17 m m^{-1}) in mean gradient. The badlands areas (0.60 m m^{-1}**)** are 61.20% higher than their corresponding catchments in mean gradient values (Table 6.2). The badlands in Tosya which are located on the North Anatolian Fault in the northern part of Turkey shows the highest mean gradient with 39.7° among the study sites. The noticeable differences in slope orientations of badland areas have been observed among the study sites (Figure 5.9). The southern and northern aspects represent majority of the hillslopes in all badland sites with 49% and 25%, respectively. Although the majority of sites have a dominant aspect to the south, the northern hillslopes appear to have a larger average area in the Saldes (41%), South Dakota (39%), and Burdur (%35) with marginal differences than southern hillslopes (30%, 32%, and 34%, respectively.). Notably, in Basilicata, southern slopes constitute 85% of the badlands' hillslopes which is a highest representation of southern aspect. The least representation of slope orientation in badland areas with eastern (13%) and western (12%) slopes slightly differ from each other.

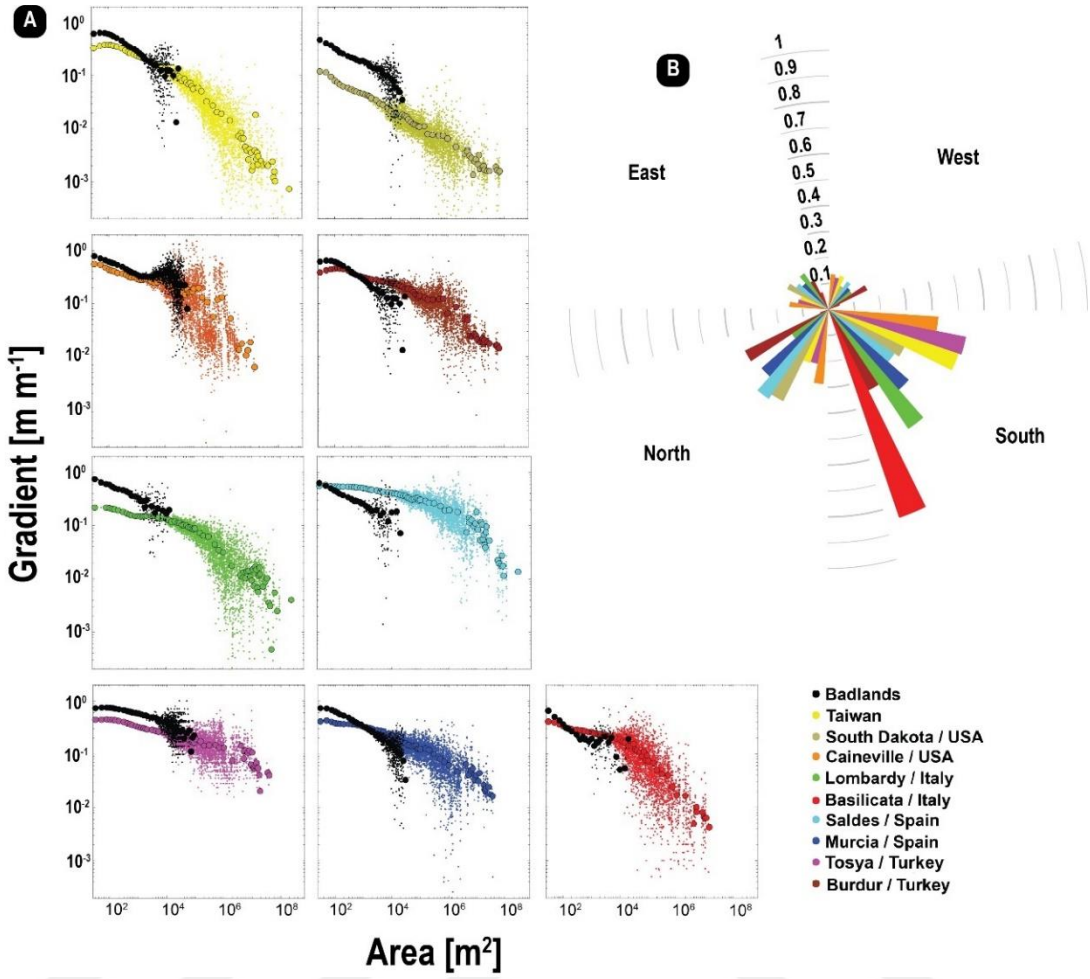

Figure 5. 9: The slope area comparison in different badland sites and their slope orientations.

6. DISCUSSION

6.1 Regional Identification and Assessments of Turkish Badlands

6.1.1 The climatic, tectonic, and geologic controls on the clustering of badlands regions

The results of regional assessment suggest that both the distribution and characteristics of Turkish badlands have been affected by the interactions of geo-environmental factors resulting from the relationship between the regional geologic and climatic settings. Badland distribution in Region 1 (Figures 6.1 and 6.2) spatially coincides with the Mediterranean climate conditions of the western coastline, which is characterized by a distinct precipitation seasonality and high rainfall erosivity, critical influencing factors for the development of badlands (Arnau-Rosalén et al., 2008; Clarke and Rendell, 2006; Higuchi et al., 2013; Vergari, 2015). In this respect, from west to east in the swath profile (Figure 6.2A and 6.2B), the observed high-precipitation

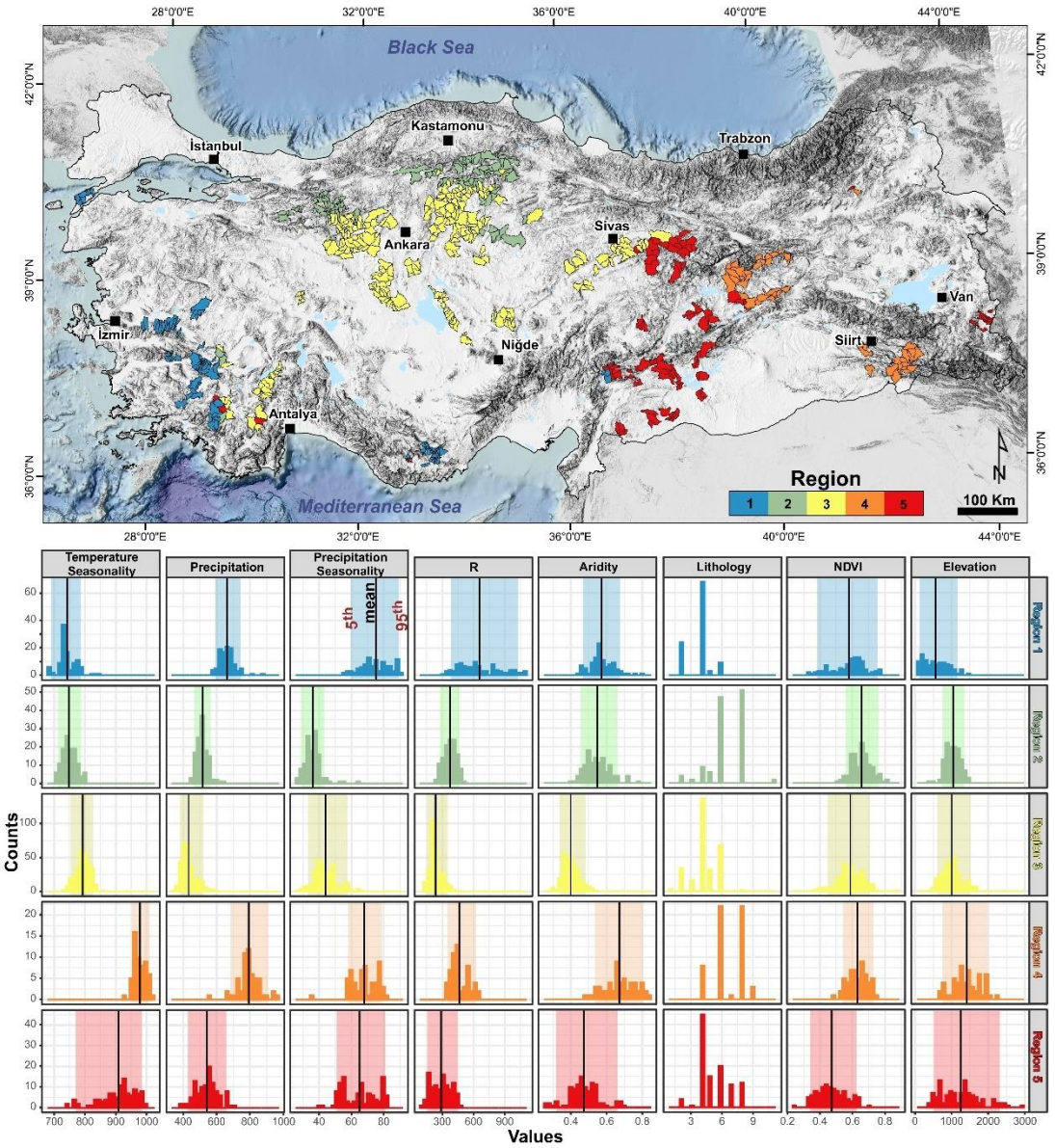

Figure 6. 1: Spatial distribution of the regions according to cluster-5. The histograms show the descriptive statistics of sub-regions. Black vertical lines indicate the mean values and shaded areas colored for each region span the interquartile range (5th and 95th percentile).

seasonality bears a clear boundary, decreasing sharply in the transition zone from the badland Region 1 in western and southern Turkey to the inner badland Region 3 in central Turkey (Figure 6.2A and 6.2B). The underlying reason for forming a sharp boundary between these two regions is caused by the presence of orographic barriers (i.e., the Taurides), controlled by neotectonic, rapid uplift, in southern Turkey (McNab et al., 2018; Schildgen et al., 2012). The climatic parameters play a crucial role in the

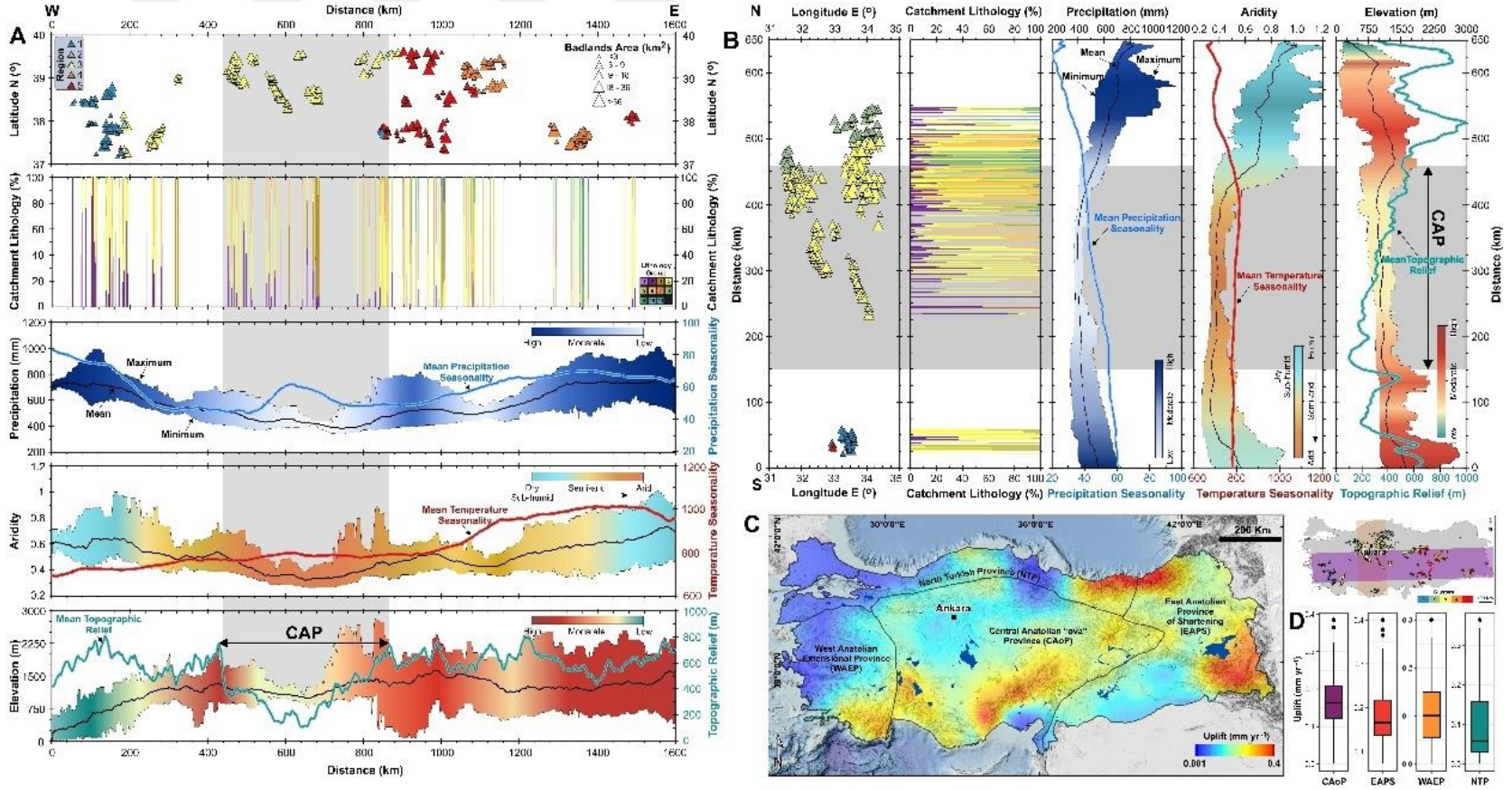

Figure 6. 2: The regional variations and comparison of the geo-environmental parameters for badland regions. The latitudinal and longitudinally oriented swath profile shows transitions in badlands regions, catchment lithology elevation, precipitation, aridity, (mean) precipitation seasonality, (mean) temperature seasonality, mean topographic relief, a) west to east, b) north to south, c) long term uplift rates compiled by McNab et al., (2018) with main tectonic provinces suggested by Şengör and Yazıcı, (2020) of Turkey, d) box plots of uplift rates in main tectonic provinces.

transition zones among the obtained badland regions, but the tectonic adjustment and its erosional response are also responsible for isolating the regions topographically in western Turkey. The extensional regime affecting western Turkey has caused successive denudational and depositional processes, constituting Plio-Quaternary terrestrial deposits (Figure 6.2A; units 2 and 4) deformed under the control of the normal faults system (Ocakoğlu, 2020; Özpolat et al., 2020). These active erosional processes have led to favorable conditions for badland formation along mountain fronts (e.g., northern and southern hillslopes of the Bozdag and Aydın mountains, respectively, along with the Western Anatolian horst-graben systems) in western Turkey. Even though the formation and the development degree of badlands are highly linked with the local structural control (Bentivenga et al., 2021), geo-environmental factors and process domains (Llena et al., 2020; Vergari et al., 2019), the tectonic and climatic settings in the regional scale are also critical factors on the evolution of badlands by adjusting regional base level (Calvo-Cases & Harvey, 1996; Faulkner, 2008; Harvey et al., 2014). In this respect, the eastern margin of the CAP, which is sculpted conformably to the NAF zone by active denudational processes such as large landslides (Görüm, 2019) and river incision, shapes the transition zone towards badland Region 3, which is tectonically less active than Region 4, in eastern Turkey.

Based on the west-to-east swath profile (Figure 6.2A), the boundary between Regions 4 and 5 is highly controlled by temperature and precipitation seasonality. These factors have been reported to be linked to badland development, as triggering factors controlling bedrock weathering processes and overland flow generation, particularly for the formation of mountain badlands (Descroix & Gautier, 2002; Moreno-de las Heras & Gallart, 2016a; Regüés et al., 1995; Regüés & Gallart, 2004). Although no apparent differences in elevation can be pointed out from the analysis of the swath profile at this transition zone for the badlands Regions 4 and 5, the large positive asymmetry in the elevation histogram for the distribution of Region 4 badlands along the range of 1000–2250 m constitutes an additional criterion of separation of these two groups of badlands (Figure 6.1B). Another associated sign for separating these two regions is the transition to the more humid conditions (i.e., the mean aridity index is 0.45 and 0.65 for Regions 5 and 4, respectively), conformably with increasing precipitation for Region 4 (Figure 6.1 and 6.2A).

The Central Anatolian Plateau (CAP) is an orogenic plateau bounded by the tectonically active faults from the southern and northern margins (Bartol & Govers, 2014; Faccenna et al., 2013; Göğüş et al., 2017; McNab et al., 2018; Schildgen et al., 2014). The swath profile that runs from north to south reflects two transition zones of badlands regions conformably with their climatic and topographic distributions (Fig. 9b). The spatial transition from Region 2 to Region 3 badlands takes place along the northern margin of the CAP, deformed by the North Anatolian Fault (NAF). The steep topography of this margin constitutes a topographic barrier limiting the amount of precipitation from the Black Sea to inland CAP, causing a distinct contrast in badland regions from sub-humid conditions in the north (Region 2) to semi-arid conditions in the CAP area (Region 3). The aridity index shows a drastic decrement from Region 2 to Region 3, which is also concurrent with a sharp precipitation reduction between these two regions caused by the orographic, rain-shadow effect exerted by the northern mountain chains over the CAP area. The controls of climatic and topographic variations are explicit for the transition on badland regions along the north to south swath profile. It is also apparent to observe that the strong variances in precipitation seasonality and mean topographic relief become dominant in separating Regions 2 – 3 – 1 along this area. The underlying reason for the partition of badland regions along the southern margin of the CAP (i.e., Regions 3 and 1, from north to south) is associated with rapid rock uplift induced steep topography (Racano et al., 2021) and its related orogenic response to increased precipitation amount and seasonality (Figure 6.2A). Schildgen et al. (2014) revealed that the southern margin (Central Taurides) of the Central Anatolian “ova” Province or CAP has been characterized by rapid uplift (~1.5 km) during the last 1.6 Ma, resulting in the formation of a natural orographic barrier (Central Taurides) that limits the movement of moisture and rainfall source from the Mediterranean Sea towards the CAP (Figure 6.2C and 6.2D). A further lithological distinction between Region 3 and Region 1 badlands along the southern CAP transition of the swath profile can be outlined (Figure 6.2B), caused by the presence of uplifted marine-borne sediments of Calabrian age in Region 1 badlands beyond the southern rim of the Central Anatolian Plateau, with important implications regarding their maximum age and tectonic control on their formation (Cosentino et al., 2012; Schildgen et al., 2012).

6.1.2 A conceptual synthesis of Turkish Badlands

Overall, our comprehensive regional assessment of Turkish badlands offers five distinguished major groups organized within the regional setting of geo-environmental terrain properties (Figure 6.3). In this context, three essential badland regions can be established: Region 1, Region 3, and Region 4, hereafter referred to as Mediterranean badlands, Central Anatolian Plateau badlands, and Eastern Anatolia Highland badlands, respectively. The other two regional groups of badlands, Region 2 and Region 5, can be interpreted as transition regions, hereafter referred to as Plateau-Margin Transition badlands and Plateau-Highland Transition badlands, respectively.

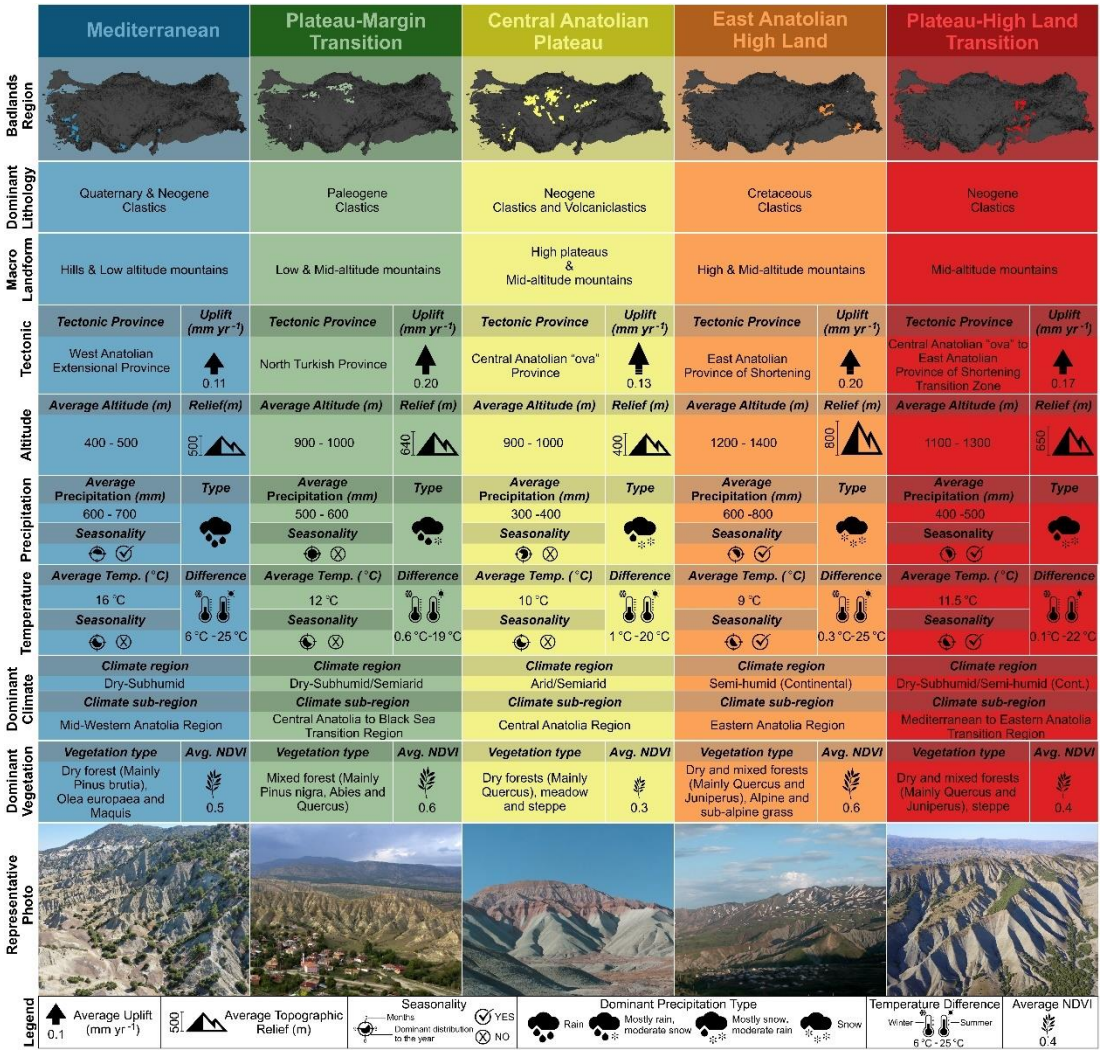

Figure 6. 3: The synthesis table illustrates the main regional characteristics and differences of five major badland regions in Turkey.

Mediterranean badlands (Figure 6.3), broadly distributed within the Western Anatolia Extensional Province (WAEP; Figure 6.2C), have been developed by the dissection of steep slopes in response to the mutual interaction of long term tectonic, climatic, and lithologic conditions. The WAEP had 3.5 km elevation in Early to Middle Miocene (Okay et al., 2020; Şengör & Yazıcı, 2020). Parallel to the onset of the neotectonics period, the escape tectonic of the Anatolian Plate together with slab retreat in the west along the Hellenic trench initiated an extensional regime to WAEP, resulting in extensive denudation, which limits the topographic relief in the long-term (Sengör & Yilmaz, 1981; Şengör & Yazıcı, 2020). Extensional tectonics further caused the formation of horst-graben systems in the WAEP. Long-term base-level changes successively led to sedimentation forming the pediment surface at the basins that are readily eroded by river systems originated in the Quaternary (Çiner et al., 2015; Westaway et al., 2004).

The regional analyses indicate that precipitation seasonality comes into prominence as one of the most critical geo-environmental parameters controlling badland development and organization for the Mediterranean badlands. Further, the presence of topographic barriers (i.e., the Taurides mountain range), which induces orographic rainfall in parallel to increased rainfall erosivity, overland flow, and soil erosion, can largely contribute to badland formation in this region. From the dominant bedrock point of view and weathering processes acting on the badland surfaces, we anticipate a more effective action of wetting – drying cycles (Cantón et al., 2002) than freezing-thawing and frost- cracking (Ariagno et al., 2022), due to the overall warm temperature of this region (mean average temperature is 16 ˚C). On the other hand, widespread river and lacustrine sediment alternation support piping and the development of intense gully networks on the side slopes of pediment surfaces, which are initiated by landsliding, pipe collapse, and headward erosion. The badlands distributed in this region share identic geo-environmental features with Italian calanchi in terms of high precipitation seasonality and the presence of sparse maquis vegetation (Farifteh & Soeters, 2006; Moretti & Rodolfi, 2000; Pulice et al., 2012). Although the marine origin of the depositional environment of Italian calanchi notably differs from the Mediterranean badlands of Turkey that are characterized by terrestrial clastics, the resemblance is relatively apparent regarding their morphological features, mostly

sharp-edged landforms sculpted by active erosion processes (e.g., shallow landslides, gullying, rilling, and piping).

The Central Anatolian Plateau badlands (Figure 6.3) represent the broadest regional distribution of these highly erosive landforms in Turkey (~42 %). The uniform climatic setting of the region stands out by having the driest, semi-arid conditions in the territory, with a 0.39 mean aridity index and 432 mm MAP values (Figure 6.1B). The CAP shows orogenic plateau characteristics similar to the Himalayan and Puna-Altiplano plateaus, which are spatially delimited by tectonically active margins that strongly constrain the passage of air masses to the interior of the plateau. This explains the scarcity of precipitation due to the reinforced emergence of rain-shadow areas that provide the regional context for the arid and semi-arid badlands of the CAP. The CAP is represented by low relief, which led to the development of pluvial lakes forming fluvio-lacustrine sediment deposits during the Pleistocene climate oscillation (Erol, 1997). Considering the current arid to semi-arid climate conditions of this region, the low annual rainfall amount levels of the CAP may significantly constrain the erosive activity and incision of these badlands, as suggested by (Gallart et al., 2002) for other badlands of arid and semi-arid character. For example, studies in the arid badlands of the Zin Valley (Israel) indicate no significant slope retreat and rather low channel incision rates at the present time, also establishing their ancient origin during a less arid phase of the late Pleistocene (Yair et al., 1980; 1982; 2013). In this sense, we can argue that, very likely, the development of the arid and semi-arid badlands of the Central Anatolian Plateau may be the result of the past active incision during a wetter phase of paleoclimate conditions, suggesting a relatively old origin as other arid and semi-arid badlands developed in different areas of the Mediterranean basin, such as the Guadix-Baza and the Tabernas badlands in Spain (Wise et al., 1982; Díaz-Hernández & Juliá, 2006; Calvo-Cases et al., 2014) or the aforementioned Zin Valley badlands in Israel (Bryan & Yair, 1982; Yair et al., 1980, 2013). Variations in parent bedrock materials and local structural differences (e.g., orientation and slope of bedding and fractures) can cause essential variations in badland morphology (Calvo-Cases & Harvey, 1996; Moreno-de las Heras & Gallart, 2016a), 2016). Although this section does not aim to describe and compare badland morphologies, we can point out some critical variations in badland morphology within the Central Anatolian Plateau badlands. Mainly, landform characteristics of the CAP badlands differ significantly

under strong lithological control of their morphologies in areas nearby Ankara and Niğde. The badlands distributed in the vicinity of Ankara are developed on sequences of terrestrial sediments and lacustrine limestones deposited successively from the Neogene to the Quaternary (Inci et al., 1988), and they are represented mainly by rounded slopes, which are formed by mutual interaction of piping and mass movements. Contrarily, the badlands located north of Niğde in Cappadocia (part of the Göreme National Park and Rock Sites of Cappadocia) were recognized by the UNESCO World Heritage List in 1985 because of their fascinating peculiar landscapes of dissected valleys, hillslopes, and fairy chimneys (Çiner &Aydar, 2019), developed on Neogene and Quate

The Eastern Anatolia Highland badlands (Figure 6.3) can be distinguished from the other Turkish badlands by their semi-humid mountain characteristics. Considering their high mean elevation (~1300 m), abundant annual precipitation (~700 mm), and large variation between minimum and maximum temperatures (0–25 ˚C), the climatic conditions of this region may imply that badland regoliths in this area are formed preferentially by the action of freezing-thawing and frost cracking weathering cycles over the bedrock materials driven by the harsh, winter thermal conditions of the mountain range. This bedrock weathering mechanism has been described as the principal regolith production mechanism in several badland areas of semi-humid and humid mountain landscapes laying in the mountain ranges of the Mediterranean basin, including the badlands of the Araguas and Vallcebre catchments, the Llobregat basin in the Spanish Pyrenees (Moreno-de las Heras & Gallart, 2016b; Nadal-Romero & Regüés, 2010; Regüés & Gallart, 2004), and the Terres Noires badlands of Draix in the French Alps (Ariagno et al., 2022; Descroix & Mathys, 2003). Frequently much younger than arid and semi-arid badlands, high production of regoliths by freezing-thawing and frost cracking weathering, and high amounts of annual precipitation provide semi-humid and humid mountain badlands with critical conditions for producing high erosion and denudation rates (Ariagno et al., 2022; Moreno-de las Heras & Gallart, 2018). The relatively high NDVI values observed for the identified Eastern Anatolia Highland badlands (0.6; Figure 6.3) point to the distribution of these erosive landforms as discrete and spatially discontinuous erosive patches within a matrix of mixed forest and alpine to sub-alpine vegetation formations, as it has been commonly described for other mountain badland systems in the Mediterranean region

(Moreno-de las Heras and Gallart, 2016). The spatial distribution of the Eastern Anatolia Highland badlands shows coherence with the southern margin of the Eastern Anatolian Plateau, which is uplifted about 2 km by the collision of the Eurasian-Arabian lithospheres causing the high relief and mountainous nature (Memiş et al., 2020). Despite the formation of a high gradient regional relief in Eastern Anatolia that has emerged from the sea level in the last 18 Ma (Memiş et al., 2020), the badlands in this area expose preferentially on Cretaceous clastics (Figure 6.2A; units 8 and 9), which overall suggests that intense denudation has caused exposing Cretaceous clastics by tearing off the upper surface lithology (mainly limestones formed on the NeoTethys Ocean) by river incision (Demir et al., 2007), large landslides (Görüm, 2019), and intense soil erosion (Erinç, 1953). These Cretaceous sediments are prominently eroded by snow-melt runoff and spring showers, which show high flow velocity conformably with the critical erosion period (March to June) in Eastern Anatolia (Yucel et al., 2015).

The Plateau-Margin Transition badlands (Figure 6.3) are distributed in the transition zone from the North Turkish Province (NTP) to the Central Anatolian "ova" Province (CaoP; Figure 6.2C) determined by Şengör (1987;2020). This region is symmetrical to the North Anatolian Fault Zone (Ketin, 1948; Şengör, 1979). The present topography of this region has been formed by fast uplift rates (~20 mm yr^{-1}; McNab et al., 2018) and river incision rates ranging between 0.15 and 0.45 mm yr^{-1} since 540 ka (McClain et al., 2020, 2021). These active processes have influenced badland formation on pediment surfaces developed on Paleogene clastics (Figure 6.2B, unit 6). The climate setting (dry sub-humid conditions), modified by the orogenic northern margin of the CAP, indicates that these badlands have been developed in a transition zone extending from the semi-arid climate conditions of the CAP (300–400 mm MAP) to the humid climate conditions (>800 mm MAP) of the Black Sea coastline. The coupled effect of dry sub-humid climate conditions and active tectonics suggests, according to the badland climate classification of Gallart et al. (2002), that these badlands may show relatively high erosion rates under the moderating control effects of mild temperatures and mixed forest vegetation (Tatli and Dalfes, 2021).

The last synthetic regional group of Turkish badlands is represented by the Plateau-Highland transition badlands (Figure 6.3), which display tectonically and climatologically rather non-uniform environmental conditions. Because of the broad

longitudinal distribution of this region in the N–S direction, changing geo-environmental factors control the distribution of badlands in this heterogeneous group that separates the Central Anatolian Plateau badlands from the Eastern Anatolian Highland badlands. The joint role of topography and climate accounts for the variation of Mediterranean climate and low relief conditions in the south of this transition region to slightly dryer conditions and higher relief in the north. Parallel to the NAF in the northern section of this region, badlands are sculpted mainly by the effect of mass wasting processes (Görüm, 2019). These geomorphic processes acting in the badland surfaces and hillslopes of this region vary from north to south due to relief- derived local base-level differences. In fact, despite the occurrence of large badlands sculpted by mass movements in the northern section of this region, patchy and smaller badlands in the southern section resulted from their relatively lower local relief.

Overall, this regional synthesis of major badland distribution characteristics offers the first effort for discussing comprehensively the role of a series of geo-environmental parameters on the organization of Turkish badlands. The analysis of the explored tectonic, climatic, lithologic, topographic, and vegetation parameters, which are commonly pointed to as major controls for badland development in the vast literature (Moreno-de las Heras and Gallart, 2018 and references therein), may show also some practical limitations for interpreting accurately the origin of the studied badlands, particularly considering the broad, regional scale approach applied in this thesis and the variable time dependence of these primary controls on badland development. These limitations may account, for example, for the impact of other geo-environmental parameters not explored in this study, such as human effects (e.g., land use, landcover, and their variations in time). In this sense, although different studies have highlighted the relevance of human activities (e.g., deforestation, mining, and agricultural activities) for the expansion and rejuvenation of badlands in areas of Spain (associated to agricultural settings and quarrying/mining; Gallart, 1992; Ballesteros Cánovas et al., 2017), France (associated to deforestation pulses; Descroix & Gautier, 2002), and Italy (associated to agricultural expansion and deforestation pulses; Marignani et al., 2008; Piccarreta et al., 2011; Torri et al., 2018), we can assume a limited imprint of human actions in the development, in general, massive badland areas explored in this study. The possible effects of early human actions (e.g., forest clearance, agriculture and grazing expansion) on the acceleration of soil erosion and sediment fluxes in

Anatolia, deciphered in the literature by climate reconstructions and palynological research (Dusar et al., 2011; Eastwood et al., 1998, 2007; Kaniewski et al., 2007), might have just boosted the erosional tempo of the analyzed badland areas, rather than developing large badland-dominated landscapes in the scope of this study. The representative temporal scale of the analyzed geo-environmental parameters, particularly climate (e.g., present precipitation, temperature seasonality, etc.), may also impose constraints on our badland development interpretations. However, the general patterns and characteristics of present climatic gradients in Turkey have been long-term structured since the Late Miocene, in response to the uplifting of the main topographic barriers (e.g., Pontides and Torides) and the formation of the Central Anatolian Plateau (Gladstone et al., 2007). Nonetheless, future works will be required to analyze and quantify in detail the long-term badland formative linkages suggested in this study between active structural (mainly tectonic, lithologic, and climatic) systems and the origin of the analyzed erosive landforms, which will require moving from the broad, regional-scale applied in this study to smaller spatial scales.

6.2 The Influences of Seasonal Variations in Climate On Weathering Processes

6.2.1 The resilience of regolith as a response of interaction between parent material and climate characteristics

Regüés et al. (1995) highlighted the constraints inherent in experimental investigations concerning the seasonal patterns of regolith behavior. These studies are limited by their focus on a single season, neglecting the diverse fluctuations in precipitation and temperature dynamics observed throughout the rest of the year. However, the following study by Regüés & Gallart (2004) has shown the importance of repeated rainfall simulations in the field to understand seasonal differences in sediment transport and regolith dynamics. Furthermore, Ariagno et al. (2022) have utilized historical meteorological and sediment records (2003-2020) to refer sediment flux to frost-cracking intensity based on daily temperature observations on Draix Catchments in SE France. Here, we take advantage of cycle-based laboratory experiments to test our hypothesis on interaction between parent badland material and different climate settings.

The differential desiccation cracks, crust, fractures, and popcorn formations have been documented in samples primarily due to their differences in mineralogical, and climatic conditions in arid and Mediterranean regions, while humid and Cappadocia

tend to maintain their shard structure over the course of cycles. Arid samples with a predominance of smectite and illite minerals interact differently with simulated climatic conditions than Mediterranean samples with dominant clay (smectite, illite, and kaolinite) and quartz minerals (Table 5.2). Even though Mediterranean samples broke down in the initial cycles, arid samples maintained their initial conditions until 2nd-year cycles (Figure 5.4). These findings are also in line with pond formations, which are strongly linked to shard breakdown, dispersion and pore blockage based on dominating mineralogy and grain size in samples. For example, arid samples showed more pond formations in the second-year cycle (Figure 5.5A), especially in the winter (6th) and spring (7th) seasons, which resulted in turning the samples into gel form when wetted (Bryan et al., 1978), increasing swelling degree and clogging the pores by filling with clay-size materials, which overall rendered the samples impermeable. The lack of pond formation in 3rd-year cycles for both in arid and Mediterranean regions also highlight the importance of highly developed cracks for maintaining infiltration capacity in the regolith. These results also confirm the observations of Faulkner (2013) on the supremacy of shrinking over swelling, which keep cracks open and results in enhanced infiltration rates (Faulkner, 1990). The cumulative volume of leachates (Figure 5.5A) displays important fluctuations, providing also evidences for the formation of ponds caused by the breakdown of the materials. This phenomenon is particularly evident during the 2nd -year cycles for arid samples, where a marked decrease (45% drop, Figure 5.5A) in cumulative volume compared to 1st -year cycles took place along with an increase in pond formation due to changing regolith conditions (i.e., increasing swelling degree and pore clogging).

Table 6. 1: The comparison of initial weights of unweathered samples and final weights of weathered samples after experiments

Sample ID	Samples (S) Weight (gr.)	Container (C) Weight (gr.)	S+C (gr.)	S+ C After Experiments (gr.)	S After Experiments (gr.)	% Weight Change
A1	283.49	46.57	325.87	290.6	244.03	-13.92
A2	280.87	53.45	327.61	304.99	251.54	-10.44
A3	285.56	47.63	324.15	297.86	250.23	-12.37
A4	280.59	46.7	320.67	311.25	264.55	-5.72
M1	281.11	50.58	327.94	277.49	226.91	-19.28
M2	281.8	40.25	314.21	247.46	207.21	-26.47
M3	282.47	47.71	323.63	245.52	197.81	-29.97
H1	280.61	41.87	317.84	308.13	266.26	-5.11
H2	280.34	45.44	321.7	314.11	268.67	-4.16
C1	283.23	47.31	330.54	331.12	283.81	0.00
C2	282.16	44.02	326.18	340.94	296.92	0.00

Across the cycles, disparities in crusts and cracks were recorded for the Mediterranean and arid samples (Fig. 5.4). In the spring and summer cycles of the 2nd and 3rd years, notably in A1 and A2 Arid samples, wetting and drying induced thick desiccation cracks that displayed a repeated pattern. However, Mediterranean samples revealed thinner, flat crusts with deep joints. Instead, humid samples are kept their physical stability through experiments due their very low SAR and EC accompanied by relatively high contents of $CaCO_3$ which may increase very importantly the stability of the materials. These records, particularly in humid samples, differ from other studies in terms of the dominant season as main contributor to regolith development. The plot-experiments showed that frost-cracking (Ariagno et al., 2021) and regolith alterations (Nadal-Romero & Regüés, 2010) become more apparent in winter seasons in Mediterranean mountain climate conditions. On the other hand, the other laboratory experiments-based studies, for example, Cantón et al. (2001) which shows the dominance of wetting and drying on weathering processes, confirm our observations for arid and Mediterranean samples. Even though weathering in nature simultaneously accompanies various physical and chemical disintegration processes over the different seasons, this might also shed light on the differential relationship between regolith development and the conditions of spring–summer seasons due to the higher insolation

and swelling potentials in the arid region. An important point that should be underlined for the Mediterranean region, is higher weight losses in samples during the simulated cycles than for other regions (Table 6.1). These findings suggest that the occurrence prolonged dry spells, which characterize summer season under Mediterranean climate (Lana et al., 2008; Akbaş, 2023), can speed up the disintegration of shards into easily transportable material. Although the primary focus of this work was the analysis of the seasonal effects of climate on weathering processes, we may also point out the significance of these results for the badland sediment fluxes throughout the year. After dry-spell induced crack formation and defragmentation of surface badland materials during summer, subsequent fall rainfalls can quickly lead to erosion and sediment mobilization, especially in the study Mediterranean and Arid region badlands.

It is also important to highlight that some limitations of cycle-based laboratory experiments such as the duration of each cycle (1 day in our experiments) may have potentially influenced our results even though every environment has its dynamics. For example, popcorn formation, which is commonly observed on marly sediments, were only recorded on A2 in the last two cycles. Furthermore, even though the humid region had harsh winter conditions, we did not observe the breaking down of the sediment which frost-cracking and freeze-thawing processes are main processes under similar conditions.

6.2.2 Geochemical proxies for weathering processes under seasonal contrast of precipitation and temperature conditions

The hypothesis that the formation of badlands is strongly linked to seasonal climatic factors has been proposed since the milestone study by Bryan and Yair (1982). However, despite previous laboratory and plot-scale experiments conducted in generally stable climatic conditions, this assumption has not been thoroughly evaluated. Conducting experiments through cycles and observing corresponding variations in geochemical indicators can give support to this overarching hypothesis, and obtained fluctuations in geochemical indicators as a response to simulated wetting and drying conditions may serve as effective proxies for investigating certain types and trends of weathering processes. Consequently, leachate chemistry properties i.e., pH, EC, cations, anions, SAR, etc. has been used extensively in research to describe the type and rate of weathering processes (Cantón et al., 2003; Faulkner et al., 2000,

2004; Kasanin-Grubin, 2013; Nadal-Romero et al., 2007; Romero Díaz et al., 2007; Summa et al., 2007; Wells et al., 2006).

These results are consistent with the findings of Xie et al. (2022), where ions, pH, and EC concentrations were shown to dominate in response to cycle-based experiments on badlands landscapes. Moreover, the high correlations observed for cations may be attributed to their major mineralogical and chemical compositions (Table 5.2) in the sediment.

The most striking result to emerge from experiments is noticeable regular trends of Na^+ over cycles, particularly in arid and Mediterranean samples (Figure 5.6). These fluctuations become more evident in the leaches of samples for the arid region characterized by dominant smectite minerals and presence of analcime and high SAR, which show a recurrent cyclic pattern of Na^+ increasing from fall to spring. Even though Ca^{2+} displays some degree similar regular trend as Na^+, we can argue that Na^+ induced-dispersion of clay minerals may surpass the stabilizing influence of Ca^{2+} that promotes aggregation of sediments via flocculation, due to the higher total concentrations of Na^+ over Ca^{2+} evidenced by the very high SAR of the arid samples. Moreover, a slight decreasing trend of pH which shifts from strong alkaline conditions to less alkaline concurrently might accelerate velocity of the weathering processes, especially in the second-year cycles in arid samples. This recurrent pattern suggests that the spring season which is marked by convectional rainfalls in arid region largely contribute to weathering processes more than other seasons. Furthermore, this rising tendency over the course of a year from fall to spring implies repeated and gradual exposure of a new regolith layers to simulations of precipitation, which can lead to the release of higher ion concentrations. Mediterranean samples, with moderate to low SAR and composed of smectite, quartz and illite (Figure 5.6), exhibit for all cations ever-increasing trends (from fall to spring) in the first-year cycles while subsequently winters come into prominence with their peak values over other seasons (Figure 5.6). This observation is also supported by EC (Figure 5.6), which has an overall strong significant correlation with K^+, Mg^{2+}, $Ca^{2+}$and Na^+ leachate contents (Figure 5.7). These results might be explained by the impacts of the seasonal precipitation regime of Mediterranean region, where climatic seasonality is evident with the supremacy of winter precipitation (Lana et al., 2008, Avcıoğlu et al. 2022, and Akbaş, 2023) that concentrates 43% of mean annual precipitation in the study Mediterranean region

badlands (Table 4.2). These winter cycles that release Na^+ and Ca^{2+} contents in the Mediterranean samples could boost the chemical reactivity of the smectite and illite minerals, which might lead to enhanced alteration of minerals (i.e., hydration) and sediment transport, as the increased water content can reduce internal friction and allow sediments to be easily transported. EC and Ca^{2+} concentrations are more likely to increase during winter cycles in the leachates of humid and Cappadocia badland samples, while other indicators remain irregular throughout the course of simulated cycles and years. This may explain the surficial responses of the humid and Cappadocia badland samples to our weathering experiments, where these samples characterized by very low SAR and EC kept their internal stability and did not break down due to the preponderance of Ca^{2+} over other indicators.

6.3. Topographic Imprints of Badlands

The quantitative catchment descriptors such as slope-area relation has been broadly used in determination of topographic thresholds of gully head (Tarolli & Dalla Fontana, 2009; Majhi et al., 2021; Rossi et al., 2022), process domains in badlands (Vergari et al., 2019), topographic signature of landslides (Meunier et al., 2008), understanding of land surface properties influences on landscape morphology (Yetemen et al., 2010). The division of the landscape into various drainage and slope regimes, such as hillslopes, unchanneled valleys, channels with the dominances debris flows, and alluvial channels has been suggested by different researchers (Ijjasz-Vasquez & Bras, 1995; Montgomery & Dietrich, 1992) to interpret and decipher the morphological evolution of landscape. Here, the slope-area relation analyses of this thesis have revealed the topographic position of badlands by comparing the badland sites from Turkey with globally known badland sites. The obtained results showed that badlands are placed up to 10^4 to 10^5 m^2 contribution areas which are considered arguably II scaling regime which refers to unchanneled valleys (Montgomery & Foufoula-Georgiou, 1993). On the other hand, it should be taken into account that average upper quantile (75^{th} percentile) of contribution areas is 177 m^2 (Table 6.2), therefore it substantially differs from maximum values and indicates that badlands are located to hillslopes and hillslope to unchanneled valley transition.

Table 6. 2: The contribution areas (m^2) comparison of badland sites and their corresponding catchments. Total area represents the polygon areas (in km^2) both in badlands and catchments.

Badlands	Utah	South Dakota	Murcia	Saldes	Lombardy	Basilicata	Burdur	Tosya	Taiwan
mean	467.2	283.4	385.7	291.9	285.4	165.0	224.2	627.3	224.2
std	1963.5	923.1	1439.3	804.7	732.9	469.7	683.8	2531.7	683.8
min	25.0	25.0	24.9	25.0	25.0	25.0	25.0	24.9	25.0
25%	50.0	25.0	49.8	50.0	50.0	49.9	50.0	49.9	50.0
50%	75.0	50.0	74.8	75.0	75.0	74.9	75.0	99.8	75.0
75%	175.0	149.9	149.5	174.9	200.0	149.8	175.0	249.4	175.0
max	4.E+04	2.E+04	4.E+04	2.E+04	1.E+04	2.E+04	4.E+04	6.E+04	4.E+04
Total Area (km^2)	9.5	10.9	5.9	1.4	2.1	0.6	32.2	4.48	5.2
Catchment									
mean	2.E+04	1.E+05	5.E+04	7.E+04	7.E+04	3.E+04	6.E+04	4.E+04	1.E+05
std	3.E+05	2.E+06	1.E+06	2.E+06	2.E+06	4.E+05	1.E+06	9.E+05	3.E+06
min	25.0	25.0	25.0	25.0	25.0	25.0	25.0	25.0	25.0
25%	50.0	50.0	49.9	50.0	50.0	49.9	50.0	49.9	49.9
50%	75.0	75.0	124.9	150.0	150.0	99.8	99.9	99.9	124.8
75%	249.9	274.9	374.6	474.9	450.0	299.4	249.8	349.6	274.5
max	1.E+07	7.E+07	4.E+07	1.E+08	1.E+08	1.E+07	6.E+07	4.E+07	2.E+08
Total Area (km^2)	15.5	67.3	44.78	102	174	13.5	56.9	40	80

The differences between upper quantile and maximum contribution area in all badland sites might point to a transition in dominant sediment processes within different section of badland landforms. In this context, diffusive (hillslope) processes are can be identified in the slopes and ridges, while gully channels of the badlands may depict a transition to linear (fluvial) processes. It also should be noted that even though slope-area relation has been highly used, there is no consensus on determination of thresholds of scaling regimes in the literature. For example, Meunier et al. (2008) interpreted that 3.2 km^2 is the break point in scaling regime from hillslopes to fluvial channels in the mountainous environment for landslides while Yetemen et al., (2010) distinguished scaling regime I and II with ~600 m^2 in two semi-arid basins with gentle topography

in New Mexico. Therefore, it is important to consider how diverse tectonic, climatic, and lithologic settings result in different scaling regimes for the slope-area relation.

Table 6. 3: The gradient (m m^{-1}) comparison of badland sites and their corresponding catchments.

Badlands	Utah	South Dakota	Murcia	Saldes	Lombardy	Basilicata	Burdur	Tosya	Taiwan
mean	0.63	0.36	0.62	0.48	0.57	0.43	0.57	0.69	0.57
std	0.39	0.34	0.29	0.28	0.37	0.32	0.26	0.29	0.26
min	0.00	0.00	0.00	0.00	0.00	0.00	0.00	0.00	0.00
25%	0.39	0.11	0.42	0.27	0.38	0.17	0.42	0.42	0.42
50%	0.66	0.26	0.66	0.47	0.54	0.37	0.58	0.71	0.58
75%	0.82	0.53	0.83	0.66	0.70	0.67	0.72	0.85	0.72
max	17.92	3.20	6.43	2.74	6.02	1.98	2.16	3.40	2.16
Catchment									
mean	0.44	0.08	0.37	0.53	0.18	0.32	0.40	0.40	0.33
std	0.56	0.17	0.25	0.39	0.20	0.28	0.23	0.28	0.25
min	0.00	0.00	0.00	0.00	0.00	0.00	0.00	0.00	0.00
25%	0.05	0.01	0.18	0.29	0.01	0.14	0.21	0.20	0.12
50%	0.32	0.02	0.35	0.49	0.14	0.25	0.39	0.40	0.31
75%	0.72	0.07	0.51	0.67	0.28	0.43	0.58	0.60	0.48
max	17.92	3.20	6.42	16.87	6.02	8.65	4.18	3.40	5.14

The slope-area relation, concurrently, might decipher the dynamics of local tectonic settings (Yetemen et al., 2010), in line with this capability of slope-area relation, the findings of this thesis also support this relation. The badland areas in Tosya and Murcia stands out with the 50^{th} percentile (i.e., median) gradient values of 0.7 and 0.66 m m^{-1} (Table 6.3) which located in close proximity to active fault zones, NAF and Alahama de Murcia Fault, respectively. While these value decrease to 0.25 in South Dakota which is tectonically inactive areas. Remarkably, Caineville badlands illustrate high gradient values of 0.66 m m^{-1} even though it is characterized by tectonically quiescent area. This finding might be explained by the badland/catchment areas ratio, 65% for Caineville. Because the overall badlands areas (avg. 0.54 m m^{-1}) are characterized by higher gradient values than catchment's gradient (avg. 0.34 m m^{-1}), as

badland/catchment ratio increases average gradient values concurrently increase in these areas. It is also possible that the fact that the Caineville badlands are primarily consist of the tablelands' escarpments, which are made up of steep hillslopes, contributes to the higher gradient values in badlands.

7. CONCLUSION

The purpose of this thesis was to clarify regional characteristics, climate weathering interaction, and topographic positions of badlands in Turkey by identifying, evaluating, and comprehending the geomorphic, geochemical, and geomorphometric properties of the Turkish badlands using a comprehensive plot to regional scale approaches.

In this context, a broad, regional inventory of badland units covering a total 4494 km^2 area over Turkey have been determined the first part of the thesis. In contrast to other site specific, local studies on badland distribution and their geomorphic characteristics, this thesis offers a first national-scale regional assessment of the distribution of badland landscapes by considering a wide set of geo- environmental conditioning factors linked to their development as proxies to characterize spatially homogeneous badland regions. Based on a machine learning algorithm (i.e., *k*-means clustering analyses) using a combination of climatic, lithologic, topographic, and vegetation parameters, we defined five distinctive badland regions over Turkey: (1) Mediterranean badlands distributed in a territory characterized by a remarkable precipitation seasonality and hilly topography; (2) Central Anatolian Plateau badlands, extensively influenced by orogenic plateau characteristics displaying the dryest (arid and semi-arid) conditions; (3) Eastern Anatolia Highland badlands, laying in a mountainous humid environment with the highest altitudes (~1300 m) and relief (~800 m); and two further regions, (4) the Plateau-Margin Transition badlands and (5) the Plateau-Highland Transition badlands, distributed within a tectonically active environment along with a climatic transition between the humid and arid regions.

Long-term topographic and climatic modifications resulting from Turkey's tectonic history play, apart from dominant lithological controls, a primary role in organizing badland landscape characteristics and their distribution in the territory. In fact, the high amount of badland units throughout the Central Anatolian Plateau (CAP) as well as their distinctive spatial patterns and diversity in transition zones across active margins (i.e., the Pontides and Taurides) suggest that superimposed effects of lithologic, tectonic, and climatic dynamics largely rule the regional characteristics of these

badland landscapes. Furthermore, results show a spatial coincidence of the distribution of confined badlands with active fault zones (i.e., NAF, EAF, and WAHG), which may have broadly contributed to the development and extension of relatively young badlands, especially in northern and western Anatolia. This spatial pattern suggests a profound link between badland generation and active structural systems that need to be analysed and quantified in detail by future studies, especially regarding long-term formative linkages.

The second part of thesis showed the sequential laboratory experiments to analyze the seasonal influences of climate on weathering processes in unconsolidated sedimentary environments of badland landscapes with contrasted climate conditions and diverse parent materials. Overall, this part demonstrated that the leachate cations and pH exhibit sinusoidal trends, especially for samples of arid and Mediterranean badland regions where marly sediments and unconsolidated sandstone are present, respectively. These trends become more evident for the release of Na^+ cation in the leachates obtained in samples of the arid region characterized by high SAR, which show a consistent increasing pattern from fall to spring seasons in our 3-years experiments. This sinusoidal pattern suggests that Na^+ induced dispersion of marly sediments composed of dominant swelling clay minerals (48-72% smectite) could potentially be accelerated during spring seasons, in line with concurrently decreasing pH that makes the environment less alkaline. In addition, winter season might contribute more than other seasons to the flocculation of sediments for samples of the Mediterranean region badlands, which could make them more stable. This result is supported by the rising Ca^+ release compared to other ions in winter, accompanied by higher leachate EC concentrations. Results of physical behavior samples, which included seasonal formation of thick crusts and desiccation cracks in spring and summer for the arid region samples as well as deep joints and thin crusts for the Mediterranean region samples, also confirm our observations regarding chemical weathering processes. Differently, samples of the humid and Cappadocia badland regions, characterized by low SAR and EC, kept their surficial and internal stabilities throughout the cycles, even though they were exposed to colder conditions than other regions, simulated by snowfall during winter cycles.

The third and last part of thesis investigated the geomorphometric properties (i.e., topographical positions of badlands) of Turkish badlands by comparing with the

globally known badlands sites from USA, Spain, Italy, and Taiwan. The results showed that the topographic imprints of badlands in the context of the sub-catchment scale may depict an appropriate instance of a transitional domain from a diffusive erosional process to a fluvial erosion process. The signature of tectonically active settings on badlands areas has been recorded with higher gradient values in Tosya, Turkey, and Murcia, Spain. On the other hand, the importance of topographic positions of badlands has been also illustrated with slope-area plots in Caineville, USA which is located on the escarpments of tablelands with higher gradient value while this site is tectonically inactive.

REFERENCES

Agostini, S., Savaşçin, M. Y., Di Giuseppe, P., Di Stefano, F., Karaoğlu, Ö., Lustrino, M., Manetti, P., Ersoy, Y., Kürüm, S., & Önal, A. Ö. (2019). Neogene volcanism in Elaziğ-Tunceli area (eastern Anatolia): Geochronological and petrological constraints. *Italian Journal of Geosciences*, *138*(3), 435–455. https://doi.org/10.3301/IJG.2019.18.

Akbas, A. (2023). Seasonality, persistency, regionalization, and control mechanism of extreme rainfall over complex terrain. *Theoretical and Applied Climatology*, *152*(3-4), 981-997.

Akbaş, A. (2014). Türkiye üzerindeki önemli kurak yıllar (Important Drought Years over Turkey). *SSRN Electronic Journal*, *12*(2), 101–118. https://doi.org/10.2139/ssrn.3417309.

Ariagno, C., Le Bouteiller, C., van der Beek, P., & Klotz, S. (2022). Sediment export in marly badland catchments modulated by frost-cracking intensity, Draix–Bléone Critical Zone Observatory, SE France. *Earth Surface Dynamics*, *10*(1), 81–96. https://doi.org/10.5194/esurf-10-81-2022.

A**rnau-Rosalén, E., Calvo-Cases, A., Boix-Fayos, C., Lavee, H., & Sarah, P.** (2008). Analysis of soil surface component patterns affecting runoff generation. An example of methods applied to Mediterranean hillslopes in Alicante (Spain). *Geomorphology*, *101*(4), 595–606. https://doi.org/10.1016/j.geomorph.2008.03.001.

Avcıoğlu, A., Görüm, T., Akbaş, A., Moreno-de las Heras, M., Yıldırım, C., & Yetemen, Ö. (2022). Regional distribution and characteristics of major badland landscapes in Turkey. Catena, 218, 106562.

Ballesteros Cánovas, J. A., Stoffel, M., Martín-Duque, J. F., Corona, C., Lucía, A., Bodoque, J. M., & Montgomery, D. R. (2017). Gully evolution and geomorphic adjustments of badlands to reforestation. *Scientific Reports*, *7*(1). https://doi.org/10.1038/srep45027.

Bartol, J., & Govers, R. (2014). A single cause for uplift of the Central and Eastern Anatolian plateau? *Tectonophysics*, *637*, 116–136. https://doi.org/10.1016/j.tecto.2014.10.002.

Bentivenga, M., Agosta, F., Palladino, G., Piccarreta, M., & Prosser, G. (2021). Structural control on badland slope evolution: A case study from the southern Apennines (Italy). *Geomorphology*, *374*, 107518. https://doi.org/10.1016/j.geomorph.2020.107518.

Bryan, R. B., & Yair, A. (1982). Perspectives on studies of badland geomorphology. *Badland Geomorphology and Piping*, *January 1982*, 1–12.

Buccolini, M., & Coco, L. (2013). MSI (morphometric slope index) for analyzing activation and evolution of calanchi in Italy. *Geomorphology*, *191*, 142–149. https://doi.org/10.1016/j.geomorph.2013.02.025.

Calvo-Cases, A., & Harvey, A. M. (1996). Morphology And Development Of Selected Badlands In Southeast Spain: Implications Of Climatic Change. *Earth Surface Processes and Landforms*, *21*(8), 725–735. https://doi.org/10.1002/(SICI)1096-9837(199608)21:8<725::AID-ESP642>3.0.CO;2-V.

Cantón, Y., Domingo, F., Solé-Benet, A., & Puigdefábregas, J. (2002). Influence of soil-surface types on the overall runoff of the Tabernas badlands (south-east Spain): Field data and model approaches. *Hydrological Processes*, *16*(13), 2621–2643. https://doi.org/10.1002/hyp.1052.

Cantón, Y., Rodríguez-Caballero, E., Chamizo, S., Le Bouteiller, C., Solé-Benet, A., & Calvo-Cases, A. (2018). Runoff Generation in Badlands. In *Badlands Dynamics in a Context of Global Change*. Elsevier Inc. https://doi.org/10.1016/b978-0-12-813054-4.00005-8.

Cantón, Y., Solé-Benet, A., & Lázaro, R. (2003). Soil-geomorphology relations in gypsiferous materials of the tabernas desert (almería, se spain). *Geoderma*, *115*(3–4), 193–222. https://doi.org/10.1016/S0016-7061(03)00012-0.

Cantón, Y., Solé-Benet, A., Queralt, I., & Pini, R. (2001). Weathering of a gypsum-calcareous mudstone under semi-arid environment at Tabernas, SE Spain: Laboratory and field-based experimental approaches. *Catena*, *44*(2), 111–132. https://doi.org/10.1016/S0341-8162(00)00153-3.

Chiba, T., Kaneta, S., & Suzuki, Y. (2008). Red relief image map: new visualization method for three dimensional data. *The International Archives of the Photogrammetry, Remote Sensing and Spatial Information Sciences*, 1071–1076. http://www.isprs.org/proceedings/XXXVII/congress/2_pdf/11_ThS-6/08.pdf.

Çiner, A., Doğan, U., Yildirim, C., Akçar, N., Ivy-Ochs, S., Alfimov, V., Kubik, P. W., & Schlüchter, C. (2015). Quaternary uplift rates of the Central Anatolian Plateau, Turkey: Insights from cosmogenic isochron-burial nuclide dating of the Kizilirmak River terraces. *Quaternary Science Reviews*, *107*, 81–97. https://doi.org/10.1016/j.quascirev.2014.10.007.

Clarke, M. L., & Rendell, H. M. (2006). Process-form relationships in Southern Italian badlands: Erosion rates and implications for landform evolution. *Earth Surface Processes and Landforms*, *31*(1), 15–29. https://doi.org/10.1002/esp.1226.

Cosentino, D., Schildgen, T. F., Cipollari, P., Faranda, C., Gliozzi, E., Hudáčková, N., Lucifora, S., & Strecker, M. R. (2012). Late Miocene surface uplift of the southern margin of the Central Anatolian plateau, Central Taurides, Turkey. *Bulletin of the Geological Society of America*, *124*(1–2), 133–145. https://doi.org/10.1130/B30466.1.

Demir, T., Westaway, R., Bridgland, D., Pringle, M., Yurtmen, S., Beck, A., & Rowbotham, G. (2007). Ar-Ar dating of late Cenozoic basaltic volcanism in northern Syria: Implications for the history of incision by the River Euphrates and uplift of the northern Arabian Platform. *Tectonics*, *26*(3), 1–30. https://doi.org/10.1029/2006TC001959.

Descroix, L., & Gautier, E. (2002). Water erosion in the southern French Alps: Climatic and human mechanisms. *Catena*, *50*(1), 53–85. https://doi.org/10.1016/S0341-8162(02)00068-1.

Descroix, L., & Mathys, N. (2003). Processes, spatio-temporal factors and measurements of current erosion in the French Southern Alps: a review. *Earth Surface Processes and Landforms*, *28*(9), 993–1011. https://doi.org/10.1002/esp.514.

Díaz-Hernández, J. L., & Juliá, R. (2006). Geochronological position of badlands and geomorphological patterns in the Guadix-Baza basin (SE Spain). Q*uaternary Research*, *65*(3), 467–477. https://doi.org/10.1016/j.yqres.2006.01.009.

Dusar, B., Verstraeten, G., Notebaert, B., & Bakker, J. (2011). Holocene environmental change and its impact on sediment dynamics in the eastern mediterranean. *Earth-Science Reviews*, *108*(3–4), 137–157. https://doi.org/10.1016/j.earscirev.2011.06.006.

Eastwood, W. J., Leng, M. J., Roberts, N., & Davis, B. (2007). Holocene climate change in the eastern Mediterranean region: a comparison of stable isotope and pollen data from Lake Gölhisar, southwest Turkey. *Journal of Quaternary Science*, *22*(4), 327–341. https://doi.org/10.1002/jqs.1062.

Eastwood, W. J., Roberts, N., & Lamb, H. F. (1998). Palaeoecological and archaeological evidence for human occupance in southwest Turkey: the Beyşehir occupation phase. *Anatolian Studies*, *48*(1998), 69–86. https://doi.org/10.2307/3643048.

Erol, O. (1997). Geomorphologic Arguments for Mid- to Late Holocene Environmental Change in Central Anatolian (Pluvial) Lake Basins. *Third Millennium BC Climate Change and Old World Collapse*, *149*, 321–350. https://doi.org/10.1007/978-3-642-60616-8_12.

Faccenna, C., Becker, T. W., Jolivet, L., & Keskin, M. (2013). Mantle convection in the Middle East: Reconciling Afar upwelling, Arabia indentation and Aegean trench rollback. *Earth and Planetary Science Letters*, *375*, 254–269. https://doi.org/10.1016/j.epsl.2013.05.043.

Farifteh, J., & Soeters, R. (2006). Origin of biancane and calanchi in East Aliano, southern Italy. *Geomorphology*, *77*(1–2), 142–152. https://doi.org/10.1016/j.geomorph.2005.12.012.

Faulkner, H. (2008). Connectivity as a crucial determinant of badland morphology and evolution. *Geomorphology*, *100*(1–2), 91–103. https://doi.org/10.1016/j.geomorph.2007.04.039.

Faulkner, H. (2013). Badlands in marl lithologies: A field guide to soil dispersion, subsurface erosion and piping-origin gullies. *Catena*, *106*, 42–53. https://doi.org/10.1016/j.catena.2012.04.005.

Faulkner, H., Alexander, R., Teeuw, R., & Zukowskyj, P. (2004). Variations in soil dispersivity across a gully head displaying shallow sub-surface pipes, and the role of shallow pipes in rill initiation. *Earth Surface Processes and Landforms*, *29*(9), 1143–1160. https://doi.org/10.1002/esp.1109.

Faulkner, H., Spivey, D., & Alexander, R. (2000). The role of some site geochemical processes in the development and stabilisation of three badland sites in Almeria, Southern Spain. *Geomorphology*, *35*(1–2), 87–99. https://doi.org/10.1016/S0169-555X(00)00024-6.

Fick, S. E., & Hijmans, R. J. (2017). WorldClim 2: new 1-km spatial resolution climate surfaces for global land areas. *International Journal of Climatology*, *37*(12), 4302–4315. https://doi.org/10.1002/joc.5086.

Gallart, F., Solé-Benet, A., Puigdefábregas, J., & Lázaro, R. (2002). Badland systems in the Mediterranean. *Dryland Rivers: Hydrology and Geomorphology of Semi-Arid Channels*, *June*, 299–326.

Genç, Y., & Yürür, M. T. (2010). Coeval extension and compression in Late Mesozoic-Recent thin-skinned extensional tectonics in central Anatolia, Turkey. *Journal of Structural Geology*, *32*(5), 623–640. https://doi.org/10.1016/j.jsg.2010.03.011.

Göğüş, O. H., Pysklywec, R. N., Şengör, A. M. C., & Gün, E. (2017). Drip tectonics and the enigmatic uplift of the Central Anatolian Plateau. *Nature Communications*, *8*(1), 1538. https://doi.org/10.1038/s41467-017-01611-3.

Görüm, T. (2019). Tectonic, topographic and rock-type influences on large landslides at the northern margin of the Anatolian Plateau. *Landslides*, *16*(2), 333–346. https://doi.org/10.1007/s10346-018-1097-7.

Hartmann, J., & Moosdorf, N. (2012). The new global lithological map database GLiM: A representation of rock properties at the Earth surface. *Geochemistry, Geophysics, Geosystems*, *13*(12), 1–37. https://doi.org/10.1029/2012GC004370.

Higuchi, K., Chigira, M., & Lee, D. H. (2013). High rates of erosion and rapid weathering in a Plio-Pleistocene mudstone badland, Taiwan. *Catena*, *106*, 68–82. https://doi.org/10.1016/j.catena.2012.11.005.

Hubert-Ferrari, A., Drab, L., Van Der Woerd, J., Benedetti, L., & Van Campenhout, J. (2021). Cosmogenic data about offset uplifted river terraces and erosion rates: implication regarding the central North Anatolian Fault and the Central Pontides. *Mediterranean Geoscience Reviews*, *3*(1), 129–157. https://doi.org/10.1007/s42990-021-00057-6.

Ijjasz-Vasquez, E. J., & Bras, R. L. (1995). Scaling regimes of local slope versus contributing area in digital elevation models. *Geomorphology*, *12*(4), 299–311. https://doi.org/10.1016/0169-555X(95)00012-T

Inci, U., Helvaci, C., & Yagmurlu, F. (1988). Stratigraphy of Beypazarı Neogene Basin, Central Anatolia, Turkey. *Newsletters on Stratigraphy*, *18*(3), 165–182. https://doi.org/10.1127/nos/18/1988/165.

Istanbulluoglu, E., Yetemen, O., Vivoni, E. R., Gutiérrez-Jurado, H. A., & Bras, R. L. (2008). Eco-geomorphic implications of hillslope aspect: Inferences from analysis of landscape morphology in central New Mexico. *Geophysical Research Letters*, *35*(14). https://doi.org/10.1029/2008GL034477.

Kaniewski, D., De Laet, V., Paulissen, E., & Waelkens, M. (2007). Long-term effects of human impact on mountainous ecosystems, western Taurus Mountains, Turkey. *Journal of Biogeography*, *34*(11), 1975–1997. https://doi.org/10.1111/j.1365-2699.2007.01753.x.

Karaca, M., Deniz, A., & Tayan, M. (2000). Cyclone track variability over Turkey in association with regional climate. *International Journal of Climatology*, *20*(10), 1225–1236. https://doi.org/10.1002/1097-0088(200008)20:10<1225::AID-JOC535>3.0.CO;2-1.

Kasanin-Grubin, M. (2013). Clay mineralogy as a crucial factor in badland hillslope processes. *Catena*, *106*, 54–67. https://doi.org/10.1016/j.catena.2012.08.008.

Keskin, M. (2007). Eastern Anatolia: A hotspot in a collision zone without a mantle plume. *Special Paper of the Geological Society of America*, *430*(January 2007), 693–722. https://doi.org/10.1130/2007.2430(32).

Liu, Y., Li, Z., Xiong, H., Gao, X., & Wu, J. (2010). Understanding of internal clustering validation measures. *Proceedings - IEEE International Conference on Data Mining, ICDM*, 911–916. https://doi.org/10.1109/ICDM.2010.35.

Llena, M., Vericat, D., Smith, M. W., & Wheaton, J. M. (2020). Geomorphic process signatures reshaping sub-humid Mediterranean badlands: 1. Methodological development based on high-resolution topography. *Earth Surface Processes and Landforms*, *45*(5), 1335–1346. https://doi.org/10.1002/esp.4821.

Maddy, D., Demir, T., Bridgland, D. R., Veldkamp, A., Stemerdink, C., van der Schriek, T., & Westaway, R. (2005). An obliquity-controlled Early Pleistocene river terrace record from Western Turkey? *Quaternary Research*, *63*(3), 339–346. https://doi.org/10.1016/j.yqres.2005.01.004.

Majhi, A., Nyssen, J., & Verdoodt, A. (2021). What is the best technique to estimate topographic thresholds of gully erosion? Insights from a case study on the permanent gullies of Rarh plain, India. *Geomorphology*, *375*, 107547. https://doi.org/10.1016/j.geomorph.2020.107547.

Marignani, M., Rocchini, D., Torri, D., Chiarucci, A., & Maccherini, S. (2008). Planning restoration in a cultural landscape in Italy using an object-based approach and historical analysis. *Landscape and Urban Planning*, *84*(1), 28–37. https://doi.org/10.1016/j.landurbplan.2007.06.005.

McClain, K. P., Yıldırım, C., Çiner, A., Şahin, S., Sarıkaya, M. A., Özcan, O., Kiyak, N. G., & Ozturk, T. (2020). Quaternary Rock Uplift Rates and Their Implications for the Western Flank of the North Anatolian Fault Restraining Bend; Inferences From Fluvial Terrace Ages. *Tectonics*, *39*(10), 0–2. https://doi.org/10.1029/2019TC005993.

McClain, K. P., Yıldırım, C., Çiner, A., Sarıkaya, M. A., Özcan, O., Görüm, T., Köse, O., Şahin, S., Kıyak, N. G., & Öztürk, T. (2021). River, alluvial fan and landslide interactions in a tributary junction setting: Implications for tectonic controls on Quaternary fluvial landscape development (Central Anatolian Plateau northern margin, Turkey). *Geomorphology*, *376*(March). https://doi.org/10.1016/j.geomorph.2020.107567.

McNab, F., Ball, P. W., Hoggard, M. J., & White, N. J. (2018). Neogene Uplift and Magmatism of Anatolia: Insights From Drainage Analysis and Basaltic Geochemistry. *Geochemistry, Geophysics, Geosystems*, *19*(1), 175–213. https://doi.org/10.1002/2017GC007251.

Memiş, C., Göğüş, O. H., Uluocak, E. Ş., Pysklywec, R., Keskin, M., Şengör, A. M. C., & Topuz, G. (2020). Long Wavelength Progressive Plateau Uplift in Eastern Anatolia Since 20 Ma: Implications for the Role of Slab Peel-Back and Break-Off. *Geochemistry, Geophysics, Geosystems*, *21*(2), 0–2. https://doi.org/10.1029/2019GC008726.

Meunier, P., Hovius, N., & Haines, J. A. (2008). Topographic site effects and the location of earthquake induced landslides. *Earth and Planetary Science Letters*, *275*(3–4), 221–232. https://doi.org/10.1016/j.epsl.2008.07.020

Montgomery, D. R., & Dietrich, W. E. (1992). Channel initiation and the problem of landscape scale. *Science*, *255*(5046), 826–830. https://doi.org/10.1126/science.255.5046.826.

Montgomery, D. R., & Foufoula-Georgiou, E. (1993). Channel network source representation using digital elevation models. *Water Resources Research*, *29*(12), 3925–3934. https://doi.org/10.1029/93WR02463.

Moreno-de las Heras, M., & Gallart, F. (2016a). Lithology controls the regional distribution and morphological diversity of montane Mediterranean badlands in the upper Llobregat basin (eastern Pyrenees). *Geomorphology*, *273*, 107–115. https://doi.org/10.1016/j.geomorph.2016.08.004.

Moreno-de las Heras, M., & Gallart, F. (2016b). Lithology controls the regional distribution and morphological diversity of montane Mediterranean badlands in the upper Llobregat basin (eastern Pyrenees). *Geomorphology*, *273*, 107–115. https://doi.org/10.1016/j.geomorph.2016.08.004.

Moreno-de las Heras, M., & Gallart, F. (2018). The Origin of Badlands. In *Badlands Dynamics in a Context of Global Change*. Elsevier Inc. https://doi.org/10.1016/b978-0-12-813054-4.00002-2.

Moretti, S., & Rodolfi, G. (2000). A typical “calanchi” landscape on the Eastern Apennine margin (Atri, Central Italy): geomorphological features and evolution. *CATENA*, *40*(2), 217–228. https://doi.org/10.1016/S0341-8162(99)00086-7.

Nadal-Romero, E., & Regüés, D. (2010). Geomorphological dynamics of subhumid mountain badland areas - weathering, hydrological and suspended sediment transport processes: A case study in the araguás catchment (central pyrenees) and implications for altered hydroclimatic regimes. *Progress in Physical Geography*, *34*(2), 123–150. https://doi.org/10.1177/0309133309356624.

Nadal-Romero, E., Regüés, D., Martí-Bono, C., & Serrano-Muela, P. (2007). Badland dynamics in the Central Pyrenees: temporal and spatial patterns of weathering processes. *Earth Surface Processes and Landforms*, *32*(6), 888–904. https://doi.org/10.1002/esp.1458.

Ocakoğlu, F. (2020). Rapid Late Quaternary denudation of the Karacasu Graben in response to subsidence in the Büyük Menderes Corridor: Insights from morphotectonics and archaeogeology. *Geomorphology*, *357*, 107107. https://doi.org/10.1016/j.geomorph.2020.107107.

Okay, A. I., & Tüysüz, O. (1999). Tethyan sutures of northern Turkey. *Geological Society Special Publication*, *156*, 475–515. https://doi.org/10.1144/GSL.SP.1999.156.01.22.

Okay, A. I., Zattin, M., Özcan, E., & Sunal, G. (2020). Uplift of anatoli. *Turkish Journal of Earth Sciences*, *29*(5), 696–713. https://doi.org/10.3906/yer-2003-10.

Özpolat, E., Yıldırım, C., & Görüm, T. (2020). The Quaternary landforms of the Büyük Menderes Graben System: the southern Menderes Massif, western Anatolia, Turkey. *Journal of Maps*, *16*(2), 405–419. https://doi.org/10.1080/17445647.2020.1764874.

Özsayin, E., Çiner, T. A., Rojay, F. B., Dirik, R. K., Melnick, D., Fernández-Blanco, D., Bertotti, G., Schildgen, T. F., Garcin, Y., Strecker, M. R., & Sudo, M. (2013). Plio-Quaternary extensional tectonics of the Central Anatolian Plateau: a case study from the Tuz Gölü Basin, Turkey. *Turkish Journal of Earth Sciences*. https://doi.org/10.3906/yer-1210-5.

Peel, M. C., Finlayson, B. L., & McMahon, T. A. (2007). Updated world map of the Köppen-Geiger climate classification. *Hydrology and Earth System Sciences*, *11*(5), 1633–1644. https://doi.org/10.5194/hess-11-1633-2007.

Piccarreta, M., Caldara, M., Capolongo, D., & Boenzi, F. (2011). Holocene geomorphic activity related to climatic change and human impact in Basilicata, Southern Italy. *Geomorphology*, *128*(3–4), 137–147. https://doi.org/10.1016/j.geomorph.2010.12.029.

Pulice, I., Cappadonia, C., Scarciglia, F., Robustelli, G., Conoscenti, C., Rose, R. De, Rotigliano, E., & Agnesi, V. (2012). Geomorphology Geomorphological , chemical and physical study of “ calanchi ” landforms in NW Sicily (southern Italy). *Geomorphology*, *153–154*, 219–231. https://doi.org/10.1016/j.geomorph.2012.02.026.

Racano, S., Schildgen, T. F., Cosentino, D., & Miller, S. R. (2021). Temporal and spatial variations in rock uplift from river-profile inversions at the Central Anatolian Plateau southern margin. *Journal of Geophysical Research: Earth Surface*. https://doi.org/10.1029/2020JF006027.

Regüés, D., & Gallart, F. (2004). Seasonal patterns of runoff and erosion responses to simulated rainfall in a badland area in Mediterranean mountain conditions(Vallcebre, southeastern Pyrenees). *Earth Surface Processes and Landforms*, *29*(6), 755–767. https://doi.org/10.1002/esp.1067.

Regüés, D., Pardini, G., & Gallart, F. (1995). Regolith behaviour and physical weathering of clayey mudrock as dependent on seasonal weather conditions in a badland area at Vallcebre, Eastern Pyrenees. *CATENA*, *25*(1–4), 199–212. https://doi.org/10.1016/0341-8162(95)00010-P.

Romero Díaz, A., Marín Sanleandro, P., Sánchez Soriano, A., Belmonte Serrato, F., & Faulkner, H. (2007). The causes of piping in a set of abandoned agricultural terraces in southeast Spain. *Catena*, *69*(3), 282–293. https://doi.org/10.1016/j.catena.2006.07.008.

Rossi, M., Torri, D., De Geeter, S., Cremer, C., & Poesen, J. (2022). Topographic thresholds for gully head formation in badlands. *Earth Surface Processes and Landforms*, *47*(15), 3558–3587. https://doi.org/10.1002/esp.5473.

Sariş, F., Hannah, D. M., & Eastwood, W. J. (2010). Spatial variability of precipitation regimes over Turkey. *Hydrological Sciences Journal*, *55*(2), 234–249. https://doi.org/10.1080/02626660903546142.

Schildgen, T. F., Cosentino, D., Bookhagen, B., Niedermann, S., Yildirim, C., Echtler, H., Wittmann, H., & Strecker, M. R. (2012). Multi-phased uplift of the southern margin of the Central Anatolian plateau, Turkey: A record of tectonic and upper mantle processes. *Earth and Planetary Science Letters*, *317–318*, 85–95. https://doi.org/10.1016/j.epsl.2011.12.003.

Schildgen, T. F., Yildirim, C., Cosentino, D., & Strecker, M. R. (2014). Linking slab break-off, Hellenic trench retreat, and uplift of the Central and Eastern Anatolian plateaus. *Earth-Science Reviews*, *128*, 147–168. https://doi.org/10.1016/j.earscirev.2013.11.006.

Schwanghart, W., & Scherler, D. (2014). Short Communication: TopoToolbox 2 – MATLAB-based software for topographic analysis and modeling in Earth surface sciences. *Earth Surface Dynamics*, *2*(1), 1–7. https://doi.org/10.5194/esurf-2-1-2014.

Şen, E., Aydar, E., Bayhan, H., & Gourgaud, A. (2014). Alkali Bazalt ve Piroklastik Çökellerin Volkanolojik Özellikleri, Kula Volkanları, Batı Anadolu. *Yerbilimleri/Hacettepe Üniversitesi Yerbilimleri Uygulama ve Araştırma Merkezi Dergisi*, *35*(3), 141. https://doi.org/10.17824/huyuamd.20663.

Sen, O. L., Ezber, Y., & Bozkurt, D. (2019). Euro-Mediterranean climate variability in boreal winter: a potential role of the East Asian trough. *Climate Dynamics*, *52*(11), 7071–7084. https://doi.org/10.1007/s00382-018-4573-9.

Şengör, A. M. C., & Yilmaz, Y. (1981). Tethyan evolution of Turkey: A plate tectonic approach. In *Tectonophysics* (Vol. 75, Issues 3–4). https://doi.org/10.1016/0040-1951(81)90275-4.

Şengör, A. M. C., & Yazıcı, M. (2020). The aetiology of the neotectonic evolution of Turkey. *Mediterranean Geoscience Reviews*, *0123456789*. https://doi.org/10.1007/s42990-020-00039-0.

Summa, V., Tateo, F., Medici, L., & Giannossi, M. L. (2007). The role of mineralogy, geochemistry and grain size in badland development in Pisticci (Basilicata, Southern Italy). *Earth Surface Processes and Landforms*, *32*(7), 980–997. https://doi.org/10.1002/esp.1449.

Tarboton, D. G., Bras, R. L., & Rodriguez-Iturbe, I. (1992). A physical basis for drainage density. *Geomorphology*, *5*(1–2), 59–76. https://doi.org/10.1016/0169-555X(92)90058-V.

Tarolli, P., & Dalla Fontana, G. (2009). Hillslope-to-valley transition morphology: New opportunities from high resolution DTMs. *Geomorphology*, *113*(1–2), 47–56. https://doi.org/10.1016/j.geomorph.2009.02.006.

Tatli, H., & Dalfes, H. N. (2021). Analysis of temporal diversity of precipitation along with biodiversity of Holdridge life zones. *Theoretical and Applied Climatology*. https://doi.org/10.1007/s00704-021-03551-x.

Tatli, H., Nüzhet Dalfes, H., & Sibel Menteş. (2004). A statistical downscaling method for monthly total precipitation over Turkey. *International Journal of Climatology*, *24*(2), 161–180. https://doi.org/10.1002/joc.997.

Torri, D., Rossi, M., Brogi, F., Marignani, M., Bacaro, G., Santi, E., Tordoni, E., Amici, V., & Maccherini, S. (2018). Badlands and the Dynamics of Human History, Land Use, and Vegetation Through Centuries. In *Badlands Dynamics in a Context of Global Change*. Elsevier Inc. https://doi.org/10.1016/b978-0-12-813054-4.00004-6.

Toté, C., Swinnen, E., Sterckx, S., Clarijs, D., Quang, C., & Maes, R. (2017). Evaluation of the SPOT/VEGETATION Collection 3 reprocessed dataset: Surface reflectances and NDVI. *Remote Sensing of Environment*, *201*(November 2016), 219–233. https://doi.org/10.1016/j.rse.2017.09.010.

Trabucco, A., & Zomer, R. J. (2018). Global Aridity Index and Potential Evapotranspiration (ET0) Climate Database v2. *CGIAR Consortium for Spatial Information (CGIAR-CSI)*, *November*, 10.

Türkeş, M. (1996). Spatial And Temporal Analysis Of Annual Rainfall Variations In Turkey. *International Journal of Climatology*, *16*(9), 1057–1076. https://doi.org/10.1002/(SICI)1097-0088(199609)16:9<1057::AID-JOC75>3.0.CO;2-D.

Vergari, F. (2015). Assessing soil erosion hazard in a key badland area of Central Italy. *Natural Hazards*, *79*(1), 71–95. https://doi.org/10.1007/s11069-015-1976-3.

Vergari, F., Troiani, F., Faulkner, H., Del Monte, M., Della Seta, M., Ciccacci, S., & Fredi, P. (2019). The use of the slope–area function to analyse process domains in complex badland landscapes. *Earth Surface Processes and Landforms*, *44*(1), 273–286. https://doi.org/10.1002/esp.4496.

Wells, T., Binning, P., Willgoose, G., & Hancock, G. (2006). Laboratory simulation of the salt weathering of schist: 1. Weathering of schist blocks in a seasonally wet tropical environment. *Earth Surface Processes and Landforms*, *31*(3), 339–354. https://doi.org/10.1002/esp.1248.

Westaway, R., Pringle, M., Yurtmen, S., Demir, T., Bridgland, D., Rowbotham, G., & Maddy, D. (2004). Pliocene and Quaternary regional uplift in western Turkey: The Gediz River terrace staircase and the volcanism at Kula. *Tectonophysics*, *391*(1-4 SPEC.ISS.), 121–169. https://doi.org/10.1016/j.tecto.2004.07.013.

Willgoose, G., Bras, R. L., & Rodriguez-Iturbe, I. (1991). A coupled channel network growth and hillslope evolution model: 2. Nondimensionalization and applications. *Water Resources Research*, *27*(7), 1685–1696. https://doi.org/10.1029/91WR00936.

Yair, A., Bryan, R. B., Lavee, H., Schwanghart, W., & Kuhn, N. J. (2013). The resilience of a badland area to climate change in an arid environment. *Catena*, *106*, 12–21. https://doi.org/10.1016/j.catena.2012.04.006.

Yair, A., Lavee, H., Bryan, R. B., & Adar, E. (1980). Runoff and erosion processes and rates in the Zin valley badlands, northern Negev, Israel. *Earth Surface Processes*, *5*(3), 205–225. https://doi.org/10.1002/esp.3760050301.

Yamazaki, D., Ikeshima, D., Tawatari, R., Yamaguchi, T., O'Loughlin, F., Neal, J. C., Sampson, C. C., Kanae, S., & Bates, P. D. (2017). A high-accuracy map of global terrain elevations. *Geophysical Research Letters*, *44*(11), 5844–5853. https://doi.org/10.1002/2017GL072874.

Yetemen, O., Istanbulluoglu, E., & Vivoni, E. R. (2010). The implications of geology, soils, and vegetation on landscape morphology: Inferences from semi-arid basins with complex vegetation patterns in Central New Mexico, USA. *Geomorphology*, *116*(3–4), 246–263. https://doi.org/10.1016/j.geomorph.2009.11.026.

Yildirim, C., Schildgen, T. F., Echtler, H., Melnick, D., & Strecker, M. R. (2011). Late Neogene and active orogenic uplift in the Central Pontides associated with the North Anatolian Fault: Implications for the northern margin of the Central Anatolian Plateau, Turkey. *Tectonics*, *30*(5), 1–24. https://doi.org/10.1029/2010TC002756.

Yucel, I., Güventürk, A., & Sen, O. L. (2015). Climate change impacts on snowmelt runoff for mountainous transboundary basins in eastern Turkey. *International Journal of Climatology*, *35*(2), 215–228. https://doi.org/10.1002/joc.3974.

CURRICULUM VITAE

Name Surname **:** Aydoğan AVCIOĞLU

EDUCATION

- **B.Sc.** **:** 2017, Çanakkale 18Mart University, Faculty of Arts and Science, Geography Department
- **M.Sc.** **:** 2019, Istanbul University, Social Science Institute, Geography Programme

PROFESSIONAL EXPERIENCE AND REWARDS:

- Visiting Scientist at Potsdam University July 2022 - July 2023.
- EGU Outstanding Student and Ph.D. candidate (OSPP) Presentation Awards 2022:
  Avcioglu, A., Antić, N., Kašanin – Grubin, M., Görüm, T., Tosti, T., Dojčinović, B., Yetemen, Ö. (2022) Seasonal influences on weathering processes in Turkish Badlands: Laboratory-based climate experiments. Abstract EGU General Assembly. Vienna.
- Visiting Scientist at Belgrade University October 2021 - November 2021.

PUBLICATIONS, PRESENTATIONS AND PATENTS ON THE THESIS:

- **Avcıoğlu, A.,** Görüm, T., Akbaş, A., Moreno-de las Heras, M., Yıldırım, C., & Yetemen, Ö. (2022). Regional distribution and characteristics of major badland landscapes in Turkey. *Catena, 218, 106562***.** **https://doi.org/10.1016/j.catena.2022.106562.**

OTHER PUBLICATIONS, PRESENTATIONS AND PATENTS:

[1] Avcioglu, A., W Schwanghart., Görüm, T., Moreno de las Heras, Ö., Yang C. J., Yetemen, Ö. (2023) Topographic signature of badlands landscapes. Abstract EGU General Assembly. Vienna.

[2] Avcioglu, A., Antić, N., Kašanin – Grubin, M., Görüm, T., Tosti, T., Dojčinović, B., Yetemen, Ö. (2022) Seasonal influences on weathering processes in Turkish Badlands: Laboratory-based climate experiments. Abstract EGU General Assembly. Vienna.

[3] Avcioglu, A., Görüm, T., Yetemen, Ö. (2021). The main geomorphological differences of badland landforms in Turkey. Abstract Mediterranean Geoscience Union Annual Meeting. Istanbul, 25-28 November 2021.

[4] Avcioglu, A., Görüm, T., Akbas, A., & Moreno de las Heras, M., Yetemen, Ö. (2021). The climatic, topographic and litho-tectonic characteristics of badlands in Turkey. Abstract EGU General Assembly. Vienna.

[5] Avcioglu, A., Görüm, T., Yetemen, Ö., & Moreno de las Heras, M. (2020). Geomorphometric characteristics of major badland landscapes of Turkey. Abstract EGU General Assembly. Vienna.

[6] Avcioglu, A., Görüm, T., Yetemen, Ö. (2020). The Geomorphological Characteristics and The Spatial Distribution of Arid and Semi-Arid Badlands In Turkey. Abstract IX. Quaternary Symposium of Turkey. Istanbul, 31 March – 4 April 2020.